ORDERED COLLOIDAL-MASK APPLICATIONS IN LIGHT MANAGEMENT

A THESIS SUBMITTED TO
THE GRADUATE SCHOOL OF NATURAL AND APPLIED SCIENCES
OF
MIDDLE EAST TECHNICAL UNIVERSITY

BY

SEYEDEHNASIM SEYEDPOUR ESMAEILZAD

IN PARTIAL FULFILLMENT OF THE REQUIREMENTS
FOR
THE DEGREE OF DOCTOR OF PHILOSOPHY
IN
MICRO AND NANOTECHNOLOGY

JULY 2021

Approval of the thesis:

ORDERED COLLOIDAL-MASK APPLICATIONS IN LIGHT MANAGEMENT

submitted by **SEYEDEHNASIM SEYEDPOUR ESMAEILZAD** in partial fulfillment of the requirements for the degree of **Doctor of Philosophy** i**n Micro and Nanotechnology, Middle East Technical U**niversity by,

Prof. Dr. Halil Kalıpçılar
Dean, Graduate School of **Natural and Applied Sciences** _____

Prof. Dr. Almıla Güvenç Yazıcıoğlu
Head of the Department, **Micro and Nanotechnology** _____

Assoc. Prof. Dr. Alpan Bek
Supervisor, **Physics, METU** _____

Assoc. Prof. Dr. Hasan Hüseyin Güllü
Co-Supervisor, **OOTM/MGEO ASELSAN** _____

Examining Committee Members:

Prof. Dr. Hamza Kurt
Electrical and Electronics Eng., TOBB University _____

Assoc. Prof. Dr. Alpan Bek
Physics, METU _____

Prof. Dr. Emrah Ünalan
Metallurgical and Materials Eng., METU _____

Assoc. Prof. Dr. Tahir Çolakoğlu
Physics Eng., Ankara University _____

Assoc. Prof. Dr. Emre Yüce
Physics, METU _____

Date: 28.07.2021

I hereby declare that all information in this document has been obtained and presented in accordance with academic rules and ethical conduct. I also declare that, as required by these rules and conduct, I have fully cited and referenced all material and results that are not original to this work.

Name, Last name: Seyedehnasim, Seyedpour Esmaeilzad

Signature:

ABSTRACT

ORDERED COLLOIDAL-MASK APPLICATIONS IN LIGHT MANAGEMENT

Seyedpour Esmaeilzad, Seyedehnasim
Doctor of Philosophy, Micro and Nanotechnology
Supervisor: Assoc. Prof. Dr. Alpan Bek
Co-Supervisor: Assoc. Prof. Dr. Hasan Hüseyin Güllü

July 2021, #104 pages

Dielectric colloidal micro-/nanospheres (CMNS) are promising candidates for different applications. In this thesis, colloidal spheres are either used for light management in photonic devices such as solar cells or surface enhanced Raman scattering (SERS) substrates.

CMNS arrays can direct the broad incident radiation into a set of tighter foci, at which light intensity becomes considerably concentrated, enabling higher conversion efficiency. Furthermore, the CMNS arrays acting as an effective medium on the device surface can reduce reflection and facilitate improved forward scattering and hence the utilization of light within the device. Therefore, uniform arrays of CMNS located on top of the photonic devices can behave as antireflection coatings or as micro-lenses which can be regarded as a surface distributed concentrator within the framework of concentrated photovoltaics (CPV). Fabrication of such a light-trapping structure is low-cost and less complicated than common alternatives such as vacuum evaporated multilayer antireflection coatings. In this thesis, experimental

demonstration and computational support of the optimal size and shape of such CMNS arrays are illustrated.

Besides, thin metallic film coated dielectric nanospheres are demonstrated to have a high potential for fabrication of cost-effective SERS substrates. In addition to the morphological advantages that nanospheres offer for attaining a high density of hot-spots, possessing shape adjustability by uncomplicated thermal treatment make them an attractive platform for tuneable SERS substrates. Furthermore, when combined with oblique angle metal deposition technique, adjustable gaps at a high density and adjustable shape of metal films, such as silver (Ag) films, can be achieved on nanospheres. Applying small changes in deposition angle can provide means for fine adjustment of the SERS enhancement factor (EF), resulting in EF up to 10^8 measured using crystal violet dye molecule as a Raman analyte. This practice paves the way for the fabrication of high EF SERS substrates at a reasonable cost using a monolayer of self-organized nanosphere pattern. An ultra-thin Ag film coated at 5^o tilt is shown to be an excellent substitute for a film deposited at 0^o with double the thickness. There is a strong agreement between the experimental results and finite element method based simulations exhibiting expected field enhancements up to 10^9 at a tilt angle of 5^o. In summary, the demonstration of several ordered colloidal mask applications in light management for photonic devices is aimed at this thesis.

Keywords: Dielectric Nanospheres, Photovoltaic, SERS

ÖZ

IŞIK YÖNETİMİNDE DİZİLMİŞ KOLLOİDAL-MASKE UYGULAMALARI

Seyedpour Esmaeilzad, Seyedehnasim
Doktora, Mikro ve Nanoteknoloji
Tez Yöneticisi: Doç. Dr. Alpan Bek
Ortak Tez Yöneticisi: Doç. Dr. Hasan Hüseyin Güllü

Temmuz 2021, #104 sayfa

Dielektrik kolloidal mikro-/nanoküreler (CMNS), farklı uygulamalar için umut vadeden adaylardır. Bu tezde, kolloidal küreler, güneş pilleri gibi fotonik cihazlarda veya yüzey artırımlı Raman saçılması (SERS) alttaşlarında ışık yönetimi için kullanılmıştır.

CMNS dizileri, geniş gelen radyasyonu, daha yüksek dönüşüm verimliliği sağlayarak ışık şiddetinin önemli ölçüde yoğunlaştığı bir dizi sıkı odak noktalarına yönlendirebilir.. Ayrıca, cihaz yüzeyinde etkili bir ortam görevi gören CMNS dizileri, yansımayı azaltabilir ve artırılmış ileri saçılımı ve dolayısıyla cihaz içinde ışığın kullanımını kolaylaştırabilir. Bu nedenle, fotonik cihazların üzerinde yer alan tek tip CMNS dizileri, yansıma önleyici kaplamalar veya konsantre fotovoltaikler (CPV) çerçevesinde yüzeyde dağıtılmış bir yoğunlaştırıcı olarak kabul edilebilen mikro lensler gibi davranabilir. Böyle bir ışık tutucu yapının üretimi, düşük maliyetli ve vakumla buharlaştırılan çok katmanlı yansıma önleyici kaplamalar gibi yaygın alternatiflerden daha az karmaşıktır. Bu tezde, bu tür CMNS dizilerinin en uygun boyut ve şeklinin deneysel gösterimi ve hesaplamalı desteği gösterilmiştir. Ayrıca,

ince metalik film kaplıdielektrik nanokürelerin, uygun maliyetli SERS alttaşlarının üretimi için yüksek bir potansiyele sahip olduğu gösterilmiştir. Nanokürelerin yüksek yoğunluklu sıcak noktalar elde etmek için sunduğu morfolojik avantajlara ek olarak, karmaşık olmayan ısıl işlemle şekil ayarlanabilirliğine sahip olmaları, onları ayarlanabilir SERS alttaşları için çekici bir platform haline getirmektedir. Ayrıca, eğik açılı metal bırakım tekniği ile birleştirildiğinde, nanoküreler üzerinde ayarlanabilir şekildeki gümüş (Ag) filmler gibi metal filmler ve yüksek yoğunlukta ayarlanabilir boşluklar elde edilebilir. Kaplanma açısında küçük değişiklikler uygulamak, SERS artırım faktörünün (EF) ince ayarı için araçlar sağlayabilir ve bu, bir Raman analiti olarak kristal mor boya molekülü kullanılarak ölçülen EF'nin 10^8'e kadar çıkmasıyla sonuçlanır. Bu uygulama, yüksek EF değerine sahip SERS alttaşlarının, kendi kendini organize eden bir nanoküre deseninin tek tabakasını kullanarak makul bir maliyetle üretilmesinin yolunu açmaktadır. 5^o eğimde kaplanmış ultra ince Ag filmin, 0^o'de iki katı kalınlıkta kaplanmış olanlar için mükemmel bir alternatif olduğu gösterilmiştir. 5^o eğim açısında 10^9'a kadar beklenen alan artırımlarını gösteren sonlu elemanlar metoduna dayalı simülasyonlar ile deneysel sonuçlar arasında güçlü bir uyum vardır. Özetle, bu tezde fotonik cihazlar için ışık yönetiminde çeşitli dizilmiş kolloidal maske uygulamalarının gösterilmesi amaçlanmaktadır.

Anahtar Kelimeler: Yalıtkan Kolloidal Nanosferler, Fotovoltaik Hücre, SERS

To my beloved family

ACKNOWLEDGMENTS

I would like to express my deepest gratitude to my supervisor, Assoc. Prof. Dr. Alpan Bek and co-supervisor Assoc. Prof. Dr. Hasan Hüseyin Güllü for their guidance, advice, patience, encouragement, and insight throughout the research. Their insightful feedback pushed me to sharpen my thinking and brought my work to a higher level.

I would like to thank Prof. Dr. Emrah Ünalan and Prof. Dr. Hamza Kurt for their support and innovative ideas during my thesis.

I would also like to thank Prof. Dr. Raşit Turan for providing high-tech infrastructure and clean room facilities in GÜNAM institute, which paves the way for me to conduct my thesis experiment.

I would like to thank to Ahmet Kemal Demir, Özge Demirtaş, Hande Çiftpinar, jamileh Hajivand, İbrahim Murat Öztürk, Hüseyin Umut Tepe for their contribution throughout my thesis work.

I would like to express my gratitude to my love, Karim Yousefi, who supported me in every step of my thesis. I could not have completed this dissertation without the happy moments he provided as distractions to rest my mind outside my research.

My parents and my brother deserve very special thanks because of their wise counsel and sympathetic ear. They are always there for me, and I could not have completed this dissertation without their support and inspiration.

My days in graduate school would not be enjoyable without the company of my friends. I have experienced memorable moments with my dear friends. I would like to thank Parisa Sharif and Mona Borra, and Salar Sedani for their support.

This work is partially funded by the Scientific and Technological Research Council of Turkey under grant number TUBİTAK 115F167.

TABLE OF CONTENTS

LIST OF TABLES

TABLES

LIST OF FIGURES

FIGURES

LIST OF ABBREVIATIONS

ABBREVIATIONS

CMNS: Colloidal Micro/Nanospheres

CL: Colloidal Lithography

RIE: Reactive Ion Etching

PS NSs: Polystyrene Nanospheres

HCP: Hexagonally Closed-Packed

NSL: Nanosphere Lithography

PR: Photoresist

UV: Ultraviolet

EBL: Electron Beam Lithography

CARS: Coherent anti-stokes Raman scattering

HML: Hole mask lithography

SERS: Surface Enhanced Raman Scattering

CHAPTER 1

INTRODUCTION

In this study, the arrays of nanospheres are utilized on top of solar cells and as SERS substrates. This chapter studies uniform arrays of periodic polystyrene nanospheres (PS NSs) and introduces the first emergence of NSs in the literature (Section 1.1). The main objectives and motivations of this work are explained in section 1.2, and a thesis outline is provided in section 1.3.

1.1 Introduction

The ordered microsphere layer was first employed as a shadow mask in 1981 to deposit silver disks by Fischer and Zingsheim [1]. Other terms are also used for this technique, including natural lithography [2], nanosphere lithography [3], [4], or colloidal lithography (CL) [5], to fabricate nanostructures.

This study introduces the optimal method to produce self-assembled arrays of nanospheres (NSs) with low defects. Monolayers of colloidal NSs are candidates for applications such as lithographic masks, optical gratings, multi-lens arrays, antireflecting surfaces, etc. In this thesis, colloidal arrays are employed in two different applications. The first application of NSs arrays is their implementation on top of Si solar cells, improving their efficiency. Secondly, Si wafers coated with NSs can be used as SERS substrates.

Colloidal lithography is of great importance as it possesses a huge potential to substitute complex and expensive techniques. In the case of Si solar cells, where NSs act as light trappers, we can easily deduce that colloidal arrays are cheaper and simpler than other predominant multilayer dielectric anti-reflective coatings (ARCs),

which are costly and time-consuming. In the case of SERS substrates, nanosphere lithography (NSL) has gained huge attention because it is a cost-effective, reproducible technique, which can produce large area, ordered metal nanostructures. Colloidal lithography possesses the benefits of both top-down and bottom-up techniques, and it can be divided into two major steps: (1) The preparation of hexagonally closed-packed (hcp) nanospheres and (2) The deposition of favorite material through the colloidal mask. The colloidal lithography process can be combined with other processes, like metal deposition (even tilted evaporation), to fabricate specific periodic nanostructures.

In this thesis, hcp NSs are coated on the surface of solar cells to manage light. Not only do NS arrays behave as antireflection coatings (ARCs), but they also concentrate light. Annealing of nanospheres can introduce shape modification of NSs, which facilitates better light concentration, and higher conversion efficiencies.

The second approach combines the colloidal mask with traditional or angled metal deposition to generate uniform, complicated metallic structures. These structures have many applications, like surface-enhanced Raman scattering (SERS), which occurs by strong near-field enhancements of metallic structures combined with polystyrene nanospheres. SERS have the capability of detection at the molecular level.

1.2 Aims and objectives

The objective of this study is to use colloidal lithography to produce periodic nanostructures and their different applications. However, to achieve high-quality self-assembled hexagonally close-packed (HCP) nanospheres, different assembly methods should be investigated. There are other challenges apart from assembly problems.

The employment of parallel fabrication methods to fabricate ordered arrays of nanopatterns and methods to remove PS spheres with minimum damage are practical

to improve the process. Besides, implementing low-cost, effective, and low defect structures is a final objective. The following steps are set out to fulfill the above-mentioned research targets.

1. Study of the cutting-edge technologies to improve colloidal lithography. This contains reviewing a wide variety of colloidal lithography steps and recently multi-step process techniques to overcome existing limitations.

2. Understanding the impact of surface hydrophilicity in the quality of nanospheres and utilizing experimental methods to increase the hydrophilicity of the substrate.

3. Fabrication of nanostructures through monolayer and bilayer dielectric spheres.

4. Fabrication of various architecture of nanostructures using the tilted evaporation method.

1.3 Thesis outline

This thesis includes five main chapters. Chapter 1 introduces the basics of nanosphere lithography. It presents the thesis goals, objectives, and thesis outline.

Chapter 2 compares the differences between conventional lithography, like photolithography and electron beam lithography, to colloidal lithography, which generates periodic structures. Furthermore, colloidal lithography (CL) is completely investigated, and various classifications and potential applications of CL-assisted periodic nanostructures are reviewed.

In Chapter 3, a single layer of hcp PS NS arrays demonstrates anti-reflective and light concentration properties for single-crystalline Si SCs, which are significantly improved by low-cost, rapid, and uncomplicated annealing-based NS shape control.

In chapter 4, polystyrene nanospheres are used in Surface-enhanced Raman scattering (SERS), which is an important spectroscopic method. In this study, SERS data were obtained from polystyrene spheres that are deposited with silver using the tilted evaporation method.

The study of colloidal lithography in nanofabrication is concluded in Chapter 5. The main findings achieved and potential future topics are mentioned in this chapter.

CHAPTER 2

BACKGROUND

This chapter studies a literature review of periodic nanostructures, such as available nanofabrication techniques and resulting nanostructures (Section 2.1).
Nanosphere lithography is explained in Section 2.2, and different applications of nanosphere lithography are shown in section 2.3. In section 2.4, angle-resolved Colloidal Lithography (CL) is presented as a promising candidate for fabricating nanostructures. Finally, the literature review is summarized in Section 2.5.

2.1 Fabrication methods for nanostructures

It has been 50 years since the renowned lecture "there's plenty of room at the bottom" by Feynman [6]. Feynman introduced straightforward approaches to work at the atomic scale, which amaze the world with extraordinary results. He has revolutionized concepts like miniature writing. Tools performing on this scale can introduce considerable progress in various applications such as advanced computers and more compact components. Applications are hugely beneficial in vast fields, like photovoltaic devices, (molecular) electronics, and biosensors. The address what Feynman has mentioned, we should answer the question of "How do we write small?" There exist two substantial techniques for nanofabrication, named the "top-down" and the "bottom-up" methods [7], [8].

2.1.1 Top-Down method

In the top-down technique, sizes of bulk materials are reduced to construct nanodevices. This is possible by the utilization of widespread approaches, such as precision engineering and lithography. It is the never-ending quest for the miniaturization of devices that further the research in such fabrication processes. The employment of different processes like subtractive and additive transfers pave the way to achieve various nanostructures.

The lithographic tools can be divided into two groups. “parallel writing” (or replication) techniques (e.g., optical lithography) and “sequential writing” (or patterning) techniques (e.g., focused-electron beam lithography).

In parallel writing, the writing process is conducted at the same time for the whole pattern employing a mask. Nevertheless, sequential lithography is a slow and expensive process since the pattern is written sequentially.

2.1.1.1 Lithography techniques

Optical photolithography (UV photolithography) is a procedure, which utilizes light to transfer required patterns to the photoresist layer from a mask. Two different approaches are practical in photolithography: (i) contact mode and (ii) projection mode.

Optical lithography resolution is limited due to the utilized wavelength of the light used for photoresist exposure [9]. The employment of short wavelengths and reduction optics between the mask and substrate will lead to downsizing the features. Conducting the procedures in deep UV and so. X-ray introduces technical complexities.

Other approaches, like electron beam lithography, have been established to overcome the limitations of optical light. While optical lithography can provide

patterns of a few micrometers, electron beam lithography provides an opportunity to get submicron resolutions.

Ideally, reaching a sub-10 nm resolution is feasible. However, the cost of such methods is tremendously high due to installing and maintaining processes of tools. In recent years, different lithographic and patterning methods have been exploited to solve existing difficulties.

The theory of soft lithography was recommended in 1988 by Whiteside's group at Harvard [10]. It consists of a set of methods [10], [11], such as microcontact printing, replica molding, etc., for producing structures by a patterned elastomer (e.g., polydimethylsiloxane (PDMS) as a mask, stamp, or mold. While these techniques can be conducted in a normal laboratory, conventional photolithography should be carried out in clean-room ambient. This is because the fabricated devices can be failed due to the existence of contamination. However, this is not the case with the PDMS stamp, as a piece of dust gets trapped between the stamp and the surface; the stamp will be functional yet.

This technology is not accurate enough to be utilized in complex nanoelectronics. As all integrated circuits possess multiple layers of various materials, small inaccuracies can cause a misalignment of the pattern with other layers.

Another technique is imprint lithography [11], which is utilized to etch a pattern into a quartz plate, applicable for replication, and polymeric master is also produced.

Table 2.1 The Properties of all these lithography techniques [12].

Technique	*feature size*	*Area*	*Cost*	*Time*
Deep UV L.	50-100 nm	Large	High	Short
Extreme UV L.	≤ 50 nm	Large	High	Short
X-Ray L.	20 nm	Large	High	Short
Electron Beam L	≈nm	Small	High	Long

Soft L	≈10nm	Large	Low	Short
Scanning Probe L	≤1nm	Small	High	Long

2.1.2 Bottom-Up method

The bottom-up method employs tiny and simple components (atoms, molecules, nanoparticles, etc.) that will self-assemble into larger, more complex structures.

Such methods are usually low-cost processes, such as Self-assembly, which is the connection of two (or more) elements to form larger components by covalent and/or noncovalent bonds [13]. Self-assembled monolayers [14] or nanostructures that self-assemble from block copolymers [15]–[17] can be fabricated by employing this technique.

These structures can be practiced by preparing metallic or semiconducting nanostructures [18]. The major benefit of this method is that nanoscale structures can be fabricated. Recent progress is achieved in the fabrication of functional nanostructures operating self-assembly like self-assembled magnetic nanoparticles [19]. Crystalline regions of magnetic nanocrystals save a vast amount of data. Nonetheless, an annealing process is critical to intensify the magnetic properties and boost the coalescence of the nanoparticles [20]. However, the existing defects in the structures make it difficult to achieve homogenous periodic structures, which makes nanofabrication a challenge with this method.

2.2 Nanosphere lithography

Nanosphere lithography (NSL) is a cost-effective, desirable technique tailored to achieve uniformly distributed arrays of nanospheres. The NSL is a combination of both the bottom-up method (self-assembly of nanobeads in HCP pattern) and the top-

down method (Nanostructured layers such as in a conventional lithography technique), as shown in Figure 2.1.

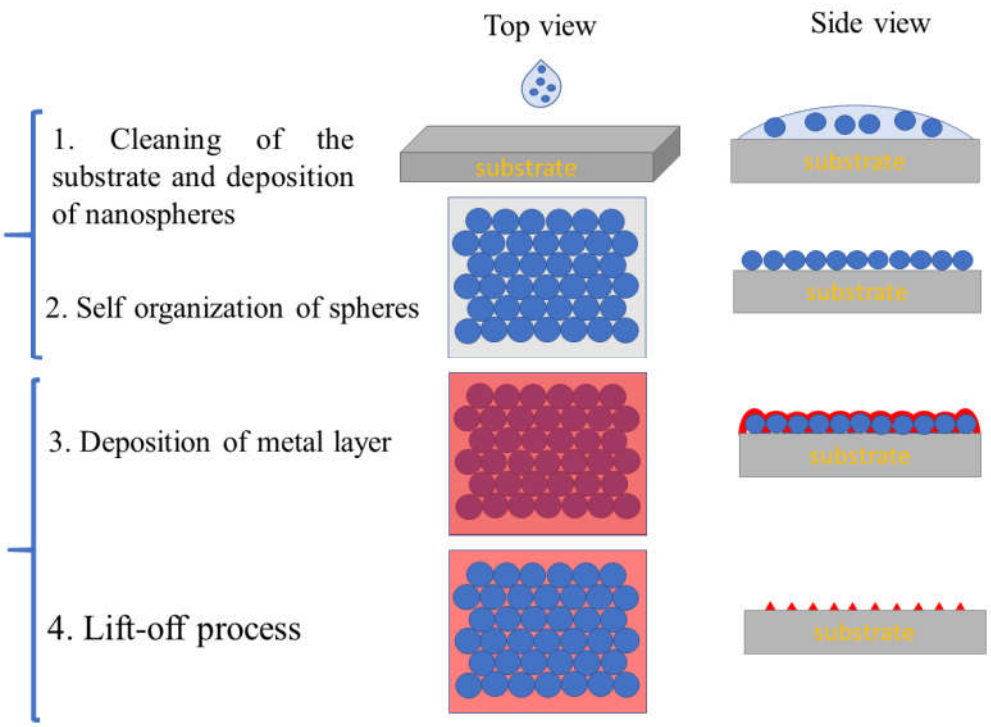

Figure 2.1. Nanosphere lithography process.

a. Mask preparation technique

The significant procedure in NS lithography is the preparation of a uniformly distributed hexagonal close-packed array of spheres. There are many methods to prepare a colloidal mask. One of the main factors which affect the quality of the mask is the physical and chemical properties of utilized spheres and the substrate. The predominantly used nanospheres are silica and polystyrene, which are preferred based on their better performance [21]. Another important criterion is the surface and techniques employed for its treatment.

For example, if the utilized surface is silicon, its surface is made hydrophilic by oxygen plasma treatment before coating with a homogenous monodisperse nanosphere (e.g., polystyrene). After the drying procedure, a hexagonal-close-packed (HCP) monolayer is shaped like Figure 2.2, which can be utilized as a mask [22]. This mask is employed to pattern the surface in selective areas due to the deposition of the favorable material through the spaces formed between ordered beads.

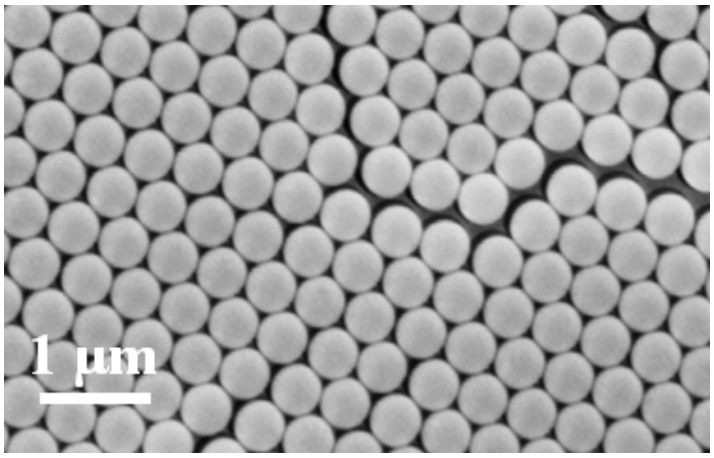

Figure 2.2. Sem image of nanospheres (Diameter 350 nm).

b. Lift -off process

After the deposition, the mask can be removed, which is called the lift-off process. This process can be conducted utilizing sonication in an adequate solvent or by stripping nanospheres employing tapes.

Nanosphere lithography is called colloidal lithography [5], [23], or natural lithography. Researchers firstly deposit nanospheres and allow them to evaporate to form an ordered monolayer on a glass substrate, which were small-area monolayers [1]. As a result, the process is named “naturally” assembled polystyrene (PS) nanospheres. Their main aim was to replicate nanopatterns by visible light.

Subsequently, [2] a monolayer of nanospheres' application has been extended to be utilized as a "deposit material" or as a lithographic mask. The nanosphere array can be deposited in an hcp order or in a random order [24].

The coating process has been established to generate microcrystalline arrays using a spin coating method. There exist some dislocations on the surface as the mask is achieved using the self-assembly method.

Another research group [25] has changed this method's name from "natural lithography" to "nanosphere lithography." This group has employed both a single layer and double layers of NSs, which produces dots as nanostructures thanks to the emerging spaces between double-layer structures.

The plasmonic resonance features of the fabricated metallic nanostructures have been studied to produce biosensors based on surface-enhanced Raman spectroscopy [7], [26], [27]. Nanosphere lithography has gained great attention as versatile one-, two-, or three-dimensional nanostructures can be fabricated using this method [28]–[32].

There are two substantial trends applied for the improvement of colloidal lithography. The first target is optimizing the self-assembly process of nanospheres to achieve a large-area layer with minimum defects. The second aim is to fabricate novel nanostructures with versatile patterns using colloidal lithography.

In addition to the effect of utilized materials, different strategies of a self-assembly method can have a profound effect on the homogeneity of the prepared mask. The offered methods can be divided into four categories, which include drain coating, drop coating, spin coating, and electrophoretic deposition.

Different methods for mask preparation

A wide variety of techniques are investigated to enhance the quality of hcp monolayers. The most practical methods will be explained in detail, focusing on two-dimensional polystyrene nanospheres lattices. The offered methods can be divided into four categories, which include drain coating, drop coating, spin coating, and electrophoretic deposition.

1. ***Self-Assembly of nanospheres during solvent evaporation:*** Self-assembly of nanospheres can happen by evaporation of a drop-casted suspension of nanosphere on a surface. The attractive capillary forces among nanospheres and convective transport of the nanospheres can accelerate the self-assembly process during the evaporation process [33]. The quality of self-assembled monolayers is critically dependent on the rates of solvent evaporation [34].

2. ***Drain coating:*** One attractive strategy is the employment of a liquid-gas interface to prepare colloidal masks [35]. The surfaces of colloidal spheres are made hydrophobic and floated on a liquid surface by a spreading solvent to achieve a high-quality mask. The self-assembly process initiates on the liquid surface after the evaporation of the solvent. For conducting the experiment, the ordering process is using a Teflon barrier. After the liquid's evaporation, the closed-pack nanospheres are carried to the submerged substrate with a slight slope. The significant issue associated with this application is the requirement to fix a substrate's location at a level below the liquid surface, which is not practical in some cases. For instance, silica spheres, which are surface-modified with chloroform solvent, start to self-assemble at the water-air interface to form hcp arrays [36]. Achieving monolayer arrays is more feasible in this technique compared to drop coating and spin coating techniques.

3. ***Dip coating:*** Dip coating is a straightforward technique in which the sample is perpendicularly dipped into a solution consist of a nanosphere solution. The sample is immersed for a considerable amount of time to enable the deposition of nanospheres on the surface, and then the sample is taken out to dry. Nevertheless, the nanospheres are coated on both sides of the substrate, which boosts the required amount of nanospheres.

4. ***Drop coating:*** A combined technique of evaporation and dip coating has been offered to resolve existing downsides [37]. In this method, a droplet of diluted nanospheres solved in water is placed onto the flat substrate [33]. Based on the hydrophilicity of spheres and surface wettability, a droplet can spread. After the evaporation of the solvent, homogenous arrays can be achieved. The slow rate of evaporation can play a pivotal role in the quality of nanosphere arrays. Some experiments are carried over a slightly tilted substrate to achieve better uniformity [38].

5. ***Spin coating:*** The colloidal mask is produced in the spin coating method by spreading the prepared dilution on the substrate's surface using centrifugation. Spin coating is considered a fast and convenient technique compared to drain coating and drop coating strategies. During the spinning process, the suspension spreads rapidly on the wettable substrate to form hcp structures. The quality of an hcp array is dependent on the parameters, like the particle/solvent ratio, the spin speed, and hydrophilicity of the surface. In some studies, the nanosphere solution is diluted with a mixture of Triton X-100 and methanol to enhance the surface's hydrophilicity [25]. Multilayer or non-close packed arrays can be achieved using different parameters in a spin coating method [39].

   The spin coating of a nanosphere suspension can not only increase the evaporation rate [2], [25], but it also provides better quality of monolayer.

There are widespread properties, like spin speed, and size of the nanospheres, wettability, which determine the quality of colloidal layer formation.

The parameters given in the literature survey are usually based on experimental trial and error [40]–[42]. The substantial aim of the NSL study is to develop optimized experimental conditions to enhance the quality of homogenous layers of nanospheres on a surface to obtain large-area structures.

The main advantage of spin coating is the possibility of mass production of a large-area coating due to quickness and compatibility with wafer-scale processes. In theoretical calculations [34], interparticle capillary forces exist between spherical particles (Figure 8). When the liquid layer thickness is reduced, it will enhance the liquid surface deformation, which boosts the capillary forces. As a result, with the direction of spheres flow into the nucleus with a convective flux mode, particles diverge from thicker places to thinner parts.

6. ***Self-assembly using electric field:*** Electrophoretic deposition or electrochemical deposition can also be utilized for the self-assembly process. In this process, the assembly of nanospheres is based on an electric field's effect on the direction of the charged particles. Therefore, negatively charged spheres move towards the positive electrode.

   Silica and polystyrene spheres can be self-assembled on a glass substrate coated with an indium tin oxide (ITO) layer [43]. Despite the speed and accuracy of this process [44], [45], its limitation is the necessity of a conductive substrate. In a typical method, nanosphere arrays are placed between two conductive Teflon electrodes. The E-field between two layers leads the direction of nanospheres.

7. ***Self-assembly at the interface of two media :***

   (a) Air-Liquid interface (Langmuir-Blodgett Coating): Langmuir-Blodgett coating is a transportation process of nanospheres from a liquid-gas interface onto a substrate by a vertical dipping of the substrate immersed on the subphase [46] or with the surface modification of the nanospheres [47] to boost the hydrophobicity characteristic.

   The colloidal solution diluted in water can be combined with ethanol and polyethylene oxide (PEO) powder to produce a low-density solution, spreading across the surface. The PEO provides a stronger connection between particles, which results in uniform arrays of nanospheres.

   (b) Liquid-Liquid interface: The self-assembly process can be initiated at the interface between two non-miscible liquids [48]. After the organization of nanospheres on the interface, the monolayer is created by the evaporation of one phase.

8. ***Prepatterned substrates:*** Template-assisted self-assembly of colloids is utilized to generate complex structures, which is not feasible to achieve with the traditional self-assembly process. Therefore, the surfaces of substrates are chemically or physically treated before the self-assembly process, which makes the process quite costly. Substrates can be physically processed using conventional lithographic methods (optical lithography [49] and electron beam lithography). Furthermore, substrates can be chemically treated [50], [51]. Figure 2.3 illustrates the schematic of colloidal mask preparation on treated surfaces. Figure 2.4 shows the SEM graph of nanosphere layer formation on chemically-treated si surface.

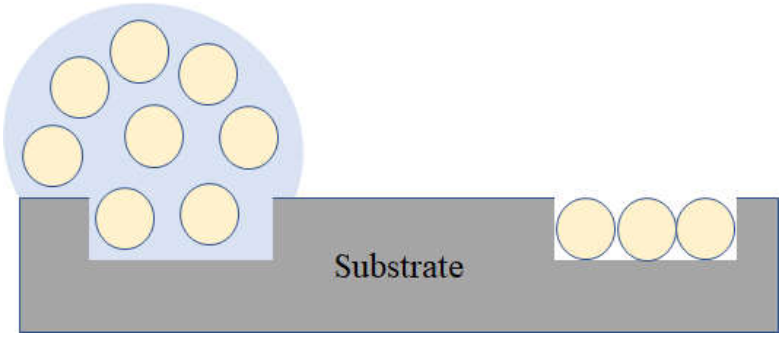

Figure 2.3. Self-assembly on a physically patterned substrate.

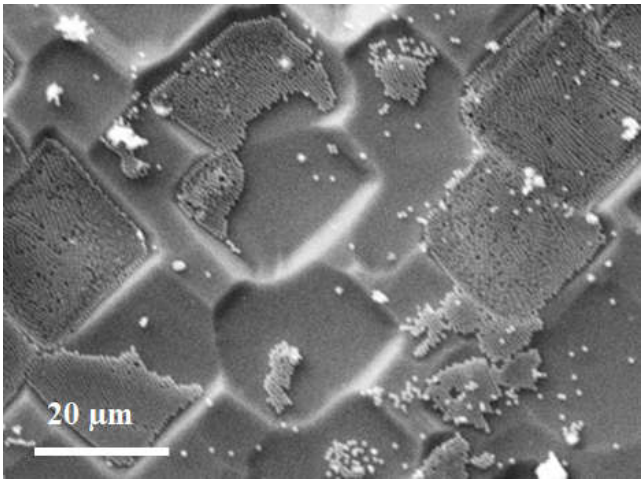

Figure 2.4. SEM image of polystyrene spheres on patterned si surface.

2.3 Applications of NSL

The arrangement of colloidal nanospheres offers a wide variety of applications in various areas.

First, NS arrays can be employed as filtration membranes in biomedical applications to segregate tiny proteins or gold nanoparticles and show the benefit of homogenous pore size distribution [52].

In addition, colloidal monolayers can be utilized as masks or templates to fabricate nanostructures. The size adjustment of structures can be achieved by changing the sphere diameters, ranging from less than ten nanometers [53] to tens of micrometers [54].

Despite the convenience and low cost of the colloidal mask, the fabricated pattern is limited to triangular shapes, which is a huge downside in comparison with traditional lithographic methods. Different strategies have been proposed to deal with this problem and obtain other structures.

Nanodots

Nanostructures can be fabricated by deposition through the colloidal mask. After the removal of nanospheres, triangular shapes remain, which are distributed in hexagonal lattices at the substrate surface. İf colloidal mask is a single layer, after the lift-off process, the emerging structures are nanotriangulars thanks to the gaps between NSs. However, if nanosphere masks are consist of double layers of NSs, the remaining structures will be nanodots, as illustrated in Figure 2.5.

One of the practical applications of fabricated nanostructures is localized surface plasmon resonance (LSPR) [55]. LSPR plays a pivotal role in nanophotonic applications, like surface-enhanced Raman scattering [56], [57] (SERS) substrates, or biosensors [58]. Ordered triangular Ag dots are studies meticulously to prove the correlation between particle sizes, shape, interparticle spacing, and LSPR [56]. (Figure 2.6). They showed that the absorption band of the metallic nanostructures could be changed from visible to near IR.

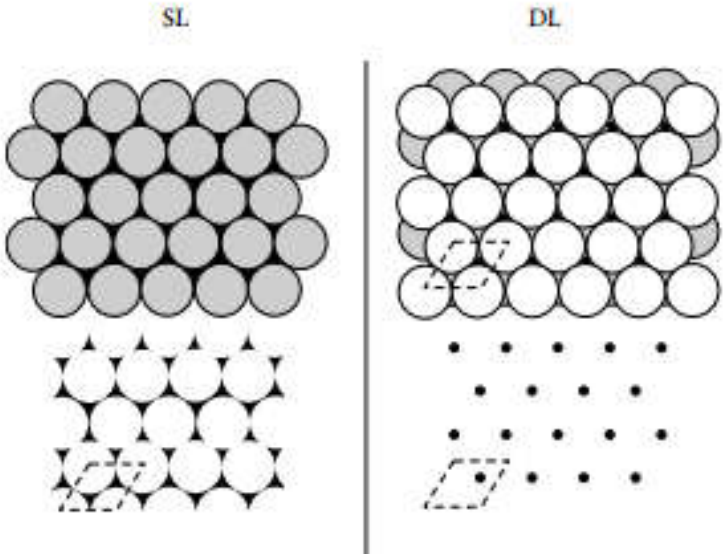

Figure 2.5. Schematic of single-layer (SL) and double-layer (DL) nanosphere mask.

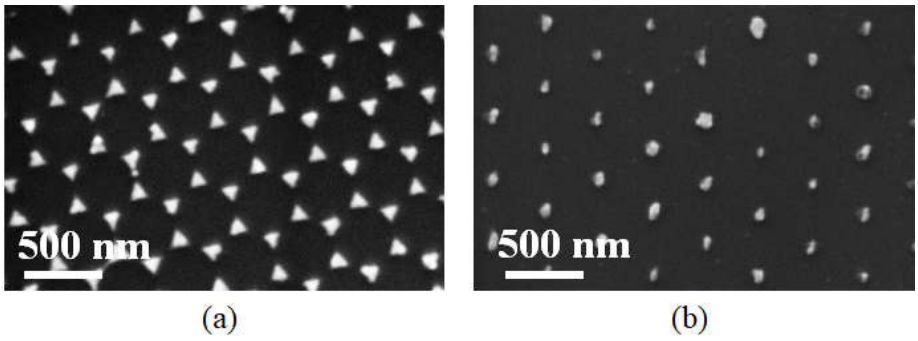

Figure 2.6. (a) SEM image of Ag triangular structures deposited through a single-layered colloidal mask. (b) SEM image of Ag nanodots deposited through a double-layered colloidal mask.

Another practical advantage of the NSL is the ultrahigh density magnetic recording which is low cost and high output [59]–[61]. Nanostructures can demonstrate better superparamagnetic behaviors if their feature sizes are reduced [18].

Some post-treatment strategies (e.g., heating (Figure 2.7) and etching (Figure 2.8)) have been developed to obtain different nanostructures through the NSL technique.

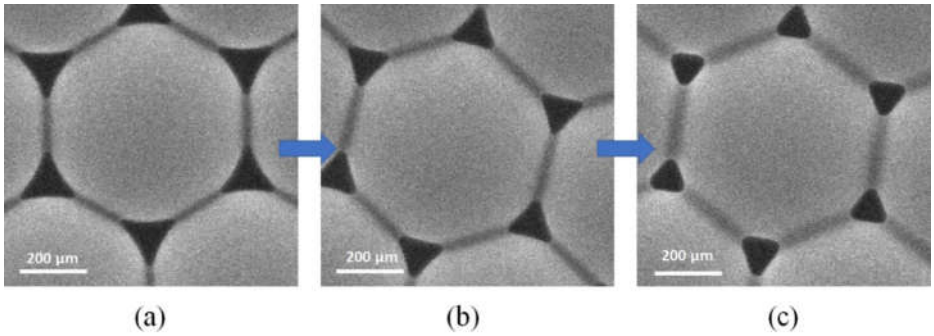

Figure 2.7. Sem graph of nanospheres at 105℃ after (a) 10 minutes annealing, (a) 20 minutes annealing, and (c) 30 minutes annealing.

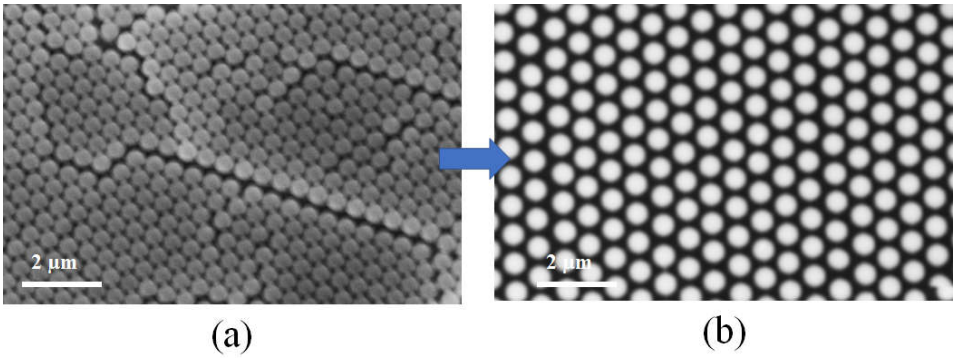

Figure 2.8. (a) Sem image of nanospheres with 350nm diameters, (b) nanospheres after oxygen plasma treatment with the aim of etching.

Another significant progress in this area was the employment of angle-resolved colloidal lithography [62].

2.4 Angle-resolved nanosphere lithography

In the above-mentioned designs, target materials are deposited at the nonzero incident angle with respect to the normal direction of the substrate. To implement novel designs using NSL, deposition is executed by changing the angle between the nanosphere mask and the beam of material being deposited, which is called angle-resolved NSL. The schematic of a motorized sample holder is demonstrated in Figure 2.9.

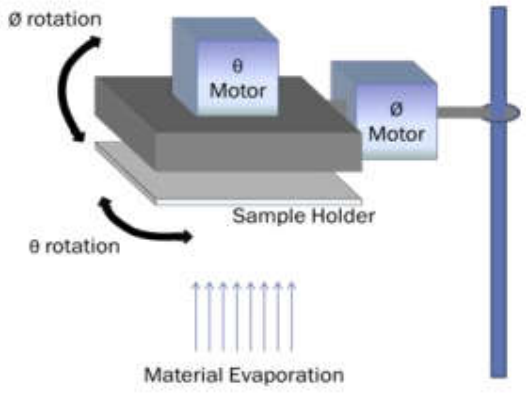

Figure 2.9. Schematic representation of motorized sample holder rotatable around two axes.

Tilted deposition technique has been employed in the fabrication of structures, like field-effect transistors, [63], [64] single-electron transistors [65],[66] tiny tunnel junctions, and optical coatings.

The size and shape of interstices between the nanosphere can be controlled by the angle of deposition. Figure 2.10 illustrates the impact of tilted evaporation on the interstices of the NSL mask from the top view. It is obvious that by increasing the angle of tilt, the projections of the interstices onto the substrate will be decreased.

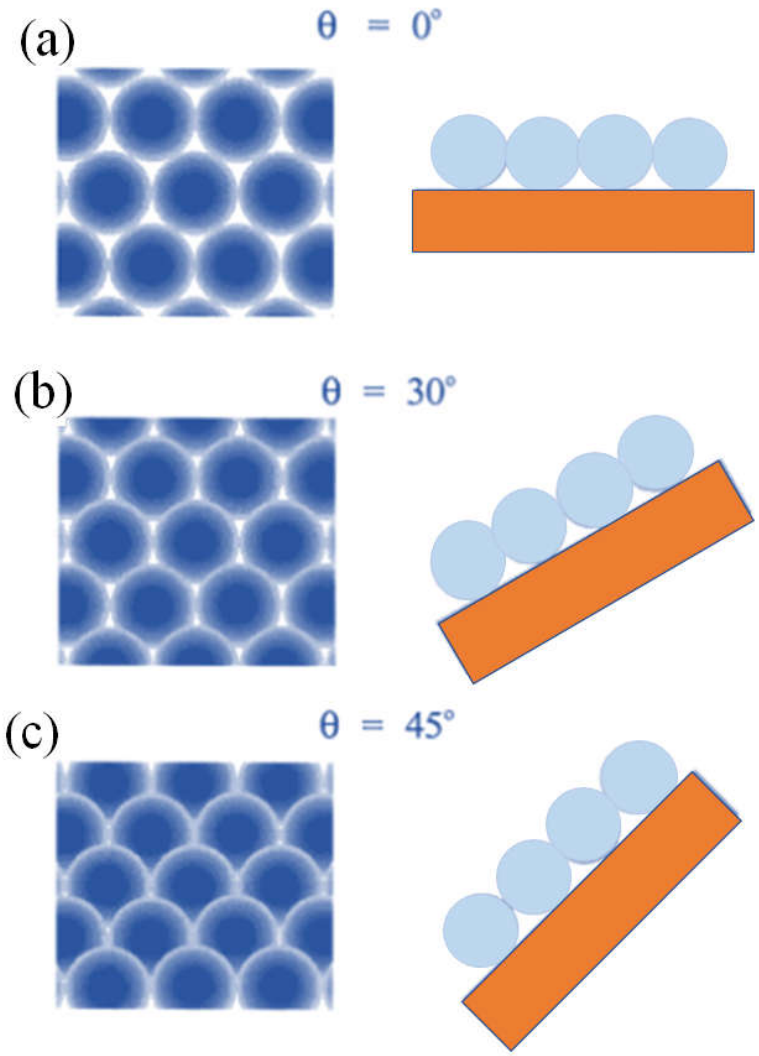

Figure 2.10. Schematic of the angle-resolved deposition process. (a) The deposition process is conducted at 0°. The size of spaces between nanospheres is the same. (b) Deposition at 30°. The space between nanospheres is smaller. (C) Deposition at 45°. The spaces between spheres are almost closed.

One of the advantages of tilted evaporation, apart from the variety of nanostructure architecture, roots in the reduction of nanosphere size. The requirement of nanostructures in the range of 1-20 nm size is because of the ever-increasing need of industries for smaller feature sizes of devices. Without the utilization of tilted evaporation, only if nanospheres with diameters on the order of 5-100 nm are employed can we obtain nanostructures with dimensions in the range of 1-20 nm size. The self-assembly of such small nanospheres is complicated as their solutions more polydisperse. Yet, with AR NSL, changing the deposition angle from 0° to 30° will reduce the in-plane dimension of nanostructures generated through both SL and DL masks by easing the self-assembly process.

Besides the variety of nanostructures with different shapes and sizes, the fabrication of other complex structures is possible using multiple deposition steps of a single target material, or multiple materials, through the same colloidal mask. By changing the deposition angle between two depositions, both nanooverlap and nanogap structures can be generated.

The diversity of nanostructures that can be produced with motorized holders through the hole mask lithography has been demonstrated in [67].

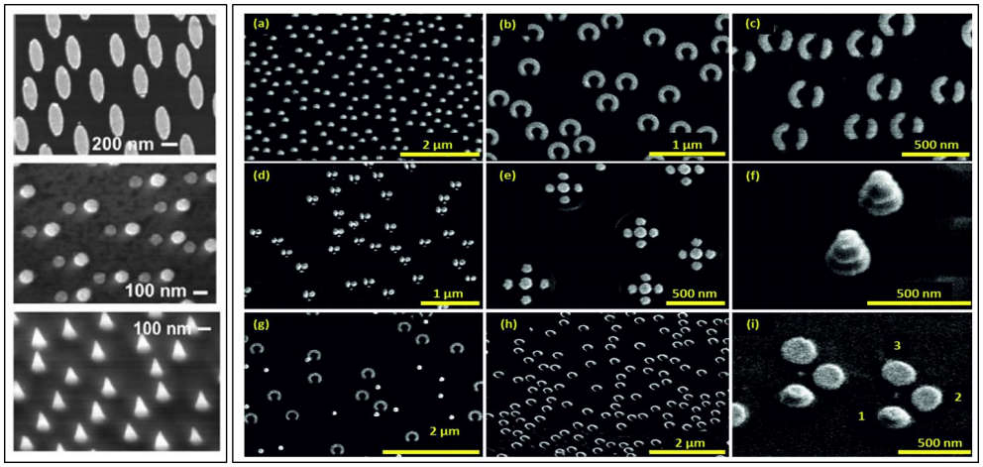

Figure 2.11. Left column: Various metal structures produced by fixed angle evaporation [68], Right column (a)-(i) Various nanostructures produced by tilted evaporation [69].

The nanostructures that are fabricated using the NSL method can be employed to enhance the plasmonic resonance on the Raman scattering effect. The effect of different geometries, such as nano cylinders, nanodiscs, and binary dimer structures produced by the NSL method, was examined on Raman enhancement [68].

2.5 Summary

In this chapter, the current lithographic techniques are studied to determine better and effective methods. Nanosphere lithography and its advantages and drawbacks are fully surveyed in this study. According to the results deducted from comparison results between various nano-patterning techniques, colloidal lithography is the most favorable tool to fabricate periodic structures.

Colloidal lithography is a decent method since it is a low-cost and large-area method. Silica and polystyrene spheres were utilized in this lithography because of their high performance in the self-assembly process.

In chapter 3, the self-assembled colloidal spheres are utilized to increase the efficiency of solar cells. Not only do the spheres reduce the reflection of photovoltaic devices, but they also concentrate light in the junction of cells which greatly increases their conversion efficiency.

In chapter 4, tilted evaporation through the colloidal sphered can be employed as an effective method to fabricate structures, which are useful for Surface Enhanced Raman Spectroscopy (SERS).

CHAPTER 3

NANOSPHERE CONCENTRATED PHOTOVOLTAICS WITH SHAPE CONTROL

3.1 Overview of light trapping methods in solar cells

Photovoltaic (PV) devices gain a considerable amount of attention to fulfill our future needs as a renewable energy source. Silicon is one of the desired candidates for PV applications due to its abundance, non-toxicity, and establishment in the semiconductor industry for large-scale production. However, there are still many struggles regarding the material and processing costs associated with traditional wafer-based designs. For instance, a significant amount of incident light is reflected due to the high refractive index of silicon, which causes a noticeable reduction in the conversion efficiency of solar cells [70].

There are different methods utilized to reduce surface reflectance and improve conversion efficiency. Light trapping methods such as surface texturing, antireflection coatings (ARCs), and optical absorption enhancement via scattering from metallic or dielectric nanoparticles are typical examples of such techniques [71]–[79]. Surface texture can increase the light trapping by utilization of secondary incidence of reflected photons. However, most techniques for texturing Si require the use of a dry or wet etching process, which can be costly, time-taking, high in the energy budget, and harmful to the environment.

Single- or multi-layered ARCs have simple, low-cost, and time-efficient fabrication processes. However, there are many limitations associated with the fabrication and performance of single- or multi-layered ARCs, such as poor adhesion, restricted working wavelength range, and limited working angle of the incident light. Furthermore, materials used for ARCs should be deposited carefully with precise refractive index and thickness control, which is quite challenging.

Alternative approaches in nanoscale light management in PV encompasses the

employment of a vast range of dielectric nanostructures, such as nanowires [80]–[85], nanoholes [86], photonic crystals [87], nanocones [88]–[90], and also metal nanostructures such as nanoparticle arrays [91]–[93], and nanogrooves [94]. However, most of these require multiple micro/nanofabrication steps, which are not readily up scalable to cope with ~km^2 surface areas covered by PV plants. Moreover, structuring of the c-Si active region or introducing additional Si/metal interfaces in many of these approaches give rise to massive internal losses due to increased surface recombination.

Metal or dielectric nanospheres can be employed as an antireflection coating to solve the drawbacks mentioned above. Metal nanoparticles, which are integrated into the surface of Si solar cells (SCs), can avoid the detrimental effects on the electrical properties at the semiconductor surface [75]. They also offer plasmonic effects and efficient radial charge-carrier collection. Furthermore, metal nanoparticles can scatter the incident light into a large span of angles, which helps increase the path length of the light inside the absorbing layer [95], [96].

However, depending on their material type, size, and shape, metal nanoparticles may have some downsides, such as a significant amount of back-reflection and large ohmic (absorptive) losses, which suppress the plasmon resonances. Besides, there are aging problems associated with metal nanoparticles in which oxidation or sulphurization of their surface detriment their optical properties in time. These drawbacks limit the applicability of metal nanoparticles as light management interfaces for SCs in comparison to dielectric nanospheres (NSs) [97].

Light management using sub-wavelength dielectric NSs has become of interest in a wide range of PV platforms, such as amorphous silicon (a-Si) thin-film SCs [98]–[101], GaAs thin film SCs [102], perovskite SCs [103], ultrathin Si/graphene SCs [104], and c-Si thin-film SCs [79]. Polystyrene (PS) NSs are one of the predominantly used dielectric NSs which can be employed in diverse applications such as antireflection coatings or micro-lens arrays in SC structures since they are scalable and low-cost [28], [105]–[108]. PS NS arrays can be coated onto large-area solar cells with a diverse nanosphere lithography technique [25], [56], [109], [110].

Naturally occurring hexagonal close-packed (hcp) arrays of NSs behave as an intermediate layer with the proper graded refractive index, which is between air and Si refractive indices. The graded refractive index facilitates the slow transition from air to Si and consequently enables light efficiently transmitting across the interface. Therefore, there is no need to use additional materials with graded refractive indices. Besides, light is scattered after passing through NS arrays, which increases the effective optical thickness of devices and light absorption through the conversion of light propagation angles from transverse to in-plane. External quantum efficiency (EQE), cell efficiency measurements, and simulation results can demonstrate the enhancement in the absorption over the solar spectrum.

An additional privilege of using PS NSs is that they can operate as optical micro-lens arrays, which concentrate the sunlight onto small regions of SC at which the radiation density can exceed typical AM 1.5 conditions where the Si SCs are more efficient [111]. A topic referred to as concentrated PV (CPV). In this approach, an apparent decrease in the required solar cell area offers an opportunity to lower the material cost as high semiconductor material costs can be substituted with low-priced mirrors or lenses.

Novel strategies and materials can be inspected to achieve a reasonable cost range in CPV devices. Standard techniques for producing micro-lens arrays have some limitations. For instance, prevalent lens materials (i.e., glass) are usually heavy, costly, and hard to manufacture. Therefore, PS NS micro-lens arrays that require a low-cost and simple spin coating process can offer a reasonable replacement.

In addition, by tuning the NS shape from that of an ideal sphere to nearly a hemispherical oblate shape can increase the amount of focused light inside the cell. Therefore, it is essential to understand the dependence of SC performance on the shape of the nanospheres.

In that respect, here we report the dependence of large-area Si SC performance characteristics on shape modification of NSs using a simple and fast annealing method, which is the main novelty of our work.

3.2 The fabrication process of solar cells coated with nanospheres

Si SCs are n^+/p junction devices, which are fabricated from p-type monocrystalline Czochralski silicon (Cz-Si) with the resistivity of 1-10 ohm.cm with saw-damage-etched front side and textured backside. We purposefully keep the front side flat so that the photon management is solely performed by NSs and not by texture. The front surface side is plasma enhanced chemical vapor deposition (PECVD) coated with silicon nitride (SiNx) for protection before KOH based texturing was applied to generate standard pyramidal texture on the backside. In the following step, $POCl_3$ diffusion in a quartz doping furnace was applied to generate the n^+ doped emitter region.

The Si surfaces were passivated together by a dry oxidation process followed by PECVD deposition of a thin SiNx layer. The oxide (~5 nm) and SiNx (~6 nm) layers are specially chosen to be thin in order to enable good passivation but not to demonstrate any ARC effect themselves so that the photonic effects of dielectric nanospheres are of the essence. To demonstrate the light concentration effect of nanospheres, 80 nm SiN_x thickness, which is generally used in standard crystalline solar cells, is reduced to 6 nm. The reason for this is that a full 80 nm SiN_x coating is not reasonable to keep since it displaces the NSs from the cell significantly, hampering the light concentration effect. Furthermore, demonstration of effective index behavior of the small-sized NSs would also not be possible. In the final step, the H-shaped silver (Ag) grid is screen printed on the front surface while the rear side is fully covered by screen-printed aluminum (Al). Activation of the screen-printed metal layers is provided by the co-firing step using an industrial conveyor belt furnace.

The surfaces of Si solar cells are made hydrophilic by the utilization of an oxygen plasma device. Then an aqueous suspension of colloidal PS NSs was spin-coated on the SCs. An hcp PS monolayer was generated by self-organization after at least 24 hours of drying. The PS NSs which are utilized in these sets of experiments are dispersed in water, and they are functionalized with hydroxyl group. The hydroxyl

polar head group (–OH) is anchored to the Si surface. After the adhesion of nanospheres to the silicon, they can only be removed either completely by dissolving in acetone or partially by ultrasonic treatment if they are not thermally treated. However, once they are thermally treated, even ultrasonication was found not to be sufficient to remove them from the surface. The PS NS monolayer was uniform on the surface of the device. Modification of the NS shapes is performed by annealing. NS coated SCs are annealed on a hotplate at a temperature of 110℃ for 10 min, 20 min, and 30 min. By annealing nanospheres at 105-110 °C, we can attain changes in the shape of nanospheres within practical processing durations in a controllable manner that enable better light concentration effect and improved efficiency. There is a narrow temperature margin of about 20 °C between which the results of treatment are completely different (100-120 °C). After extensive shape optimization studies on nanospheres, we have found that at ≥120 °C, nanospheres can be completely molten, from which experimentally determined glass transition temperature (T_g) of PS NSs is ~110 °C which agrees with the literature[112]. The heat treatment induces the spherical shapes of the NSs to modify into oblate spheroids, which leads to improvement in light focusing, in the sense that the foci of such formed micro-lens arrays shift more into the device, better overlapping with the junction region and hence introducing improved efficiency. A perfect sphere, on the contrary, generates a premature focus close to the top surface and with severe chromatic aberration.

In our premises, we have conducted studies on the temperature rise of the Si cells on a clear summer day previously. The temperature of cells was found to reach as high as ~60 °C [113], which is well below the minimum temperature at which nanosphere shapes start to change (>~105 °C) at reasonable process durations. From our extensive optimization studies, we determined that temperatures up to 95 °C are found to show no detectable influence on the nanosphere's shape/size regardless of the duration of temperature treatment. Thus, we can safely conclude that the nanospheres on the surface of solar cells are expected to hold their shape/size even on a clear summer day.

Two different dielectric nanosphere types are used during experiments. Silica NSs

with diameters of 880 nm are spin-coated on the surface of SC. However, as shape modification is not possible in Silica NSs, detailed experiments are conducted on PS NSs, which can be shape-modified by the annealing process. The diameters of PS NS employed here are 350 nm, 500 nm, 750 nm, and 4.75 µm. The layout of fabrication is illustrated in Figure 3.1.

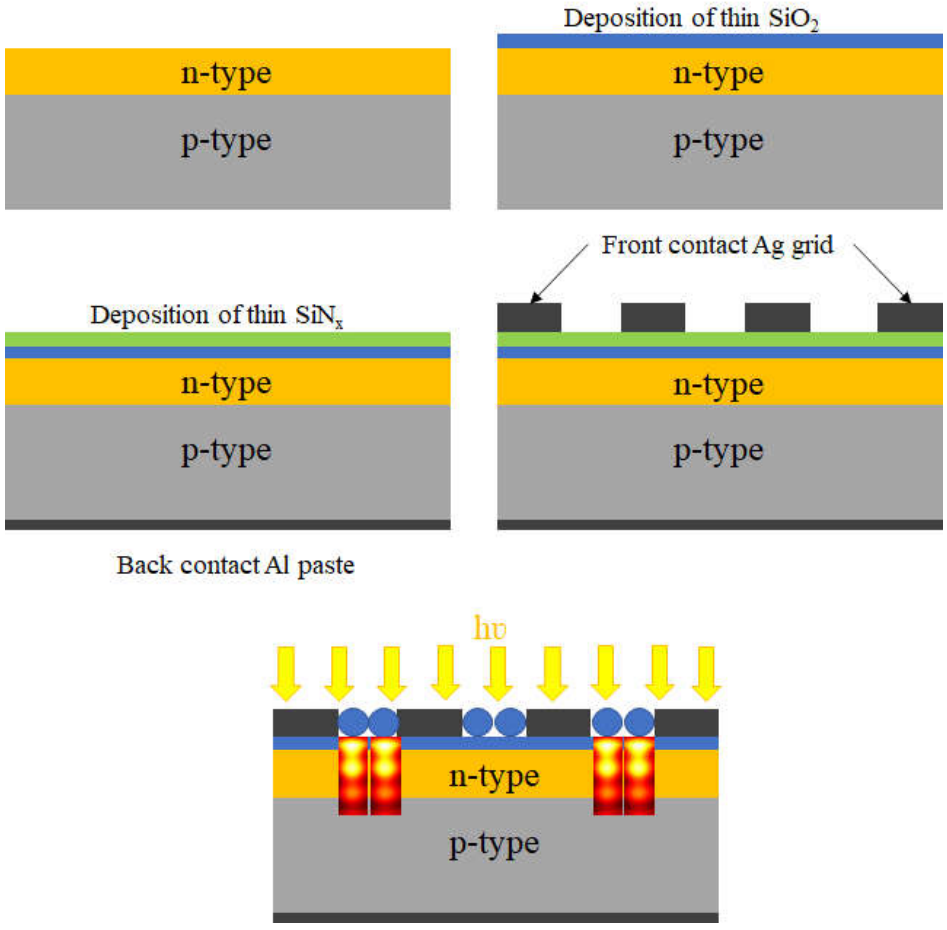

Figure 3.1. Cross-section schematics of a c-Si solar cell decorated with NS.

3.3 Solar cells deposited with Silica nanospheres

3.3.1 Simulation results of solar cells with Silica nanospheres

Maxwell solutions are carried out numerically using the finite elements method (FEM) for 880 nm silica (SiO_2) NS decorated in Figure 3.2. The wavelength of the incident light is adjusted to 600nm.

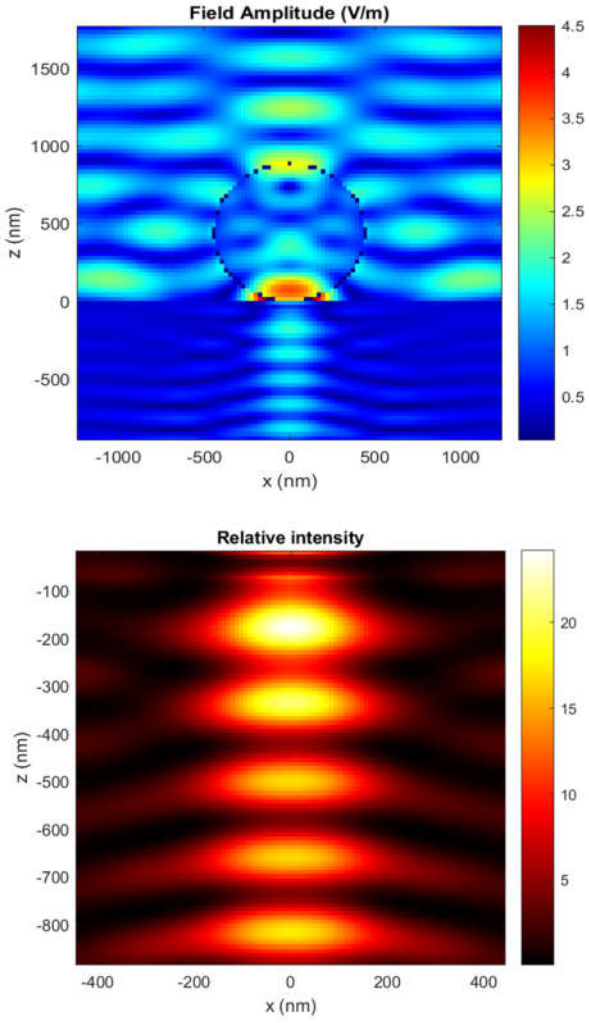

Figure 3.2. Maxwell simulation of Silica nanosphere with 880nm diameter.

3.3.2 Experimental results of solar cells with Silica nanospheres

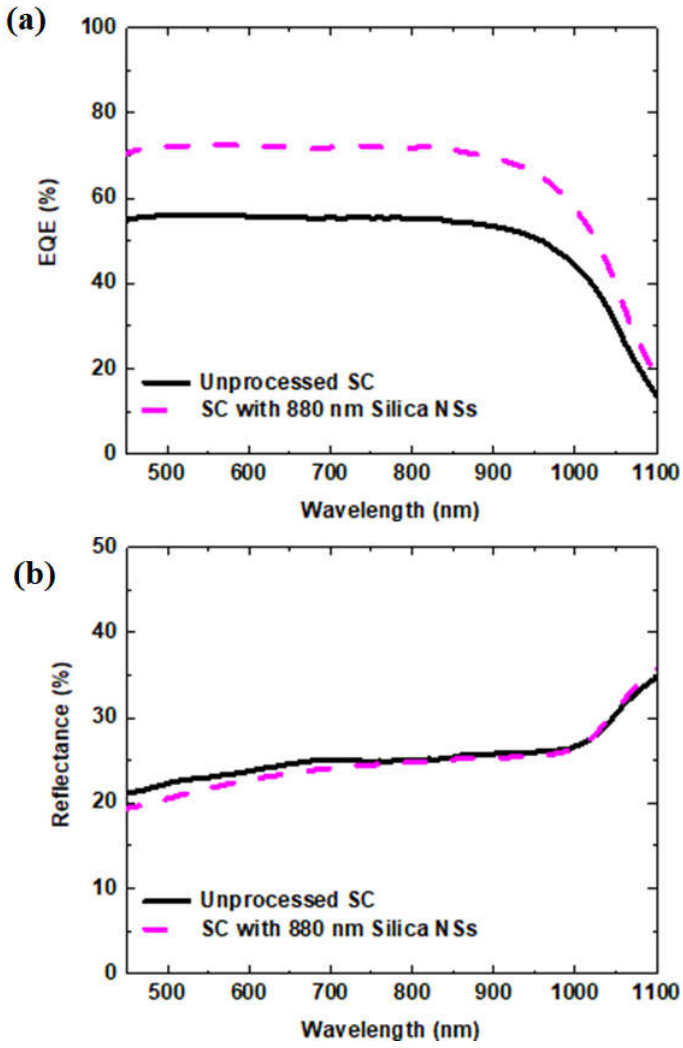

Figure 3.3. Experimentally determined curves for Silica NSs (a) EQE, (b) Reflectance.

The experimental results in Figure 3.3 show that there is a significant improvement of 12 % in external quantum efficiency of solar cells with silica nanospheres of 880 nm. The reflectance is reduced only about an absolute 1% by 880 nm NSs in as

deposited form. For a more direct representation of the effect, experimentally obtained J-V curves are illustrated in Figure 3.4.

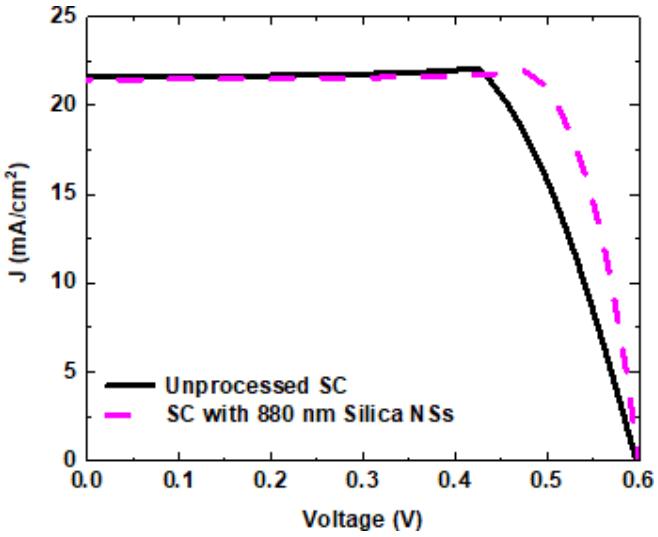

Figure 3.4. J-V measurements of SC with 880 nm Silica NSs.

Table 3.1 J_{sc} and efficiency of SC with Silica NSs

	J_{sc}	*% Increase in* J_{sc}	η	*% Increase in* η
Unprocessed SC	22.07	----	9.3	----
SC with 880 nm SiO_2 NS	27.11	22.83	10.02	7.74

Table 3.1 summarizes the measured improvement of Jsc for SCs with Silica NSs, and efficiency. So, there is an increase in the photocurrent, which demonstrates enhanced absorption in the active layer due to the nanospheres' light concentration effect. As the annealing process is not feasible for Silica NSs, shape modification cannot be applied to such NSs. Therefore we plan to extend our studies in the field of PS NSs, which enable us to reach further improvement in the efficiencies due to

better light trapping effect thanks to the shape modification of NSs.

3.4 Solar cells deposited with polystyrene nanospheres

The electromagnetic simulations are performed using a finite elements method (FEM) Maxwell's equations solver, COMSOL [114], to calculate the distribution of electric fields across the boundaries of Si SCs, which can explain the light-harvesting effect of shape-controlled NSs and the absorption behavior of the devices. In these simulations, all the boundaries of the calculation box *(4000 nm x 4000 nm x-y)* were furbished with a perfectly matched layer (PML) boundary conditions (BCs).

The reflectance of bare and NS coated SC surface, and the effect of shape-modified NSs on reflectance is calculated using the finite-difference time-domain (FDTD) method. Polarization-dependent simulations are carried out using an FDTD Maxwell solver, Lumerical [115], and were conducted between 0 to 30 degrees due to the symmetry of the hcp configuration. In all simulations, wavelength-dependent refractive indices and extinction coefficients of PS NSs and Si (dispersion effects) are taken into account [116]. In the FDTD simulation, a calculation box with dimensions of *(4000 nm x 4000 nm x 1000 nm x-y-z)* has been implemented with PS NSs in hcp configuration on the surface. Along with the x and y directions, BCs are chosen to be periodic and symmetric. Boundaries along the z-direction are furbished with PML BCs in order to avoid the reflection of electromagnetic waves from the box boundaries.

Extensive simulations are conducted to choose the optimum size limit of PS NSs, which is provided in Figure 3.5.

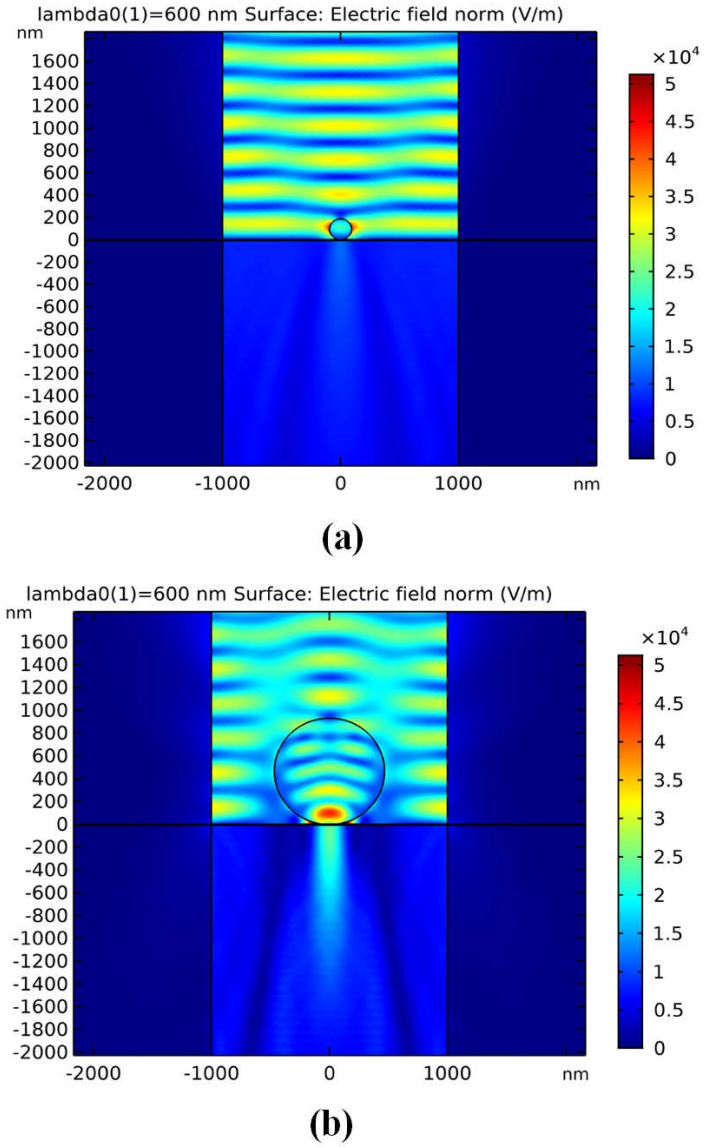

Figure 3.5. 2D cross-sectional E-field distribution at 600 nm wavelength calculated by the FEM (COMSOL) with PS NSs on Si SC: (a) as deposited 200 nm perfect sphere, (b) as deposited 1 µm perfect sphere.

According to Figure 3.5, NSs with sizes of 200 nm demonstrate a negligible amount of e-field inside the solar cell, and for NSs with sizes larger than 1 µm, the considerable amount of E-field resides inside the NS above the Si surface. Therefore,

the NSs which are chosen here are between the range of 200 nm-1 μm. So, the diameters of PS NS employed here are 350 nm, 500 nm, 750 nm. However, to investigate the response of large microspheres, the effect of NSs with the size of 4.75 μm is also examined in this study.

The layout of Si SCs with colloidal PS NSs is sketched in Figure 3.6.a, and a top-view SEM image of the SC surface is shown in Figure 3.6.b. The low-magnification SEM image is demonstrated in Figure 3.6.c proves the uniform distribution of PS NS arrays. It can be seen that a single layer of PS NSs is self-organized uniformly in hcp configuration on the surface of the SC, where the diameters of the PS NSs are confirmed to be ~350 nm, ~500 nm, and ~750 nm with good mono-dispersity. 350 nm and 750 nm NSs are shown in Figure 3.6 for comparison. Figure 3.6 d,f,h illustrate the annealing effect on the shape of 350 nm NSs after 10, 20, and 30 min at 110℃, which manifests itself in reduction of the gap size between hcp NSs. Figure 3.6 e,g,i show tilted side-view SEM images of 750 nm NSs at increasing annealing times.

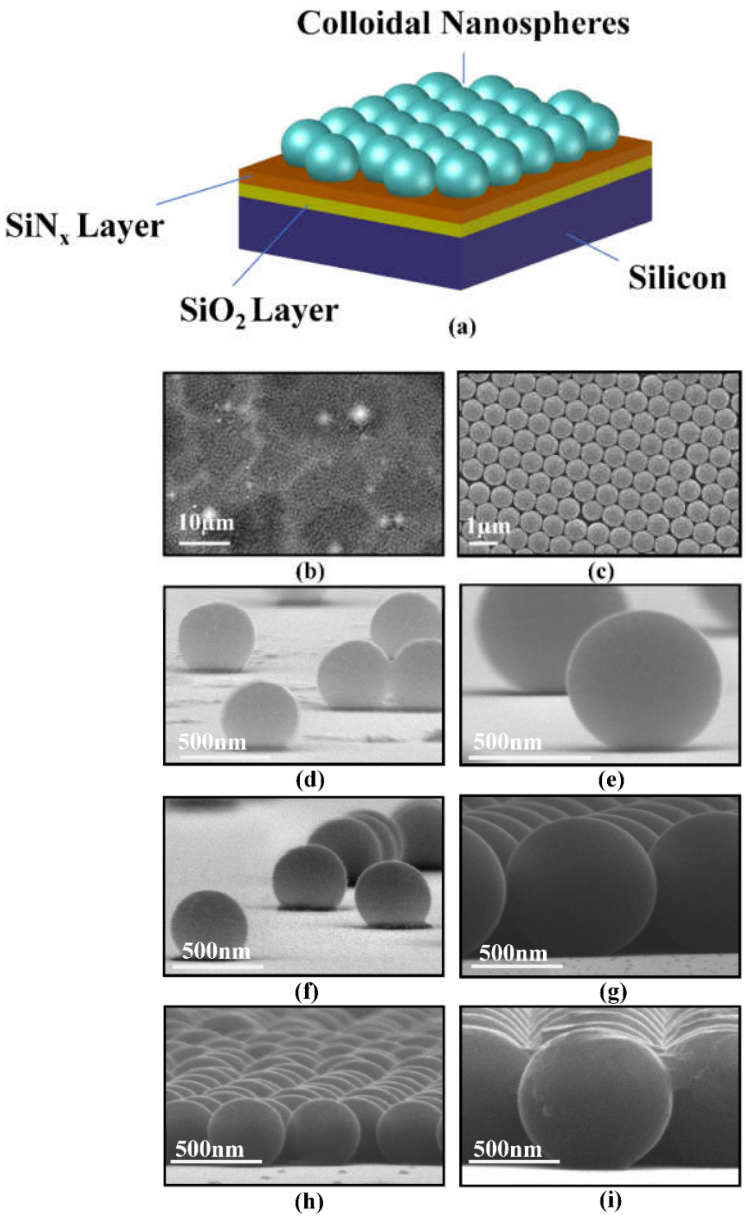

Figure 3.6. (a) The layout of the Si SC with colloidal PS NSs. (b) Low-magnification top view of large-area hcp colloidal PS NSs on a Si SC. (c) High-magnification top view of 750 nm colloidal PS NSs on Si SC (d), (f) and (h) Side-view of 350 nm colloidal PS NSs on a Si SC after 10, 20, and 30 min of annealing, respectively. (e), (g), and (i) Side-view of 750 nm colloidal PS NSs on Si SC after 10, 20, and 30 min of annealing, respectively.

Careful measurements of the spheroid dimensions are performed on close-up, side-view SEM images for detection of the differences between spheroid shapes meticulously, and simulations are carried out based on the shape data extracted from SEM images, which are illustrated in Figure 3.7 and Figure 3.8.

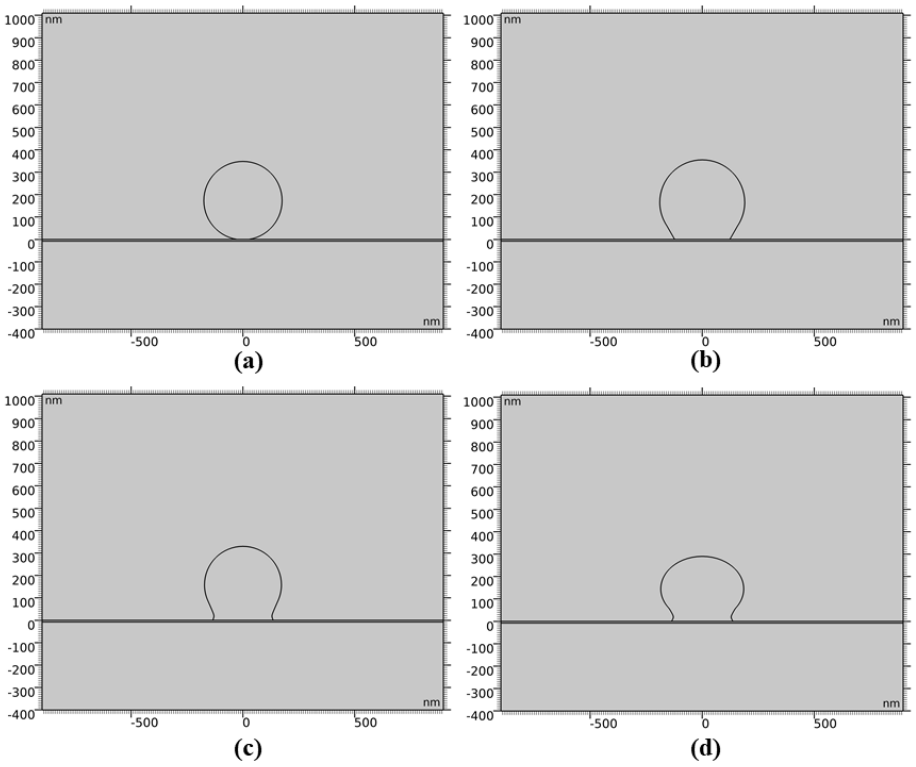

Figure 3.7. Dimensions extracted from SEM images for Si SC with 350 nm NSs: (a) as deposited perfect sphere, (b) after 10 min, (c) after 20 min, (d) after 30 min annealing.

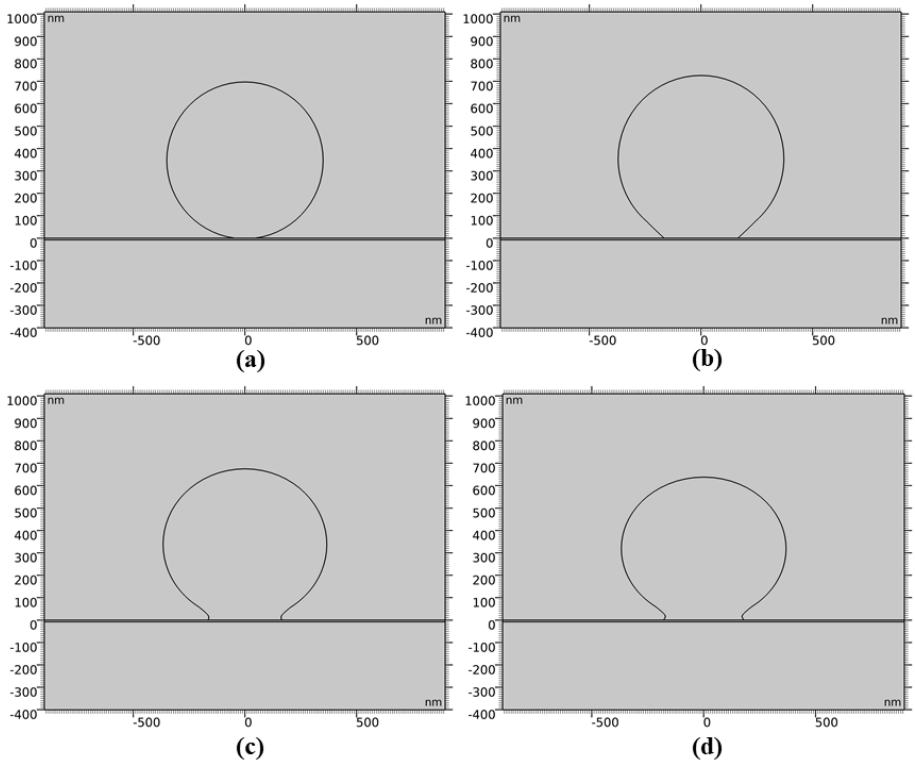

Figure 3.8. Dimensions extracted from SEM images for Si SC with 750 nm NSs: (a) as deposited perfect sphere, (b) after 10 min, (c) after 20 min, (d) after 30 min annealing.

3.4.1 Simulations and experimental results supporting the light trapping (anti-reflective) effect

We have conducted electromagnetic simulations on reflectance from SCs with and without PS NSs at various incidence polarization angles only for 350 nm and 750 nm NSs since 500 nm NSs were experimentally found to produce an average photonic activity monotonously lying between the two. Figure 3.9a shows that 750 nm NSs are effective as a broadband ARC coating, whereas 350 nm NSs do perform best in the 500 – 800 nm wavelength range, which is because of light forward scattering. Figure 3.9b and Figure 3.9c demonstrates that the ARC effect for both

350 and 750 nm NSs show little dependence on polarization, with 350 nm NSs demonstrating better ARC activity at polarization angles greater than 15° and 750 nm NSs virtually showing no significant dependence on polarization.

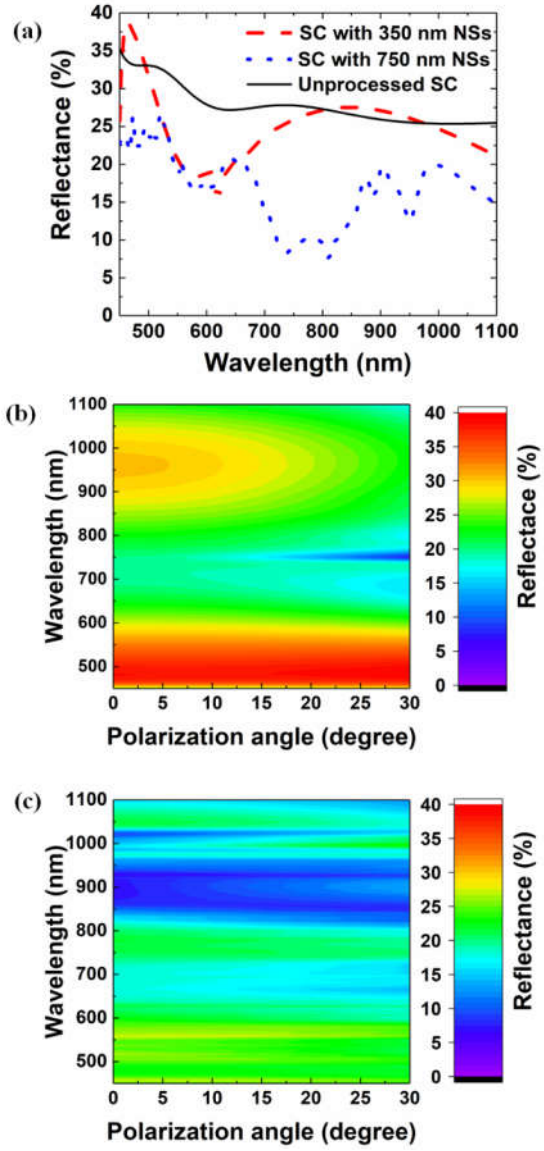

Figure 3.9. (a) Simulated reflectance for unprocessed SC and with 350 nm and 750 nm colloidal PS NS coating. Simulated reflectance spectra versus polarization angle with (b) 350 nm and (c) 750 nm PS NSs.

In order to have an understanding of the overall effect of the NSs, we have calculated weighted total reflectance as a function of the polarization angle, which is shown in Figure 3.10 for SCs with the two NS sizes before and after annealing. Small NSs with 350 nm diameter act as an effective index medium, exhibiting a thin-film interference pattern in the reflectance spectrum (Figure 3.9a). Their light concentration (micro-lens focusing) effect is negligible as compared to their effective index property. However, the light concentration effect takes the lead for NSs with a larger diameter (750 nm), and the effective index effect is reduced.

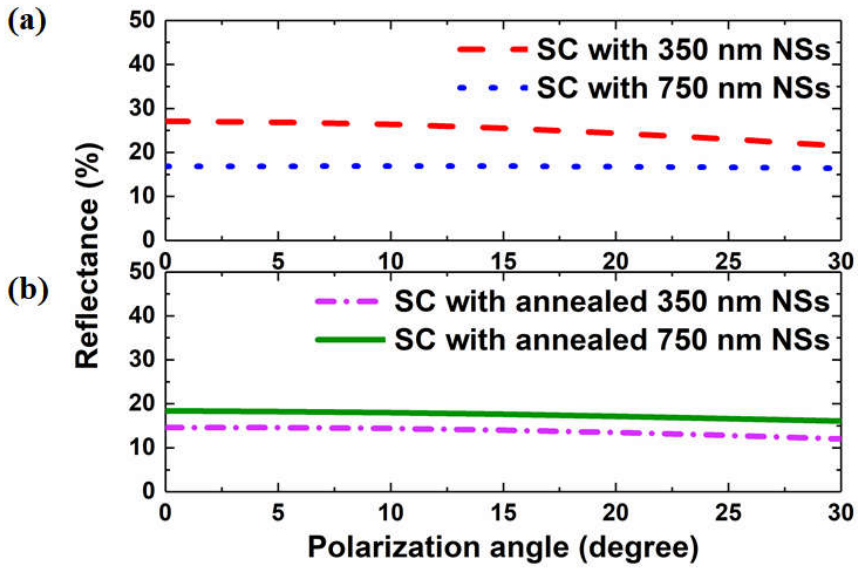

Figure 3.10. (a) Simulated weighted total reflectance (over 450-1100 nm wavelength range) as a function of polarization angle for SCs with PS NSs. (b) Same with annealed NSs.

Figure 3.10 shows that shape control plays a crucial role in improving the graded-index behavior for all polarizations. The weighted reflectance of solar cells with NSs can be reduced significantly (>5%) by shape modification through an annealing method for NSs of a significantly smaller size than the wavelength (350 nm). The change in the reflectance for larger particles (750 nm) does show a similar reduction

effect, albeit to a lesser extent (~1%). Polarization-dependent simulations are performed between 0 to 30 degrees due to the symmetry of the hcp configuration.
The experimental results in Figure 3.11 show that there is a significant improvement in the external quantum efficiency of solar cells with shape-controlled nanospheres of 350 nm. The reflectance is reduced only about an absolute 1% by 350 nm NSs in as deposited form, which increases up to a reduction of absolute ~10% over the entire spectrum with shape control.

Mie resonances emerge at various wavelengths depending on NS size. These peaks are in great consistency with reflection and EQE spectra in solar cell. Nanospheres with the size of 350 nm indicate a forward scattering property at resonant wavelengths.
Once the nanospheres with a diameter of 350 nm are placed on top of Si SC, a significant amount of backward scattering can be happened due to the mismatch of refractive indices existing at the air/Si interface. Especially, the backward scattering takes the lead compared to the forward scattering at wavelengths above 550 nm.

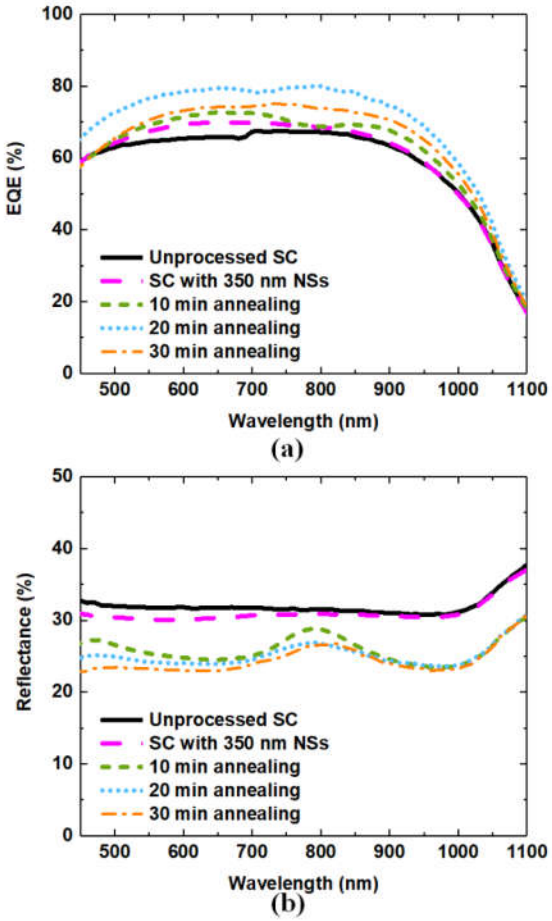

Figure 3.11. (a) Experimentally determined EQE curves for shape-controlled NSs of 350 nm, (b) Experimentally determined reflectance curves for shape-controlled NSs of 350 nm.

Figure 3.12 shows that the reflectance is reduced about an absolute 5-10% by 500 nm NSs in as deposited form, which increases up to a reduction of absolute ~15% over the entire spectrum with shape control.

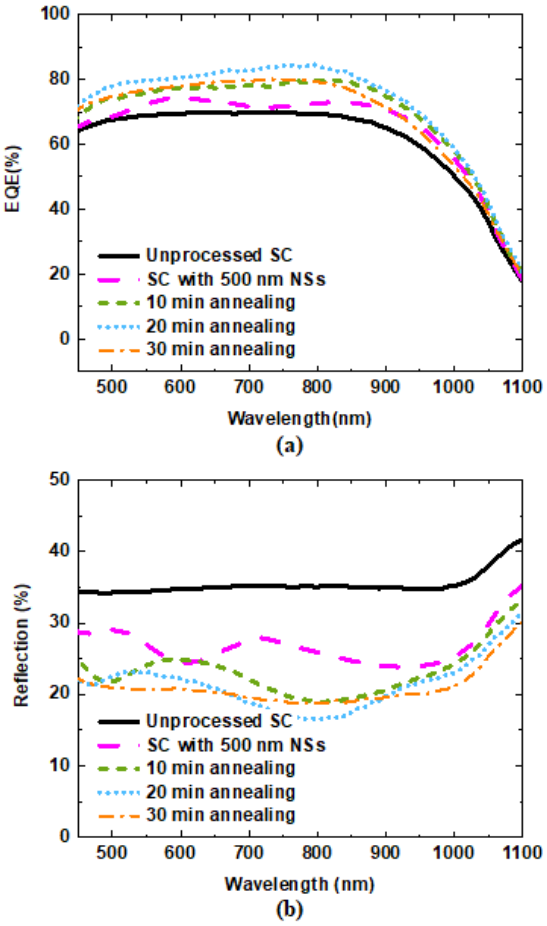

Figure 3.12. (a) Experimentally determined EQE curves for shape-controlled NSs of 500 nm, (b) Experimentally determined reflectance curves for shape-controlled NSs of 500 nm.

The effect is similar in 750 nm spheres but to a greater extent. The reflectance reduces already by about absolute 5-10% in as deposited form, which increases to about 10-15% absolute reduction with shape control. It is obvious that a significantly improved anti-reflective effect of NSs is possible through shape control, as shown in Figure 3.13.

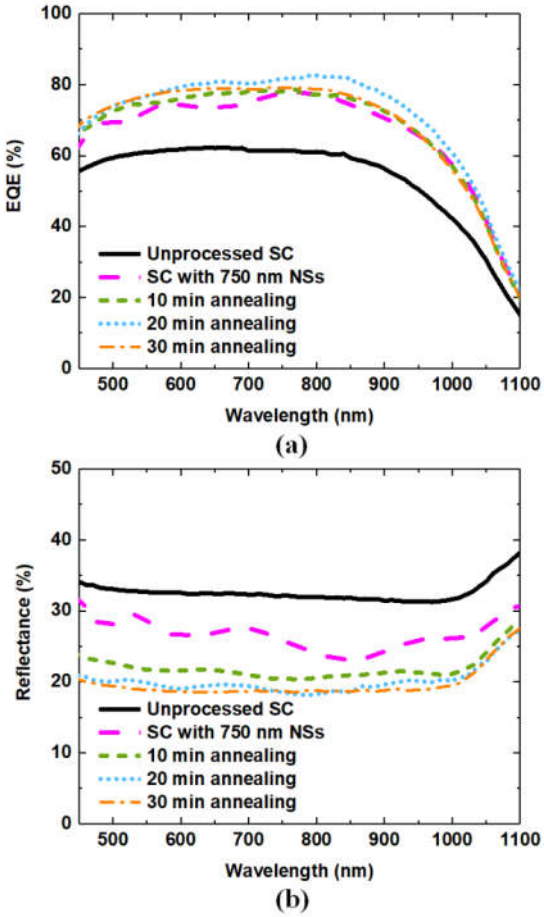

Figure 3.13. (a) Experimentally determined EQE curves for shape-controlled NSs of 750 nm, (b) Experimentally determined reflectance curves for shape-controlled NSs of 750 nm.

The reflectance of SC with 4.75 µm reduces already by about absolute 5-10% in as deposited form, which increases to about 15% absolute reduction with shape control. It is obvious that a significantly improved anti-reflective effect of NSs is possible through shape control, as shown in Figure 3.14.

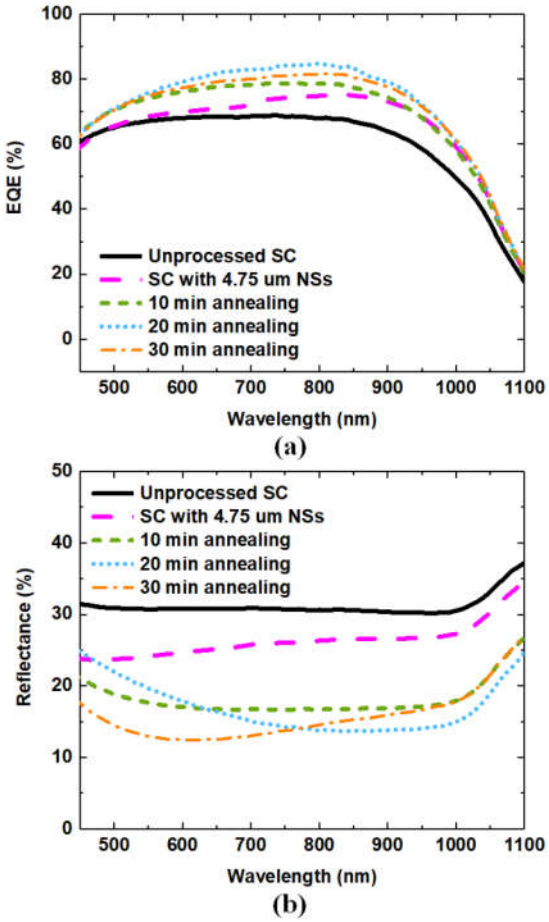

Figure 3.14. (a) Experimentally determined EQE curves for shape-controlled NSs of 4.75 μm, (b) Experimentally determined reflectance curves for shape-controlled NSs of 4.75 μm.

Figure 3.15 displays the experimentally determined effect of annealing time on EQE and reflectance. At an annealing temperature of 110°C, the ideal annealing time to achieve minimum reflectance and maximum EQE is found to be around 20 minutes.

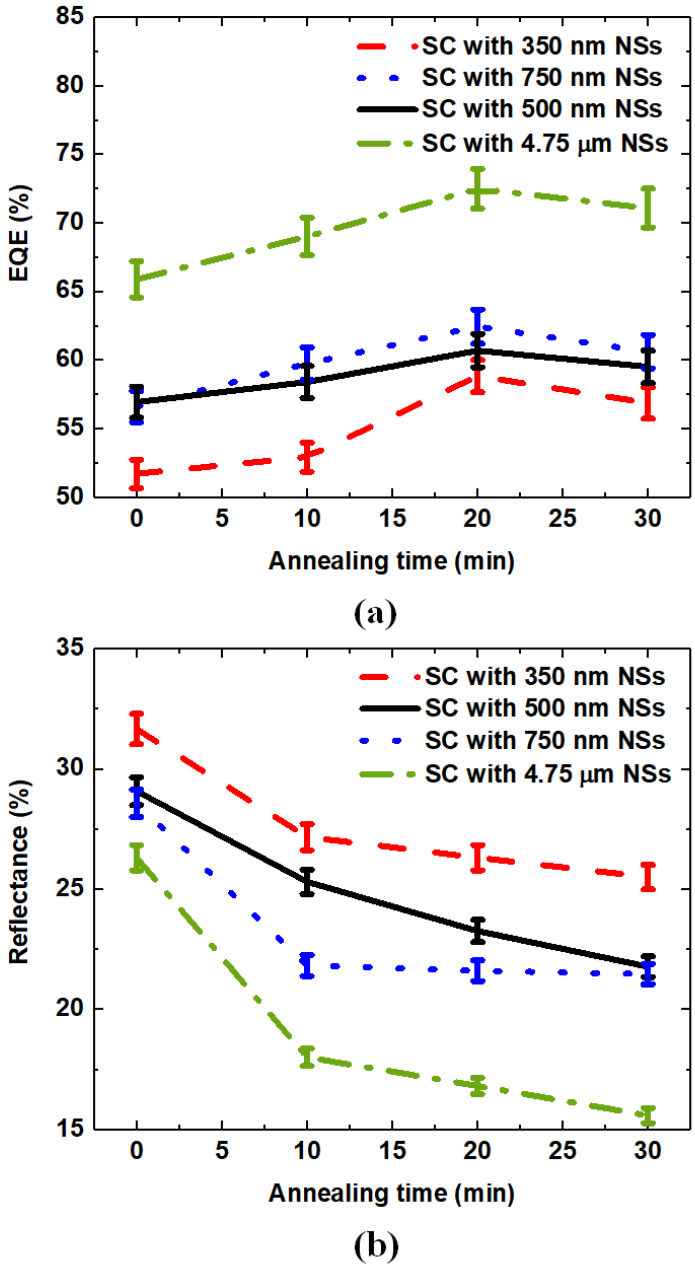

Figure 3.15. Experimentally determined weighted total EQE (over 450-1100 nm wavelength range) as a function of annealing time for NSs of 350, 500,750 nm , and 4.75 μm size, (b) weighted total reflectance for NSs of 350, 750 nm , and 4.75 μm size.

3.4.2 Simulations and experimental results supporting the light concentration effect

In order to demonstrate efficient control of the light concentration effect of NSs through shape control, E-field distribution profiles along the x-z plane are calculated at various wavelengths using the FEM algorithm (COMSOL). Figure 3.16 and Figure 3.17 show time-averaged E-field amplitudes calculated at 600 nm wavelength for the as deposited spherical 350 nm and 750 nm NS on the SC as well as for its three different shape modified versions. In order to conduct the simulations, the shapes of the NSs are determined from high magnification SEM images. Thereby, dimensions and oblate spheroid shapes attained through annealing processes are transferred to the simulations precisely as possibly representing the experimentally obtained shapes.

The main reason why annealing can improve the light concentration is the contact surface. The behavior of NSs is strongly dependent on the nature contact surface between the surface and solar cell.

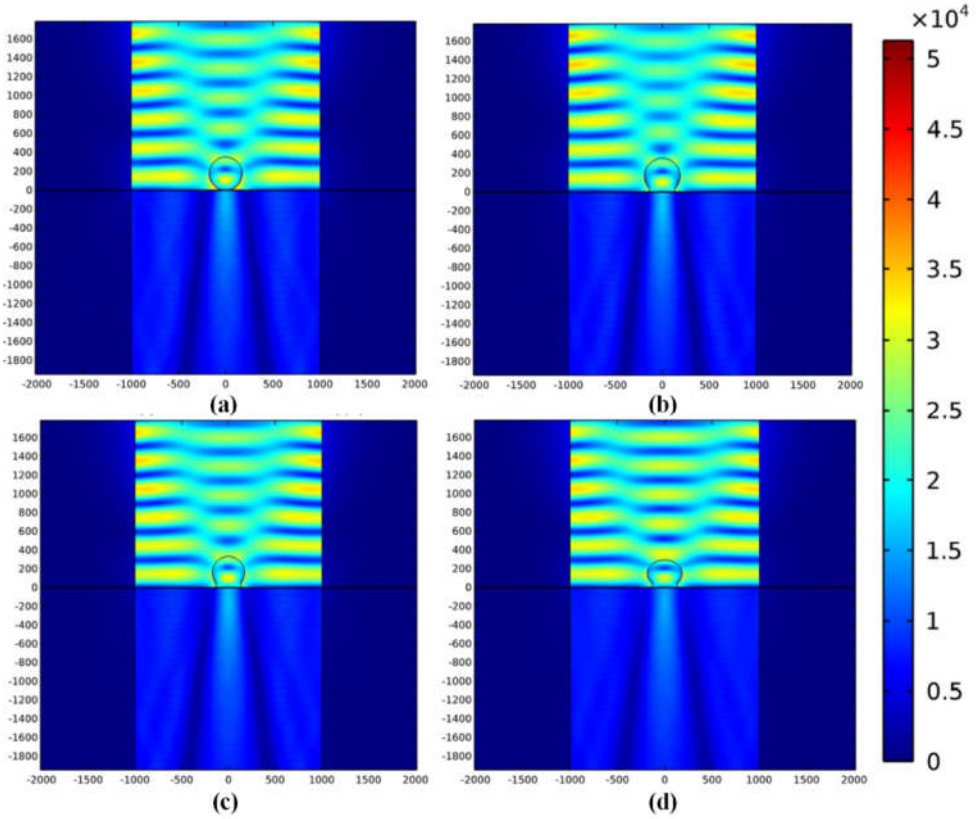

Figure 3.16. 2D cross-sectional E-field distribution at 600 nm wavelength calculated by the FEM (COMSOL) with 350 nm NS on Si SC: (a) as deposited perfect sphere, (b) after 10 min, (c) after 20 min, (d) after 30 min annealing. Box dimensions 4000 nm x 4000 nm x-y. Arbitrary unit linear color map.

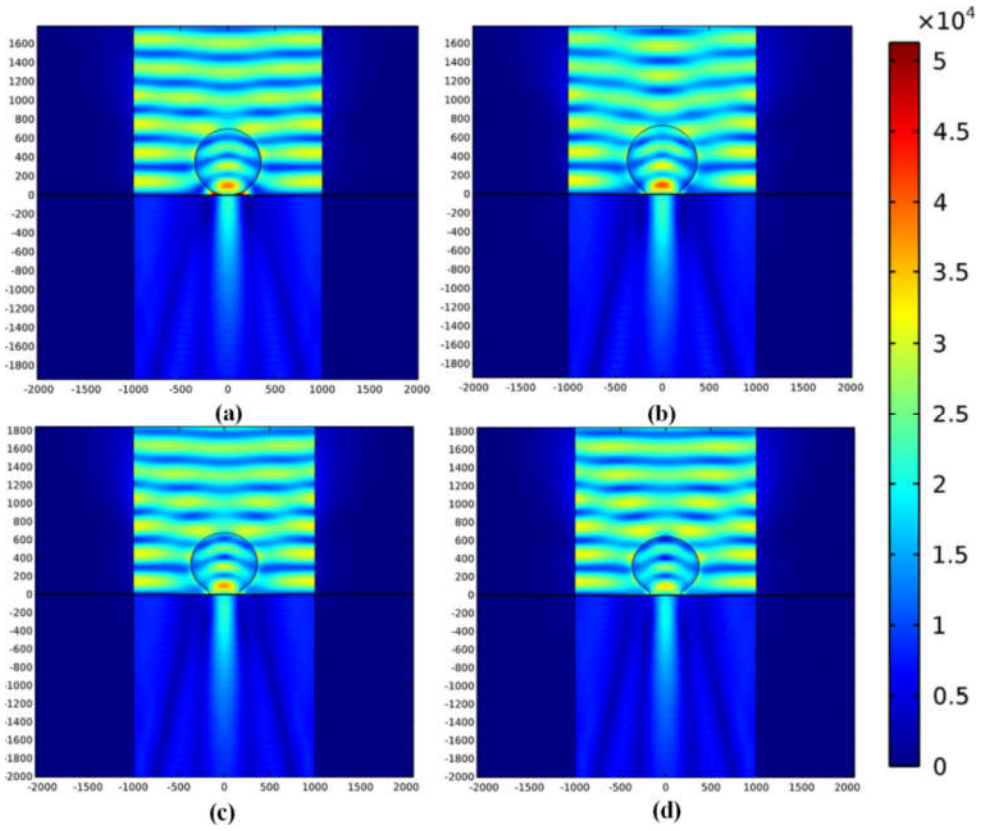

Figure 3.17. 2D cross-sectional E-field distribution at 600 nm wavelength calculated by the FEM (COMSOL) with 750 nm NS on Si SC: (a) as deposited perfect sphere, (b) after 10 min, (c) after 20 min, (d) after 30 min annealing. Box dimensions 4000 nm x 4000 nm x-y. Arbitrary unit linear color map.

As it is not easy to discern the subtle-at-first-sight differences between the cases in the overall look given in Figure 3.16, and Figure 3.17, we have decided to conduct our more detailed analysis close to the junction region. In order to understand the effect of light concentration, cross-section averaged E-field intensities are calculated over a 200 nm thick region surrounding the junction plane at 400 nm below the surface in all cases. The average field intensities are given as a function of wavelength in Figure 3.18 for both 350 and 750 nm NSs. In order to have a sensible comparison between E-field profiles and experimental measurement of efficiencies,

the mean E-field intensity of each configuration is multiplied with the solar simulator spectrum, utilized in experimental I-V measurements.

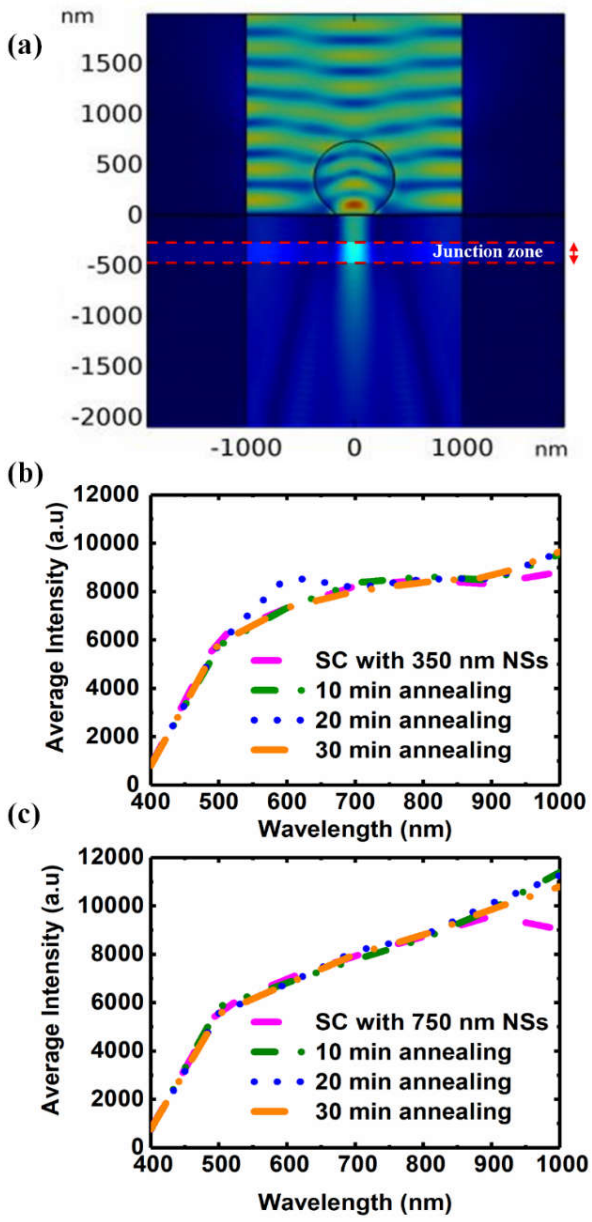

Figure 3.18. (a) 2D cross-sectional E-field distribution at 600 nm wavelength calculated by the FEM method (COMSOL) for 10 minutes of annealing. Box dimensions 4000 nm x 4000 nm x-y. Same color map as in Fig. 6. The junction zone

is highlighted where the averaging is performed for parts b and c. Calculated average intensity for different time-controlled shapes for (b) 350 nm NSs, (c) 750 nm NSs.

The resulting spectrally weighted average intensities are plotted against annealing time, as shown in Figure 3.19. The result shows that the optimal light concentration effect is expected from NSs annealed for 20 minutes, which agrees very well with the experimentally determined conclusion of Figure 3.15.

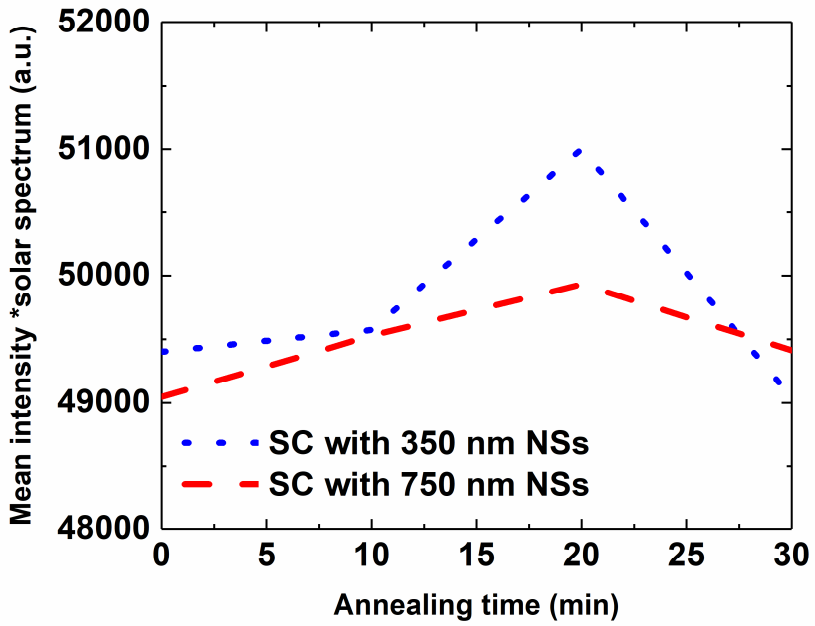

Figure 3.19. Simulated AM 1.5 solar spectrum weighted mean spectral intensity for 350 nm (blue dotted line) and 750 nm (red dashed line) NSs.

For a more direct representation of the effect, experimentally obtained I-V curves are illustrated in Figure 3.20 for 350, Figure 3.21 for 500 nm NSs, Figure 3.22 for 750nm, and Figure 3.23 for 4.75 µm NSs. Here we see again that the annealing time of 20 minutes optimized the light concentration effect. Namely, at the particular spheroid shape and size attained by 20 minutes of annealing time, the light focus is

aligned to overlap best with the junction.

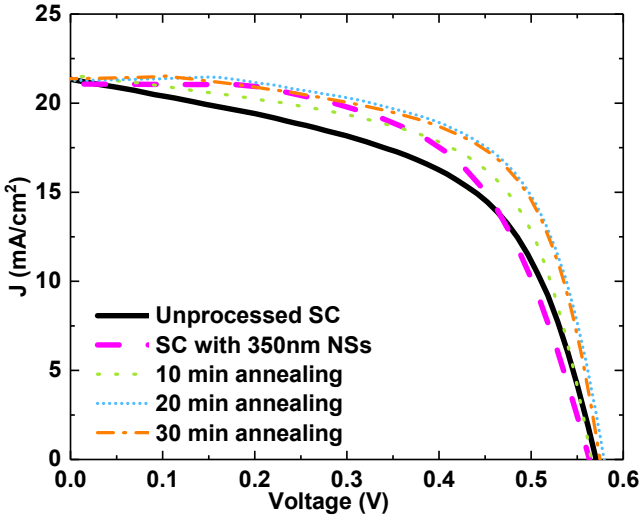

Figure 3.20. J-V measurements of SCs with 350 nm NSs at different annealing times.

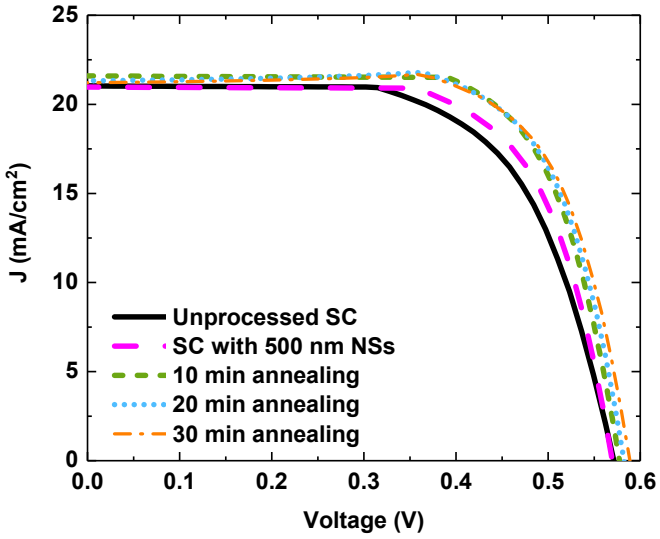

Figure 3.21. J-V measurements of SCs with 500 nm NSs at different annealing times.

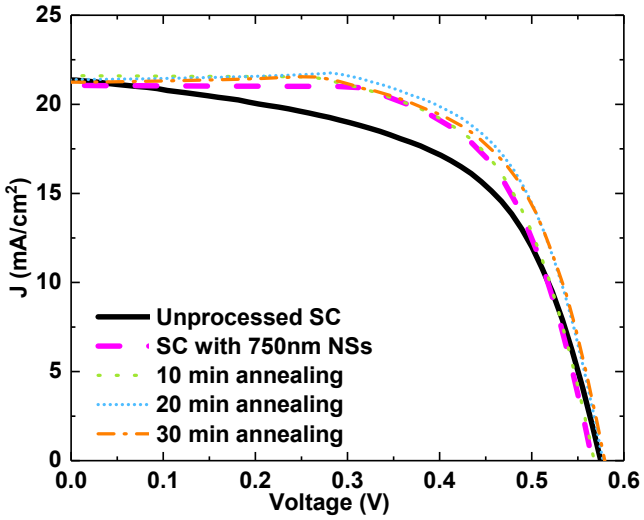

Figure 3.22. J-V measurements of SCs with 750 nm NSs at different annealing times.

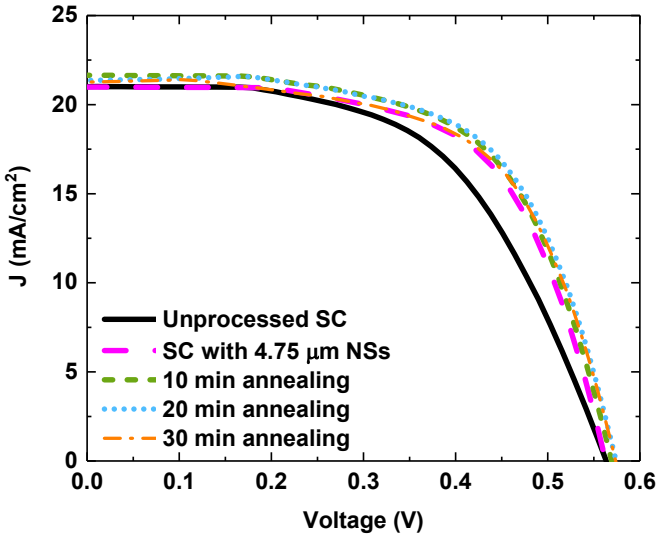

Figure 3.23. J-V measurements of SCs with 4.75 μm NSs at different annealing times.

We observe a similar improvement trend for both the efficiency and the fill factor (FF) in hcp NS covered SCs as shown in Figure 3.24, both of which agree with the simulation results of spectrally weighted average intensities given in Figure 3.19.

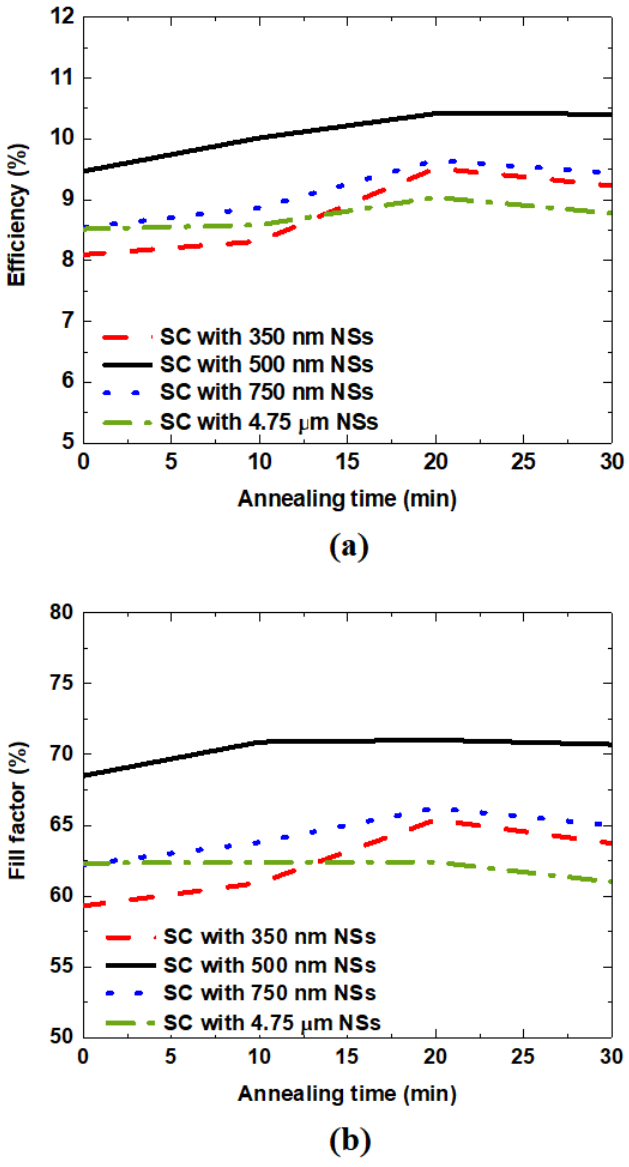

Figure 3.24. Experimentally determined (a) photoconversion efficiencies (b) FFs for SCs with different NSs versus annealing time.

Table 3.2 summarizes the measured improvement of conversion efficiencies and fill factors for SCs with NSs and shape-controlled NSs. By employing a shape control mechanism, conversion efficiencies can be enhanced by >27% as compared to pristine NS light management and by >8% as compared to unprocessed SC.

Table 3.2 Efficiency and fill factor of shape-controlled NS SCs

Sample	*FF*	*% increase in FF*	*η*	*% increase in η*
Unprocessed SC	55.1	-	7.5	-
350 nm NSs	59.3	7.7	8.1	8.6
SC with 350 nm NSs after 20 min annealing	65.4	18.8	9.5	27.6
Unprocessed SC	64.37	-	8.90	-
500 nm NSs	68.50	6.41	9.47	6.4
SC with 500 nm NSs after 20 min annealing	71.02	10.33	10.42	17.07
Unprocessed SC	57.7	-	7.9	-
750 nm NSs	62.2	7.9	8.6	8.1
SC with 750 nm NSs after 20 min annealing	66.2	14.8	9.7	22.0
Unprocessed SC	55.81	-	7.60	-
4.75 μm NSs	62.33	11.68	8.52	12.10
SC with 4.75 μm NSs after 20 min annealing	62.40	11.80	9.04	18.94

Since the used NSs are polymeric insulators, the corresponding cell FF values could not be directly related to NSs. The resulting improvement in FF values is probably because of the extra annealing step. Considering the current-voltage curve given in Figure 3.20, the cells with NSs already have some series resistance problems right after the solar cell fabrication. Observed poor FF values are basically due to the saw damage removed the shiny front and lack of SiNx with a proper thickness, both of which would reduce FF in turn. Any thermal treatment is expected to improve the adhesion of the screen-printed high-temperature Ag-paste, which will improve corresponding FF values at the cell level. Although FF is found to improve by thermal processing of the cells, the observed improvement of cell efficiencies is due to the improved photoconversion efficiency due to improved photon management of the cells.

Table 3.3 summarizes the measured improvement of Jsc for SCs with 350 nm NSs and shape-controlled NSs. So, there is an increase in the photocurrent, which demonstrates enhanced absorption in the active layer due to the nanospheres' light concentration effect. Therefore, it can be concluded that enhanced photovoltaic performance is not merely because of improved fill factor but mainly because of improved absorption.

Table 3.3 Jsc of shape-controlled 350 nm NS SCs

	Jsc	*% increase in Jsc*	*± %2*
Unprocessed SC	25,68	----	0.5136
SC with 350 nm NSs	26,57	3,4	0.5314
SC with 350 nm NSs after 10 min annealing	27,39	6,65	0.5478
SC with 350 nm NSs after 20 min annealing	30,41	18,41	0.6082
SC with 350 nm NSs after 30 min annealing	29,04	13,08	0.5808

Table 3.4 summarizes the measured improvement of Jsc for SCs with 500 nm NSs and shape-controlled NSs.

Table 3.4 Jsc of shape-controlled 500 nm NS SCs

	Jsc	*% increase in Jsc*	*± %2*
Unprocessed SC	26,93	----	0.5386
SC with 500 nm NSs	28,37	5,34	0.5674
SC with 500 nm NSs after 10 min annealing	30,61	13,66	0.6122
SC with 500 nm NSs after 20 min annealing	31,55	17,15	0.631
SC with 500 nm NSs after 30 min annealing	30,35	12,69	0.607

Table 3.5 summarizes the measured improvement of Jsc for SCs with 750 nm NSs and shape-controlled NSs

Table 3.5 Jsc of shape-controlled 750 nm NS SCs

	Jsc	*% increase in Jsc*	*± %2*
Unprocessed SC	23,50	----	0.47
SC with 750 nm NSs	29	23,4	0.58
SC with 750 nm NSs after 10 min annealing	30.41	29.40	0.6082
SC with 750 nm NSs after 20 min annealing	31,55	34.25	0.631
SC with 750 nm NSs after 30 min annealing	31,16	32.59	0.6232

Table 3.6 summarizes the measured improvement of Jsc for SCs with 4.75 μm NSs and shape-controlled NSs

Table 3.6 Jsc of shape-controlled 4.75 µm NS SCs

	Jsc	*% increase in Jsc*	*± %2*
Unprocessed SC	23,35	----	0.467
SC with 4.75 µm NSs	26,58	13,83	0.5316
SC with 4.75 µm NSs after 10 min annealing	30.61	31,09	0.6122
SC with 4.75 µm NSs after 20 min annealing	30,82	31.99	0.6164
SC with 4.75 µm NSs after 30 min annealing	30,14	29.07	0.6028

Figure 3.25a and Figure 3.26a show polarization-dependent E-field amplitude depth profile at a wavelength of 600 nm within the Si SC calculated below the NS with 350 nm and 750 nm PS NSs, respectively. Figure 3.25b and Figure 3.26b show the same calculations conducted for the shape-controlled PS NSs. It is evident that with shape control, the light concentration effect is enhanced for both NS sizes. Moreover, it can be observed that shape control does enable less polarization dependence and more omnidirectional activity. The extent of the omnidirectional polarization improvement in 750 nm NSs is far better than that of 350 nm with expressing virtually no dependence. The E-field intensity is found to be stronger for shape-controlled 750 nm NSs over a larger SC depth range, which indicates a better performance in light concentration than that of 350 nm NSs taking the long electron diffusion length in Si into account. Moreover, these results are found to be in good agreement with the experimental results of Figure 3.15.

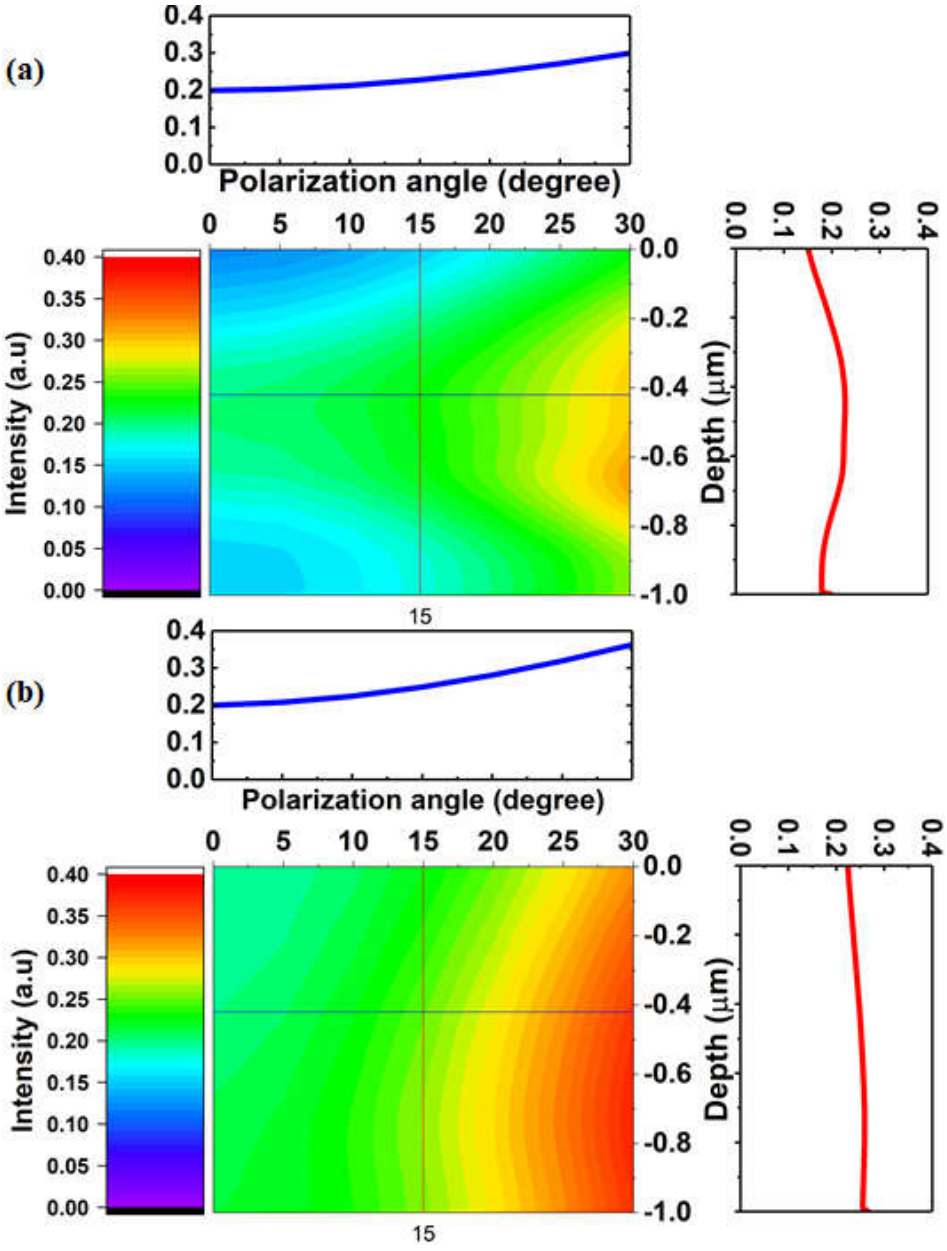

Figure 3.25. Simulated depth profile of E-field intensity versus polarization angle with (a) as deposited 350 nm PS NSs and (b) 20 min annealed PS NSs. The horizontal line marks the approximate location of the junction, where the E-field amplitude profile is shown above the 2D plot. The vertical line marks 15-degree polarization where the depth profile to the right of the 2D plot is shown.

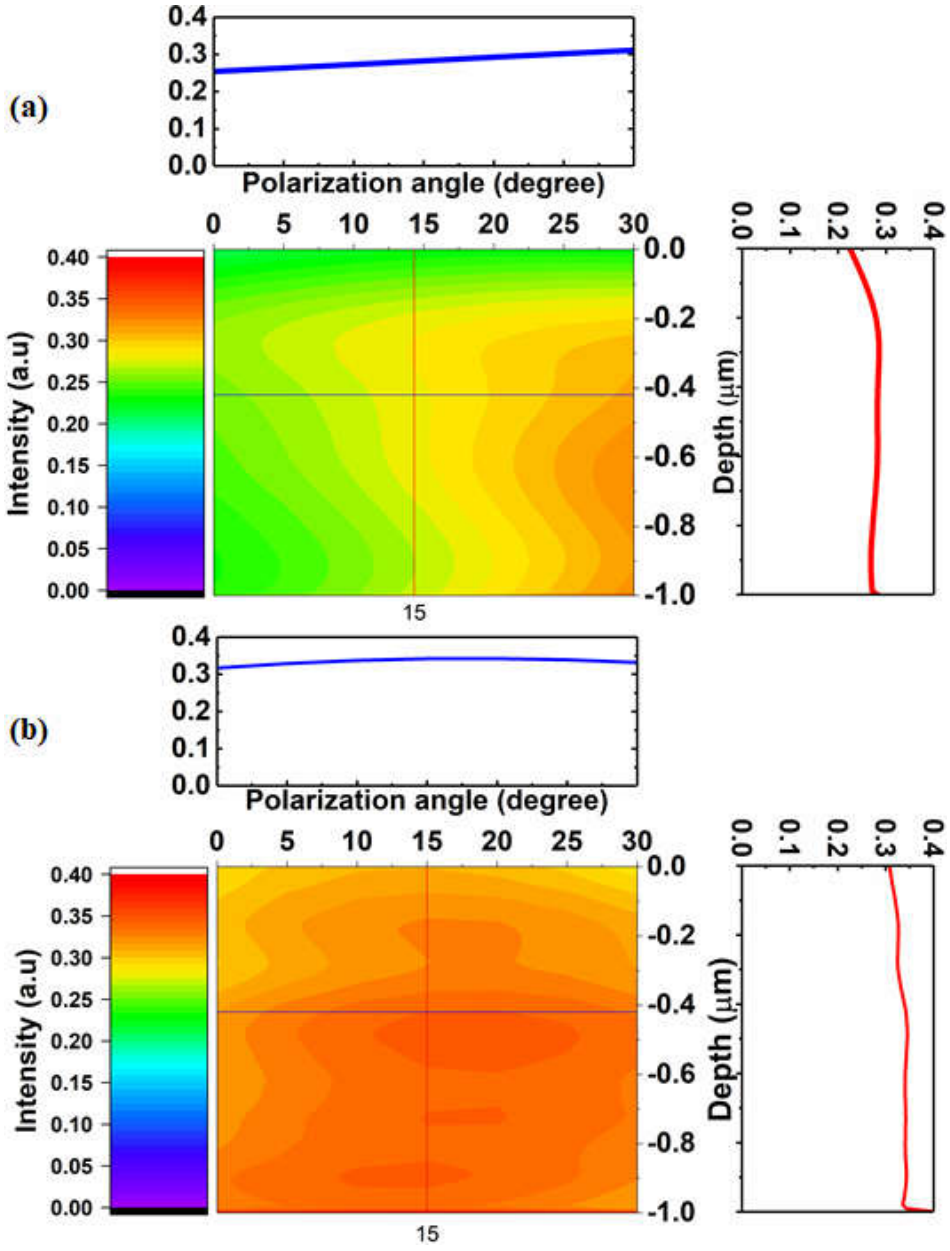

Figure 3.26. Simulated depth profile of E-field intensity versus polarization angle with (a) as deposited 750 nm PS NSs and (b) 20 min annealed PS NSs. The horizontal line marks the approximate location of the junction, where the E-field amplitude profile is shown above the 2D plot. The vertical line marks 15-degree polarization where the depth profile to the right of the 2D plot is shown.

3.5 Conclusion

In conclusion, a single layer of hcp PS NS arrays with 350 nm, 500 nm, 750 nm, and 4.75 μm in diameter demonstrate anti-reflective and light concentration properties for single-crystalline Si SCs, which are significantly improved by low-cost, rapid, and uncomplicated annealing-based NS shape control. There is a reduction of absolute 1% in reflectance for Si SCs with 350 nm NSs, which improves to an impressive absolute ~10% over the entire spectrum with shape control. For Si SCs with 750 nm NSs, the reflectance is already reduced by about an absolute 5-10%, which reaches a striking absolute of ~10-15% with shape control. It is evident that the anti-reflective properties of NSs can be intensified through shape control.

Furthermore, the shape-controlled PS NSs lead to a better light concentration effect, which results in further improvements in conversion efficiency by a factor of 27% for SCs with shape-controlled 350 nm NSs and by a factor of 22% for SCs with shape-controlled 750 nm NSs. The novel idea of the shape-modification method for improved light management through NSs introduces an easily applicable and feasible way to achieve high-efficiency solar cells and has the potential for utilization in light management of many other kinds of photonic devices.

Annealing of PS NSs improves efficiency by improving photon management of cells through shape control which influences the photonic effects. There are two different photonic mechanisms through which the annealing of NSs helps in improving efficiency. One is the effective index effect in which small NSs such as those of 350 nm size act as an anti-reflective coating (ARC). By annealing NSs as the shape of the NSs change, the average thickness and the volume fraction of PS versus air in the NS layer changes, and hence the photonic action of the PS decoration gets modified. When nanospheres are in a complete sphere shape, there are air gaps between the contact surface of Si and PS NSs. Meanwhile, annealing nanospheres leads to a better contact surface of spheres to Si, which leads to the removal of air gaps between NSs and Si. So, the light refracted through polystyrene to Si instead of air to Si substrate. Moreover, a large contact area between particles and substrate

facilitates preferential scattering of light into the high-index substrate [117] and keeping the light trapped within the substrate due to enhanced contact surface. Figure 3.27. The effective index of refraction versus height for (a) as deposited NSs on Si, (b) annealed NSs demonstrates a modification of the effective index in spherical and annealed NSs. As $\Delta n_B < \Delta n_A$ reflectance is expected to drop for annealed NSs.

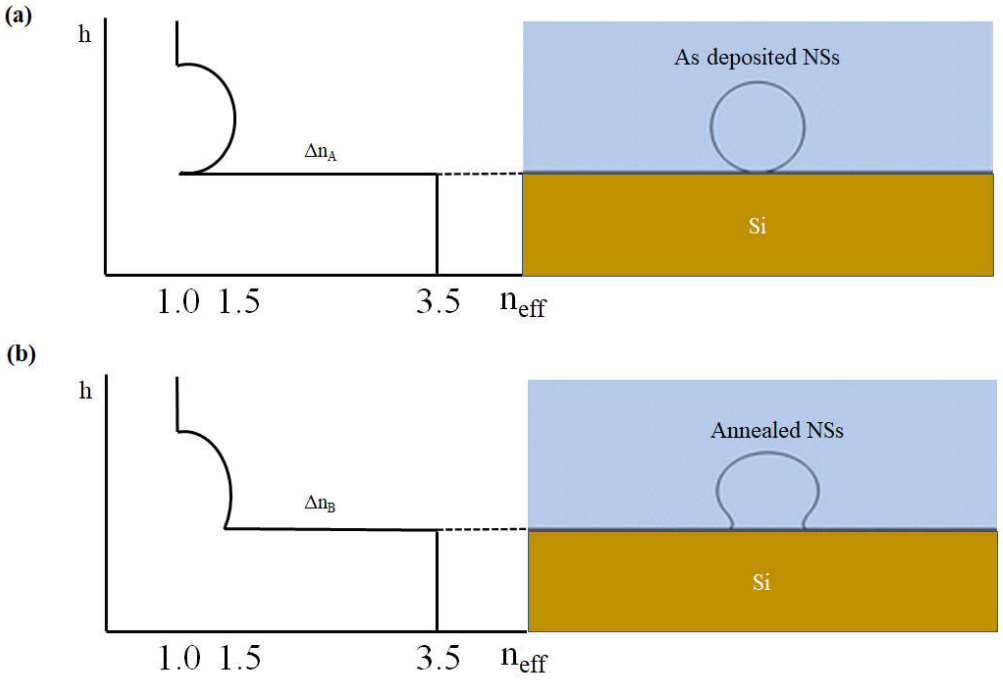

Figure 3.27. The effective index of refraction versus height for (a) as deposited NSs on Si, (b) annealed NSs on Si.

The second photonic effect is the micro-lensing which is more dominant in larger (750 nm) NSs, in which the light concentrated at the foci is expected to exceed AM 1.5 conditions, a condition at which the Si cells are known to have higher conversion efficiency [118].

An issue regarding the use of PS NSs for photon management of Si solar cells is the stability of the PS NSs under operational temperatures. We have previously

performed experiments on the temperature increase of Si cells on clear summer days in Ankara-Turkey, where this thesis work is conducted. Cells were found to reach temperatures up to a maximum of 60 °C, which is much lower than the temperature at which nanosphere forms begin to deform (≳105 °C). After extensive shape optimization studies on NSs, we have found that at ≥120 °C, NSs can be completely molten, from which experimentally determined glass transition temperature (T_g) of PS NSs is found to be ~110 °C which agrees with the literature. Our thorough optimization experiments revealed that temperatures up to 95 °C had no discernible effect on the shape/size of the nanosphere regardless of the length of the temperature treatment. As a result, we may confidently assume that the nanospheres on the surface of solar cells will retain their shape/size even on a clear summer day under equatorial conditions. We do make this statement under the reservation that, of course, under extreme desert climates, the situation may be different. Our approach would still find applicability over an extensive global coverage and hence is significant.

Another point we would like to make is that, in order to minimize the environmental effects on NS-based SCs, including humidity, air, and freezing, a thin protective layer can be used on top of SCs.

As the last discussion, it should be noted that we have conducted our studies on bulk mono-crystalline Si solar cells, a platform that has already been studied extensively for optimal light management. KOH-based pyramidal texturing followed by a passivation and ARC deposition is the gold-standard process that ensures reflectance below 5% over a broad spectral range. We have chosen this platform since its remaining process steps are highly reproducible, and hence the sample-to-sample variation is minimal. However, the expectation of the actual benefit from our PS NS-based light management approach is maximum for thin-film solar cells, and multi-crystalline Si solar cells where KOH base pyramidal texturing is not applicable.

CHAPTER 4

METAL FILM ON NANOSPHERES SERS SUBSTRATES

4.1 Overview of SERS substrates

Raman spectroscopy is a highly sensitive optical characterization technique, which identifies the chemical components of a material employing inelastic scattering of incident electromagnetic radiation due to vibrations of chemical groups constituting the material.

The Raman scattering, however, is a non-resonant low probability process as compared to resonant scattering processes such as elastic (Rayleigh) scattering or fluorescence. Inherently low signal/noise in Raman measurements leading to low molecular detectivity has urged scientists to employ several signal amplification schemes such as surface-enhanced Raman spectroscopy (SERS) [119]–[122], resonant Raman scattering [123], [124], and coherent anti-Stokes Raman scattering (CARS) [125] , [125].

Resonant Raman scattering and CARS techniques involve highly specific light sources such as tunable lasers and a high level of experimental complexity. Therefore, SERS stands out as the most widely utilized signal amplification technique in Raman spectroscopy. SERS has two main origins: chemical and physical enhancement [127]–[130]. Chemical processes such as charge transfer can lead to 10^3 fold enhancement [131], where physical processes can lead to 10^9-10^{12} fold enhancement [132], [133] of the Raman signal. The physical enhancement in SERS is based on enhanced localized electromagnetic fields, which can be achieved by surface plasmon resonances (SPR) of metal nanostructures [119]–[122], [134]. Commonly, SERS enhancement factors [EFs] are found to be highest in nanostructured noble metal film surfaces [135] or noble metal nano/microparticles that sustain strong field localization due to the presence of localized surface plasmon

resonances (LSPR) and a high density of so-called hot spots [136], [137]. Based on electromagnetic simulations such as Maxwell's equations solvers and experimental results, it can be concluded that EFs in SERS can be considerably improved if the LSPR band center is close to the excitation wavelength [138]–[141]. Due to its straightforward integration into standard Raman spectroscopy systems, as simple as the replacement of standard substrates with SERS substrates, SERS has found its place in a wide variety of applications in chemical and biological sensing [142]–[145].

4.2 Metallic films on nanospheres SERS substrates

SERS substrates based on metallic structures can be fabricated using a wide variety of approaches, such as nanoparticle self-assembly [146], e-beam lithography [147], and nanosphere lithography (NSL) [56]. Among these methods, NSL has attracted considerable interest since it is a low-cost, robust, and reproducible method used for the fabrication of large area, ordered metal nanostructures. In NSL, hexagonally close-packed (hcp) polystyrene (PS) or silica nanosphere (NS) arrays are used as 2D masks to deposit metal nanostructures using thermal evaporation followed by removal of colloidal masks to form ordered triangular metallic nanostructures [148]–[151]. Another effective approach to achieve SERS substrates is keeping the colloidal NSL mask after metal evaporation. This is because the metal film on the nanospheres has a considerable roughness, which can improve the Raman signal substantially [57], [152]–[157]. This method, also referred to as a metal film over nanospheres (FONs) or metal-capped nanospheres, can be employed for SERS detection of anthrax, glucose, biotin, and DNA [158]–[163].

The main privilege of the NSL method is that the tunability of the LSPR wavelength to the exciton wavelength is feasible as the plasmonic characteristics can be easily tuned by changing the size of nanospheres and thickness of the evaporated metal film [149]. There are several reports in literature targeting improvement or tunability of NSL based SERS substrate design. In one such work, it is targeted to increase the

tunability of FON structures by deposition of Ag FONs on PDMS [164]. In another work, a proposed method for improvement is to coat the NSL mask with a bilayer of Ag and Au at the same thickness and determine optimized values for strong SERS signals [165]. In another study, the LSPR wavelength is tuned by using silica nanospheres with different diameters, but the thickness of Ag is constant [166]. Despite the practicality of such methods, it is beneficial to employ a technique that does not require different nanosphere diameters, and the LSPR wavelength shift can be achieved by Ag films over the NSL mask (AgFONs) with shape modification. In that respect, the oblique angle deposition method can pave the way to tune the LSPR wavelength by changing the vapor incident angle relative to the surface normal of the substrate. The Raman enhancement in such a structure is mainly due to the Ag film on the nanosphere rather than the underlying triangular islands [167].

In our study, we show that a novel approach that combines two simple strategies can lead to attaining higher EF in SERS. Firstly, a single-size NSL mask is shape-modified using a simple and swift annealing-based technique to enhance electric field concentration, consequently leading to high SERS EFs [168]. Secondly, oblique deposition of Ag films on shape-modified NSL mask, albeit at low tilt-angles, is employed for fine-tuning the EFs. The idea of oblique angle deposition was previously used in [167] using larger θ resulting in not only a smaller Ag coating area but also in anisotropic thickness, which is not always desirable. Therefore, in our work, a custom-built thermal evaporation chamber is utilized to enable depositions at smaller angles, which enable fine adjustment of the LSPR wavelength. Crystal Violet (CV), one of the most popular tracer dyes, was opted as the analyte to check the SERS response. The molecular structure of the CV is illustrated in Figure 4.1. CA index name of CV molecule is Methanaminium, N-[4-[bis[4-(dimethylamino) phenyl]methylene]-2,5- cyclohexadien-1-ylidene]- N-methyl-, chloride (1:1) with a chemical formula of $C_{25}H_{30}ClN_3$.

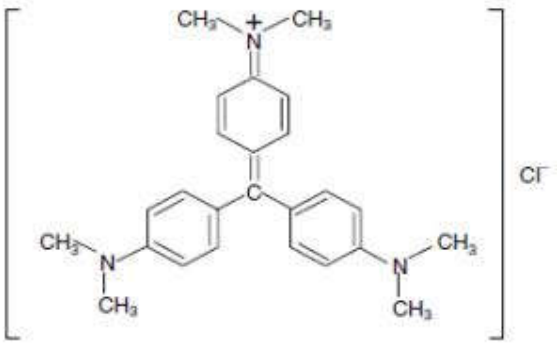

Figure 4.1. Molecular structure of the CV.

The maximum absorption wavelength of CV solution is in the UV spectrum, as illustrated in Figure 4.2.

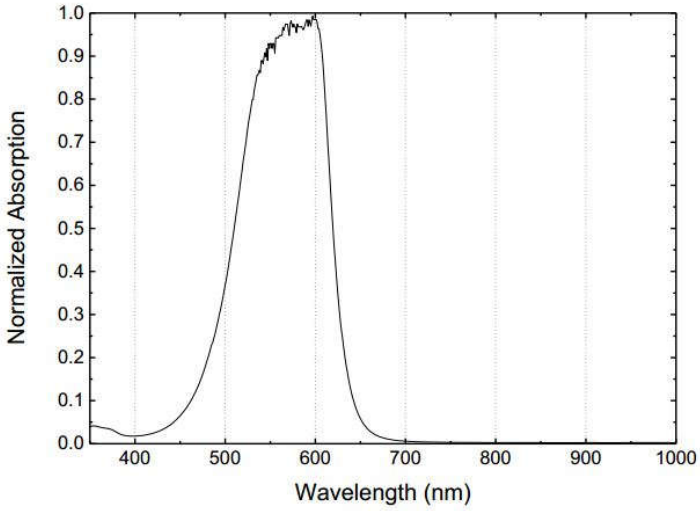

Figure 4.2. The UV-Visible absorption spectrum of CV solution.

Then, a relative EF is calculated by comparing the SERS spectra of CV acquired on AgFON substrates with Ag coated and bare Si wafers.

The SERS activity is measured using population statistics, which demonstrates that shape controlled AgFON monolayer substrates are very promising for a trace amount of molecule detection offering EFs up to 10^8, which is in good agreement with the finite element method (FEM) based Maxwell solver simulations.

4.3 Fabrication process of AgFON arrays

2 cm x 2 cm pieces of single-side polished silicon (Si) wafers are ultrasonically cleaned using acetone, isopropanol, and deionized water in sequence. A mild oxygen plasma treatment is carried out to make the surface of silicon samples hydrophilic. The solution of colloidal NSs, dispersed in water and functionalized with a hydroxyl group, was spin-coated on the Si samples. PS NSs self-organize in the hcp structure during the natural evaporation at room temperature, which is commonly used as the NSL mask in literature.

Subsequent thermal treatment of NSL mask improves adhesion of PS NSs to the Si surface. We have experienced that the NSs tend not to stay fixed on the surface of Si during coating of the dye molecules from aqueous solution unless this thermal treatment is employed, which is done at 110 °C for 20 min [168].

The diameters of PS NS employed for SERS substrates are 350 nm. Ag films are deposited at two different thicknesses of 10 nm and 20 nm on a monolayer PS NS based NSL mask using a custom-built thermal evaporation deposition system at incidence angles of $\theta = 0°, 5°, 10°, 15°$.

The fabrication steps are shown in Figure 2.1. First, a PS NS-based NSL mask is fabricated and annealed at 110°C for 20 minutes on a hot plate (Figure 2.1a). Next, thermal evaporation-based oblique angle Ag deposition is performed on the NSL mask, and fabrication of the AgFON array is finalized, as shown in Figure 2.1b. CV

molecules are spin-coated on an AgFON array from an aqueous solution at 10^{-4} mol/L concentration. Figure 2.1c shows the field enhancement of nanospheres.

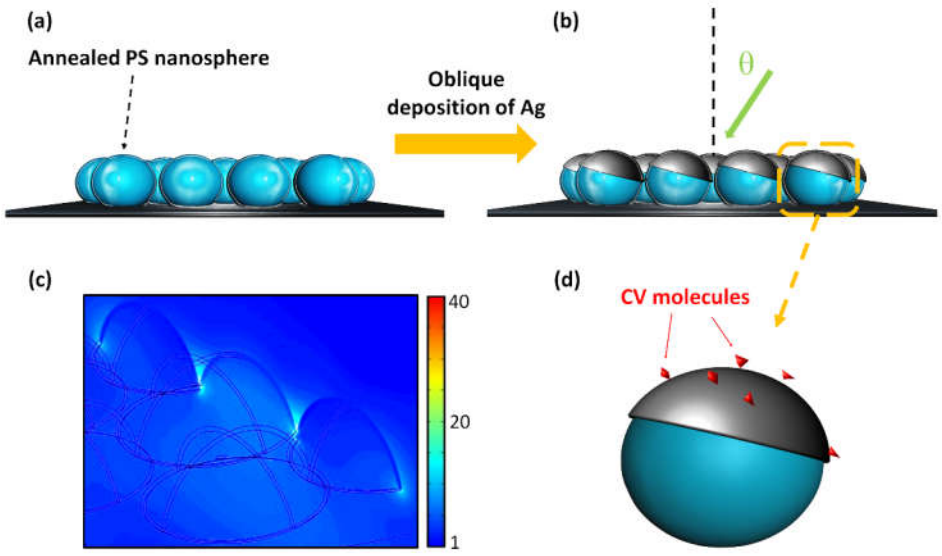

Figure 4.3. (a) Shape-modified hcp PS NSs on Si wafer, (b) Oblique angle deposition of an Ag film over PS NSs, (c) Field enhancement of nanospheres, (d) Nanosphere deposited with CV molecule.

4.4 Characterization of AgFON arrays

The SEM images in Figure 4.4 display the AgFON array structure from different angles and at different magnifications. Figure 4.4.a shows a top-view image of the AgFON array in which a uniform self-organized hcp configuration of 350 nm size NSs is clearly visible. Figure 4.4.b shows a side-view image of NSs after annealing for 20 min at a temperature of 110 °C. Figure 4.4.c displays the shadowing effect due to tilted evaporation.

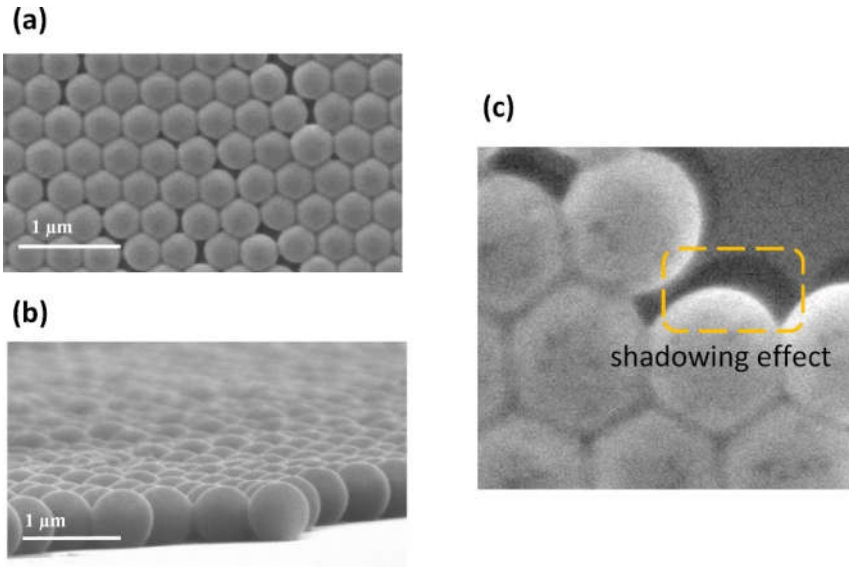

Figure 4.4. SEM images of (a) as-deposited hcp PS NSs with 350 nm size in top view, (b) 20 min 110°C annealed PS NSs in side-view, (c) 5° tilt Ag deposited annealed PS NSs showing the shadowing effect.

4.4.1 SERS measurements

A 10^{-4} M CV solution was used as an analyte for SERS measurements. AgFONs were spin-coated with CV molecules. The SERS signals were excited by using a linearly polarized continuous wave (CW) 532 nm wavelength laser source (Coherent Verdi) multimode (MM) fiber coupled to a modified upright microscope (Nikon Eclipse LV100) equipped with a 100X/0.90 NA objective. The excitation power is adjusted to 1.8 mW on the sample surface over a 17 µm diameter round illumination spot. The incident polarization of the originally linearly polarized excitation laser is scrambled due to MM fiber delivery. The Raman signal was collected in epi-configuration by the same objective lens and coupled into another multimode fiber through a suitable dichroic mirror (Semrock) and a notch filter (Semrock). The Raman signals were analyzed by a f/9.8, 750 mm spectrometer (Andor SR750) with 150 l/mm grating and an EMCCD camera (Andor Newton). The schematic diagram of the SERS setup is shown in Figure 4.5.

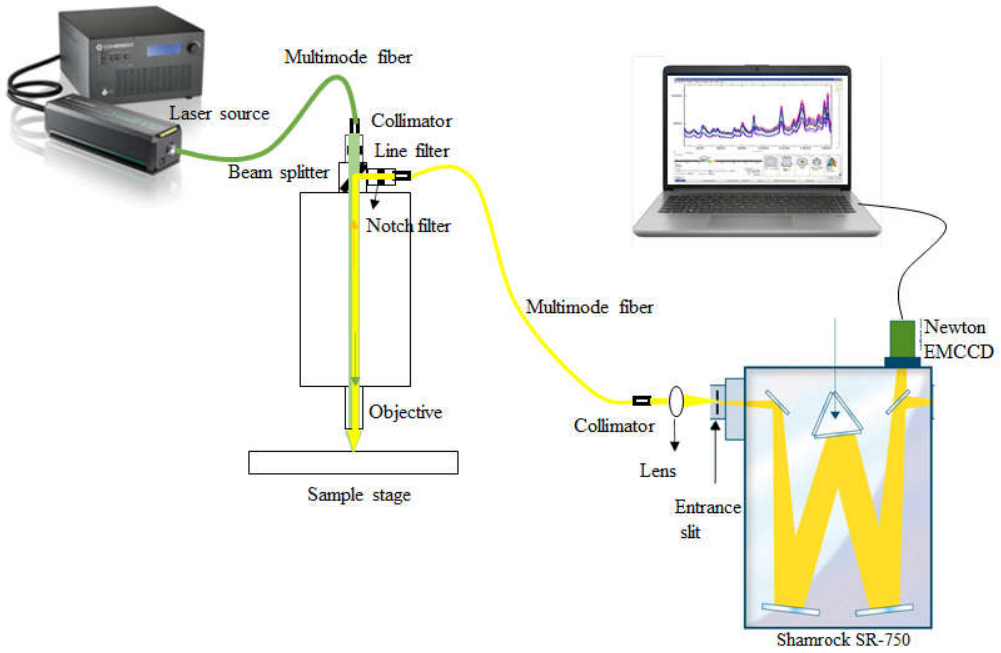

Figure 4.5. Schematic diagram of the SERS setup.

4.5 Simulations of AgFON arrays

COMSOL Multiphysics was employed to carry out FEM-based Maxwell simulations. A 3-dimensional model of the AgFON was designed based on SEM images using Autodesk Meshmixer. The simulations were conducted to calculate the field enhancement of AgFON at different Ag deposition angle (θ) values from 0° to 15° (Figure. 4.6). The SEM images show that the Ag patch on each nanosphere is smaller than a half-circle. A linearly polarized CW plane wave at 532 nm wavelength is used in the simulations. The shape and coverage of the AgFON are specified considering the θ and the relative orientation of the NS monolayer domain with respect to polarization direction (φ) of light. It is important to simulate different incidence polarization angles to ensure that the results are not specific to a single chosen configuration, and the results adequately represent the experimental

conditions. The dielectric function of Ag was taken from Johnson and Christy [169].

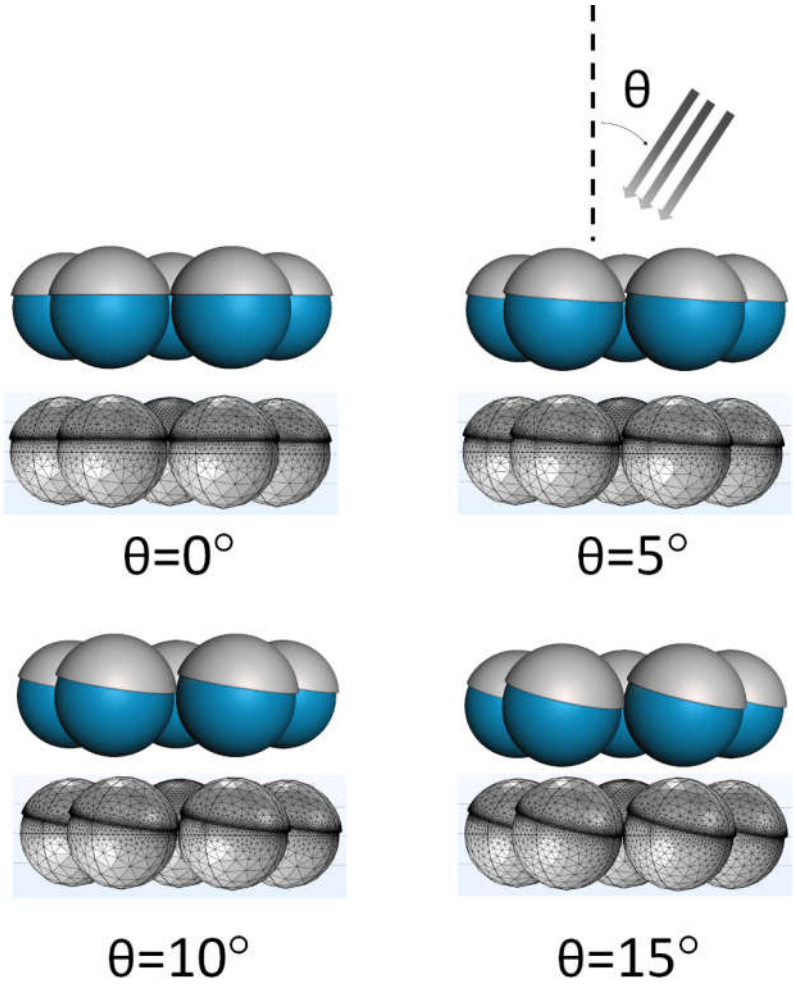

Figure. 4.6. Explanation of θ angle.

The evaporation angle has a vital role to play as it can finely adjust the LSPR wavelength of AgFONs [38]. The optical response of AgFONs is dependent on Ag nanostructures and Ag film on NSs for small θ. The larger the deposition angle becomes, the smaller the intersphere gaps become due to the shadowing effect. There is a critical θ_c with no nano triangles (around 55°) [167]. As we target SERS due to

AgFONs and not the triangular Ag nanostructures, we have carried out our experiments and simulations at smaller θ to study fine-tuning. The simulation results of the maximum Raman EF as a function of polarization angle for deposition angle θ of 0°, 5°, 10°, and 15° are shown in Figure. 4.7. In the Raman EF calculations, we employ the well-accepted approximation of $EF=E_{loc}^4/E_0^4$ where E_{loc} and E_0 are the local and the incident field magnitudes, respectively. It is found that the Raman EF is maximized for θ=5° for all incidence polarizations.

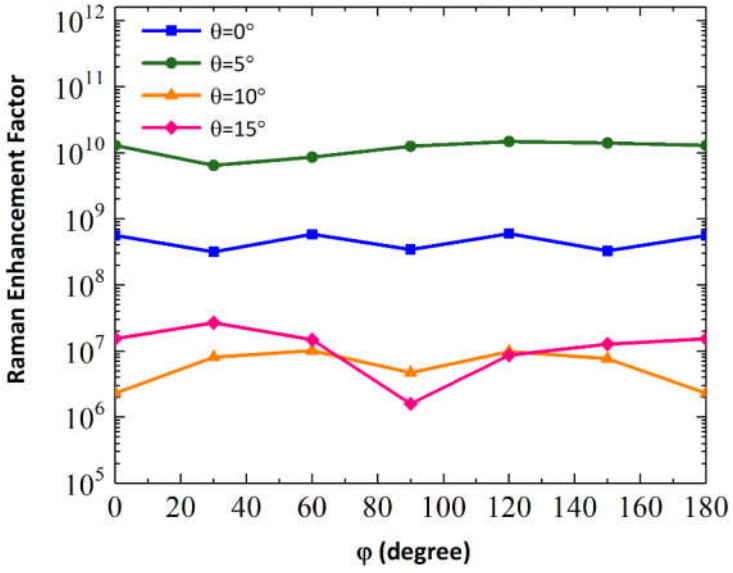

Figure. 4.7. Raman EF calculated using FEM simulations of AgFONs deposited at various θ as a function of incident polarization angle.

When θ > 5°, the EF has a considerable drop. The connection between EF and θ can be explained by the variation in the shape and coverage of Ag film, which takes place during oblique angle deposition. Dark field scattering spectroscopy measurements also display great agreement with FEM results, which can be seen in Figure 4.8.

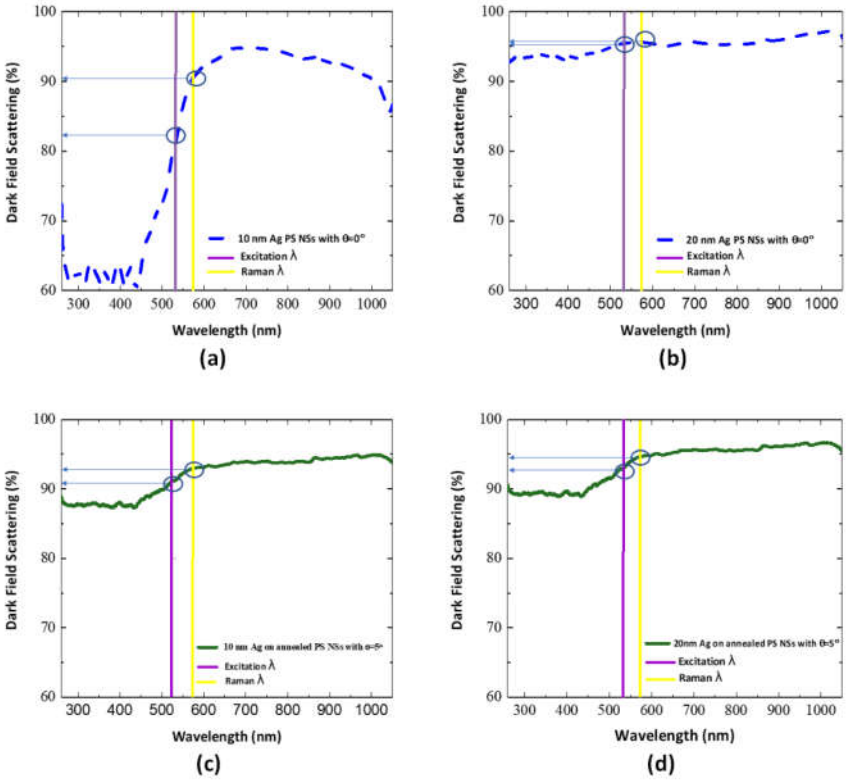

Figure 4.8. Dark field scattering spectra of SERS substrates: (a) AgFON with 10 nm Ag deposited at 0° on as-deposited NSs, (b) AgFON with 20 nm Ag deposited at 0° on as-deposited NSs (c) AgFON with 10 nm Ag deposited at 5° on annealed NSs, (d) AgFON with 20 nm Ag deposited at 5° on annealed NSs (purple and yellow vertical lines represent Raman excitation (532 nm) and Raman scattered (574 nm) wavelength positions, respectively).

Based on values derived from dark field scattering plots at Raman excitation and Raman scattering wavelengths, it can be deduced that EF of SERS substrates can be improved by 26% if nanospheres are thermally treated and then deposited with 10 nm Ag film at 5°.

$$\text{EF improvement}=\frac{Annealed\ NSs\ deposited\ at\ 5\ tilt\ with\ 10\ nm\ Ag}{As-deposited\ NSs\ deposited\ at\ 0\ tilt\ with\ 10\ nm\ Ag}$$

EF improvement=$\left(\frac{0.83}{0.74}\right)^2 = 1.258$

For Ag film with thickness of 20 nm, the Raman enhancement of SERS substrates can be improved by 2.1 % if nanospheres are thermally treated and then deposited at 5° tilt angle.

EF improvement=$\frac{Annealed\ NSs\ deposited\ at\ 5\ tilt\ with\ 20\ nm\ Ag}{As-deposited\ NSs\ deposited\ at\ 0\ tilt\ with\ 20\ nm\ Ag}$

EF improvement=$\left(\frac{0.90}{0.89}\right)^2$=1.0207

4.6 Results and discussion

4.6.1 SERS intensity spectra

SERS intensity spectra of AgFONs spin-coated with CV 10^{-4} M from 10 different selected spots of the substrate are shown in Figure 4.9. 1312 and 1412 cm^{-1} intervals of 10 peaks were baseline corrected, and peak areas were obtained.

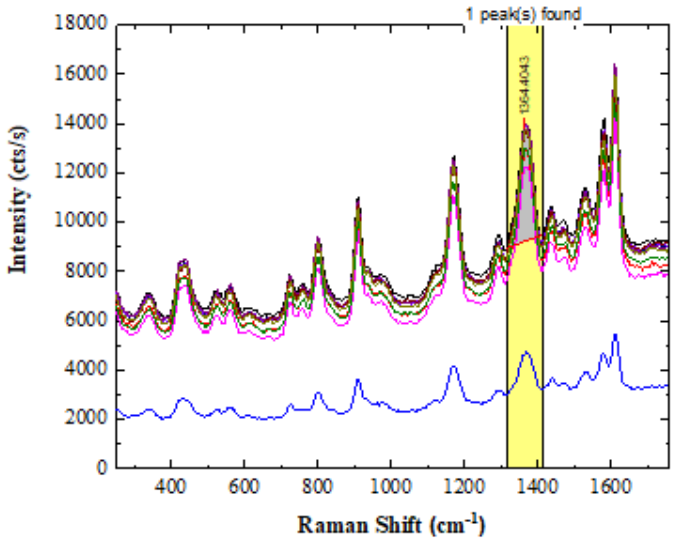

Figure 4.9. SERS intensity spectra of AgFONs deposited with 10nm Ag film at θ=5° on thermally treated spheres (integrated between the 1312 and 1412 cm^{-1} to be employed for SERS statistics).

4.6.2 EF calculation

A schematic diagram of Raman measurement from a droplet of 10^{-4} M CV molecule on a Si wafer is illustrated in Figure 4.10.

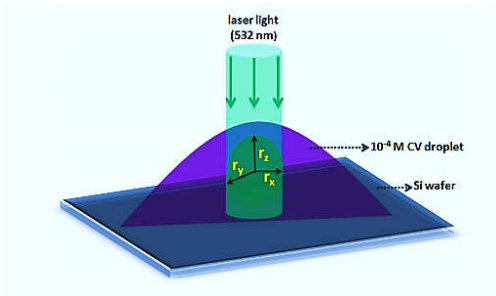

Figure 4.10. Schematic representation of Raman measurement from a droplet of 10^{-4} M CV molecule.

In normal Raman spectroscopy (NRS) inside liquid samples, the 3-dimensional Raman probe volume can be determined by considering a prolate spheroid focal volume, which in our case have dimensions of r_x = 8.5 μm, r_y = 8.5 μm and r_z (depth of focus) = 17 μm, yielding V_{probe} = (4π/3) x 8.5 μm x 8.5 μm x 17 μm = 5144.88 μm^3 = 5.14 x 10^{-12} L of probe volume. For our 10^{-4} M solution, the total number of molecules ($N_{NRS} = C_{NRS}$ X V_{probe}) in the measurement volume can be found as N_{NRS} = 10^{-4} mol/L x 6.02 x10^{23} molecules/mol x 5.14 x 10^{-12} L = 3.09 x 10^8 molecules. After baseline correction, I_{NRS} is calculated through the area under the peak (1370 cm^{-1}) with a width between 1350 and 1386 cm^{-1} and is found as 322 cts s^{-1}.

The molecules in the near field extend to around 2 nm from the surface of the metal film, resulting in a probe volume of V_{probe}= 2 nm x 227x10^6 nm^2 x 2= 9.08 X 10^{-16} L. Therefore, the total number of CV molecules in the SERS measurement can be calculated as N_{SERS}= 10^{-4} mol/L x 6.02 x10^{23} molecules/mol x 9.08 x 10^{-16} L = 5.46 x 10^4 molecules. With the measured I_{NRS} and I_{SERS} values, the EF for surface averaged structures can be calculated using EF = (I_{SERS}/N_{SERS})/(I_{NRS}/N_{NRS}), which is usually considered as the best estimate of the average SERS EF for a given SERS substrate.

Figure 4.11 shows the corresponding values and ranges in a box chart which is employed using OriginLab software. The box plot includes five data values and illustrates the outliers. The box portion lies between two lines called the 25th percentile and 75th percentile. 75th percentile refers to the line where 25% of the answers lie above that value, and 75% of the answers lie below that value. The 25th percentile refers to the line at which 25% of the data values are below this value.

The median line divides the box into two parts in a way that half of the data are greater than or equal to this line and half are less. Points at minimum and maximum values are plotted individually as asterisks.

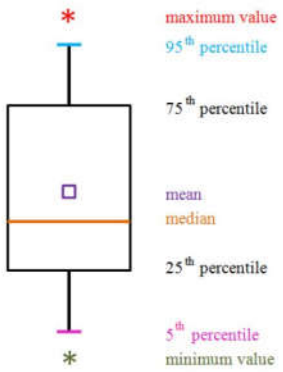

Figure 4.11. Corresponding values and ranges for box charts.

Figure 4.12 shows the experimentally determined EFs where statistics of SERS measurements cover spectra acquired from 10 different random spots on each substrate prepared at different θ and Ag coating thicknesses before and after annealing of PS NSs.

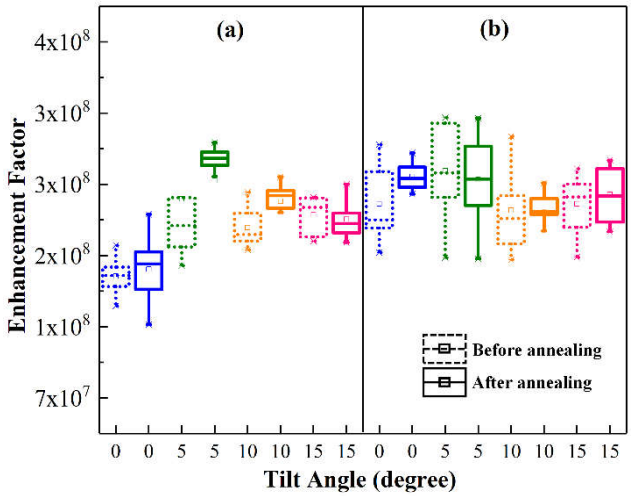

Figure 4.12. Box charts displaying the population statistics of SERS EFs of (a) 10 nm and (b) 20 nm Ag coated PS NSs before (dotted lines) and after (solid lines) annealing with θ values of 0°, 5°, 10°, and 15°.

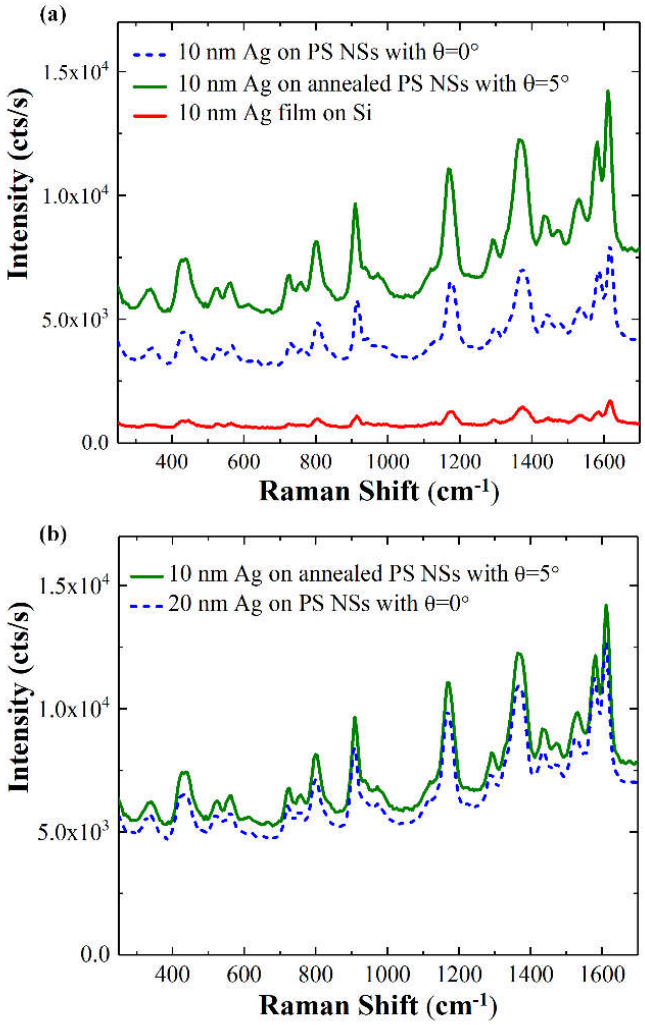

Figure 4.13. SERS spectra of 10^{-4} M CV spin-coated on (a) 10 nm Ag on non-annealed PS NSs (dotted blue line), annealed PS NSs with θ=5° (solid green line), and 10 nm Ag coating on Si (solid red line), (b) 10 nm Ag on annealed PS NSs with θ=5° (solid green line) and 20 nm Ag on non-annealed PS NSs without tilting (dotted blue line).

Statistics show that maximum EF is obtained from 10 nm Ag coating with θ=5° on annealed PS NSs, which is consistent with the simulation results. It is evident that

with increasing the deposition angle, the shadowing effect causes reduction of the Ag coating area and increase of the Ag film thickness variation.

Figure 4.12 shows that heat treatment-based shape control of PS NSs is a simple yet effective way to achieve homogeneous SERS substrates, as shown in the reduction of the population range in the box chart. Box charts show that not only does AgFON with 10 nm of thickness result in more homogenous SERS substrates but also enables significant material cost reduction. This is because by applying simple annealing-based shape control and oblique angle Ag deposition, we can achieve EFs even better than that of the AgFON with 20 nm thickness coated at a normal deposition angle. So, it can be said that at least half the amount of Ag material can be saved using this method. It is also evident from Figure 4.12 that at a thickness of 20 nm, the shape control, and tilt angle do not yield statistically significant changes in the EF. So, it can be said that these tuning parameters are most effective in achieving high EF SERS substrates with ultra-thin Ag layers. For a clear understanding of the effect, the corresponding averaged SERS spectra are shown in Figure 4.13.a. It is evident that at the same Ag coating thickness of 10 nm, the Raman intensity can be enhanced around 10^3 times on NSs with respect to flat Ag film on Si. Moreover, a shape adjustment of the NSs followed by an oblique angle Ag evaporation at $\theta=5^o$ can further improve the Raman signal substantially. Figure 4.13.b clearly illustrates that with shape adjustment and oblique angle deposition, the necessary amount and hence the cost of Ag material can be cut by half. It should be noted that the consumed amount of evaporation material can easily be 3 to 4 orders of magnitude larger than the actual coated amount in thermal evaporators (depending on the source-sample distance).

4.7 Conclusion

In this study, annealing-based nanosphere shape adjustment and oblique angle deposition of Ag film have been utilized as a method to fabricate SERS substrates at a low cost. The small variation in deposition angle enables fine-tuning of the Raman

enhancement factors of the AgFON structure. Raman enhancement factors as high as 10^8 are achieved utilizing this technique from crystal violet dye molecule. This method enables cost-effective fabrication of SERS substrates with ultra-thin Ag films deposited at 5^o tilt can replace SERS substrates fabricated by deposition of Ag films with double thickness in normal deposition angle. FEM simulations show excellent agreement with the experimental results and demonstrate expected field enhancements up to 10^9 at a tilt angle of 5^o.

CHAPTER 5

CONCLUSIONS AND FUTURE PROSPECTS

The objective of this thesis is to fabricate colloidal arrays and investigate applications of dielectric nanospheres.

Chapter 2 discusses different techniques for producing ordered two-dimensional nanosphere colloidal films: spin coating was shown to be one of the most advantageous methods of coating nanospheres, which is utilized in this thesis.

Dielectric NSs can be used either in the form of uniform arrays of uniformly closed-pack ordered arrays of nanospheres for light trapping or as colloidal masks to deposit metallic films. In this work, uniformly ordered arrays of nanospheres are employed in two different applications, including solar cells and SERS substrates.

In chapter 3, dielectric colloidal nanospheres (NSs) can be employed for light management in photonic devices like solar cells (SCs). They are potential nano-optical platforms as adjustable light management interfaces in solar cells because they both behave as antireflection coatings (ARCs) and also as microlenses for light concentration.

NS arrays enable the focusing of solar radiation into tighter foci, which leads to concentration of light intensity and higher photovoltaic conversion efficiency. In addition, the NS arrays can be considered as an effective layer on the surface of PV, which can decrease reflectance and enables improved forward scattering. As a result, homogenous arrays of NSs on the surface of SC can operate as antireflection coatings or as micro-lenses, which can be considered as a light concentrator in the structure of concentrated photovoltaics.

SC with NSs can act as light-trapping structures, which are low-cost and uncomplicated fabrication steps than conventional, yet costly, time-taking vacuum-

evaporated multilayer dielectric ARCs. Moreover, conventional ARCs are not post-deposition tunable for attaining improved efficiency. In this work, both simulation and experimental work confirm that the shape adjustment of such NS structures can improve light harvesting and, consequently, efficiency in Si SCs. The light conversion efficiency of Si SCs is enhanced by about 27% with shape adjustment of NS arrays.

The unique novelty of this work is the post-deposition adjustability of an ARC, which is simple to implement for improved light trapping and light concentration in Si solar cells. Our adjustable light management interfaces are broadband, omnidirectional and show minimal polarization dependence.

In chapter 4, NSs arrays are used in a two-step procedure that combines the advantages of top-down and bottom-up methods: (1) preparing homogenous mask of nanospheres and (2) Deposition of metallic films using the colloidal layer as a mask.

This method is employed for the purpose of fabricating SERS substrates at a cheap cost. The novelty of this work is to utilize annealing-based nanosphere shape modification and oblique angle deposition of Ag film to improve the performance of SERS substrates. The considerable improvement of the Raman enhancement factors of the AgFON structure is made possible by the tiny variations in deposition angles. Raman enhancement factors as high as 10^8 have been obtained by using this method from crystal violet dye molecules. Using this technique, it is possible to manufacture SERS substrates with ultra-thin Ag films deposited at a 5^o tilt at a low cost, which may be used to replace SERS substrates fabricated by deposition of Ag films with double thickness at the usual deposition angle. The findings of the FEM models, which show great consistency with the experimental data, indicate the anticipated field enhancements up to 10^9 at a 5^o tilt angle.

5.1 Future prospects

The future prospects of this work are to employ different methods to improve the quality of self-assembled NS arrays and colloidal lithography. Furthermore, there are different grains, grains boundaries, and dislocations in uniformly hcp monolayers of NSs. Sometimes, there are even double layers or multilayers of NSs layers. These defects cannot be put into consideration in our simulation or experimental results. These criteria can be considered in future studies. This improvement can pave the way to fabricate and diversify micro/nanostructures produced through colloidal lithography.

Furthermore, by etching the colloidal crystal masks, a wide variety of nanostructures can be presented. NSL can be employed to fabricate noble metal structures, such as holes, cones, pillars, bowls, rings, shells, and triangles, which are beneficial in the field of plasmonics. They have been extensively studied for usage as nanoantennas, color displays, plasmonic sensors, and SERS substrates, among other applications.

There will be more studies focused on colloidal crystals and their architectures to fabricate a range of periodic 3D hierarchical nanostructures that may be customized for use in nanophotonics, optoelectronics, electronics, metamaterials, and biology.

Regarding NS-based solar cells, it is true that that the fabrication of NS-based light-trapping bulk solar cells can be more costly and less applicable than conventional KOH-based texturing methods. However, the main objective of utilizing NSs is investigating light management of NSs, which can be used extensively in different thin-film devices, including thin-film solar cells or detectors, where texturing is impossible. Furthermore, the light management scheme can be taken into longer or shorter wavelength depending on the application, which is not applicable using conventional light trapping methods such as pyramidal texturing.

The main novelty of this study is to use the annealing method to change the shape of nanospheres utilized on top of SC to improve the light concentration effect. Our deduction for the reason of better light concentration after annealing of NSs is the extended contact surface. Further studies can be conducted to survey the effects of annealing on the structural, surface morphology, and dielectric properties of annealed PS NSs on Si, as well as the surface passivation effects using FTIR spectra and dielectric measurements.

REFERENCES

[1] U. C. Fischer and H. P. Zingsheim, “Submicroscopic Pattern Replication With Visible Light.,” *J. Vac. Sci. Technol.*, vol. 19, no. 4, pp. 881–885, 1981, doi: 10.1116/1.571227.

[2] H. W. Deckman and J. H. Dunsmuir, “Natural lithography,” *Appl. Phys. Lett.*, vol. 41, no. 4, pp. 377–379, 1982, doi: 10.1063/1.93501.

[3] C. H. John and P. V. D. Richard, “Nanosphere lithography: A materials general fabrication process for periodic particle array surfaces,” *J. Vac. Sci. Technol. A Vacuum, Surfaces, Film.*, vol. 13, no. 3, pp. 1553–1558, 1995, [Online]. Available: http://link.aip.org/link/?JVA/13/1553/1.

[4] J. C. Hulteen, D. A. Treichel, M. T. Smith, M. L. Duval, T. R. Jensen, and R. P. Van Duyne, “Nanosphere lithography: Size-tunable silver nanoparticle and surface cluster arrays,” *J. Phys. Chem. B*, vol. 103, no. 19, pp. 3854–3863, 1999, doi: 10.1021/jp9904771.

[5] G. Zhang and D. Wang, “Colloidal Lithography — The Art of Nanochemical Patterning,” *Chem. Asian J.*, vol. 4, pp. 236–245, 2009, doi: 10.1002/asia.200800298.

[6] W. G. Eberhard and W. T. Wcislo, “Plenty of room at the bottom?,” *Am. Sci.*, vol. 100, no. 3, pp. 226–233, 2012, doi: 10.1511/2012.96.226.

[7] P. A. Sabatier, “Top-down and Bottom-up Approaches to Implementation Research : A Critical Analysis and Suggested Synthesis Authors (s): Paul A . Sabatier Published by : Cambridge University Press Stable URL : http://www.jstor.org/stable/3998354 Accessed : 28-03-2016 21,” *J. Public Policy*, vol. 6, no. 1, pp. 21–48, 1986.

[8] H. Zheng and S. Ravaine, “Bottom-up assembly and applications of photonic materials,” *Crystals*, vol. 6, no. 5, 2016, doi: 10.3390/cryst6050054.

[9] S. Okazaki, “Resolution limits of optical lithography,” *J. Vac. Sci. Technol. B Microelectron. Nanom. Struct.*, vol. 9, no. 6, p. 2829, 1991, doi: 10.1116/1.585650.

[10] Y. Xia and G. M. Whitesides, “Soft lithography,” *Angew. Chemie - Int. Ed.*, vol. 37, no. 5, pp. 550–575, 1998, doi: 10.1002/(sici)1521-3773(19980316)37:5<550::aid-anie550>3.3.co;2-7.

[11] B. D. Gates, Q. Xu, M. Stewart, D. Ryan, C. G. Willson, and G. M. Whitesides, “New approaches to nanofabrication: Molding, printing, and

other techniques," *Chem. Rev.*, vol. 105, no. 4, pp. 1171–1196, 2005, doi: 10.1021/cr030076o.

[12] P. Colson, C. Henrist, and R. Cloots, "Nanosphere lithography: A powerful method for the controlled manufacturing of nanomaterials," *J. Nanomater.*, vol. 2013, 2013, doi: 10.1155/2013/948510.

[13] J. M. Lehn, "Perspectives in supramolecular chemistry: From molecular recognition towards self-organisation," *Pure Appl. Chem.*, vol. 66, no. 10–11, pp. 1961–1966, 1994, doi: 10.1351/pac199466101961.

[14] H. Kind *et al.*, *Patterned films of nanotubes using microcontact printing of catalysts*, vol. 11, no. 15. 1999.

[15] J. C. Meiners, H. Elbs, A. Ritzi, J. Mlynek, and G. Krausch, "Chemically functionalized surfaces from ultrathin block-copolymer films," *J. Appl. Phys.*, vol. 80, no. 4, pp. 2224–2227, 1996, doi: 10.1063/1.363114.

[16] G. Krausch and R. Magerle, "Nanostructured thin films via self-assembly of block copolymers," *Adv. Mater.*, vol. 14, no. 21, pp. 1579–1583, 2002, doi: 10.1002/1521-4095(20021104)14:21<1579::AID-ADMA1579>3.0.CO;2-6.

[17] M. Lazzari and M. Arturo López-Quintela, "Block Copolymers as a Tool for Nanomaterial Fabrication," *Adv. Mater.*, vol. 15, no. 19, pp. 1583–1594, 2003, doi: 10.1002/adma.200300382.

[18] J. I. Martín, J. Nogués, K. Liu, J. L. Vicent, and I. K. Schuller, "Ordered magnetic nanostructures: Fabrication and properties," *J. Magn. Magn. Mater.*, vol. 256, no. 1–3, pp. 449–501, 2003, doi: 10.1016/S0304-8853(02)00898-3.

[19] Y. He *et al.*, "RSC Advances Fabrication of SERS-active conjugated copolymers / gold nanoparticles composite fi lms by interface- directed assembly †," *RSC Adv.*, vol. 5, pp. 39697–39704, 2015, doi: 10.1039/C5RA05430C.

[20] T. Huang, K. Yu, Y. Liao, and C. Lee, "Enhance the structural stability of the FePt nanoparticle monolayer by adding gold overlayer," *Colloids Surfaces A*, vol. 285, pp. 603–606, 2006, doi: 10.1016/j.colsurfa.2006.02.046.

[21] Y. Xia, B. Gates, Y. Yin, and Y. Lu, "Monodispersed Colloidal Spheres: Old Materials with New Applications," *Adv. Mater.*, vol. 12, no. 10, pp. 693–713, 2000, doi: 10.1002/(sici)1521-4095(200005)12:10<693::aid-adma693>3.3.co;2-a.

[22] H. Li, J. Low, K. S. Brown, N. Wu, and W. V. Nano, "Large-area well-ordered nanodot array pattern fabricated with self-assembled nanosphere template," *IEEE Sens. J.*, vol. 8, no. 6, pp. 880–884, 2008, doi: 10.1109/JSEN.2008.923266.

[23] S. Yang, S. G. Jang, D. Choi, and S. Kim, "reviews Nanomachining by

Colloidal Lithography," *Small*, vol. 2, no. 4, pp. 458–475, 2006, doi: 10.1002/smll.200500390.

[24] H. W. Deckman and J. H. Dunsmuir, "Applications of Surface Textures Produced With Natural Lithography.," *J. Vac. Sci. Technol. B Microelectron. Nanom. Struct.*, vol. 1, no. 4, pp. 1109–1112, 1983, doi: 10.1116/1.582644.

[25] J. C. Hulteen and R. P. Van Duyne, "Nanosphere lithography: A materials general fabrication process for periodic particle array surfaces," *J. Vac. Sci. Technol. A*, vol. 13, no. 24, pp. 1553–1558, 1995, doi: 10.1116/1.579726.

[26] T. R. Jensen, G. C. Schatz, and R. P. Van Duyne, "Nanosphere lithography: Surface plasmon resonance spectrum of a periodic array of silver nanoparticles by ultraviolet - Visible extinction spectroscopy and electrodynamic modeling," *J. Phys. Chem. B*, vol. 103, no. 13, pp. 2394–2401, 1999, doi: 10.1021/jp984406y.

[27] X. Zhang, C. R. Yonzon, and R. P. Van Duyne, "Nanosphere lithography fabricated plasmonic materials and their applications," *J. Mater. Res.*, vol. 21, no. 5, pp. 1083–1092, 2006, doi: 10.1557/jmr.2006.0136.

[28] L. Li, T. Zhai, H. Zeng, X. Fang, Y. Bando, and D. Golberg, "Polystyrene sphere-assisted one-dimensional nanostructure arrays: Synthesis and applications," *J. Mater. Chem.*, vol. 21, no. 1, pp. 40–56, 2011, doi: 10.1039/c0jm02230f.

[29] Y. Li, N. Koshizaki, and W. Cai, "Periodic one-dimensional nanostructured arrays based on colloidal templates, applications, and devices," *Coord. Chem. Rev.*, vol. 255, no. 3–4, pp. 357–373, 2011, doi: 10.1016/j.ccr.2010.09.015.

[30] Y. Li, W. Cai, and G. Duan, "Ordered micro/nanostructured arrays based on the monolayer colloidal crystals," *Chem. Mater.*, vol. 20, no. 3, pp. 615–624, 2008, doi: 10.1021/cm701977g.

[31] J. Dewalque, R. Cloots, O. Dubreuil, N. Krins, B. Vertruyen, and C. Henrist, "Microstructural evolution of a TiO 2 mesoporous single layer film under calcination: Effect of stabilization and repeated thermal treatments on the film crystallization and surface area," *Thin Solid Films*, vol. 520, no. 16, pp. 5272–5276, 2012, doi: 10.1016/j.tsf.2012.03.044.

[32] X. Ye and L. Qi, "Recent advances in fabrication of monolayer colloidal crystals and their inverse replicas," *Sci. China Chem.*, vol. 57, no. 1, pp. 58–69, 2014, doi: 10.1007/s11426-013-5018-2.

[33] O. D. Velev, N. D. Denkov, P. A. Kralchevsky, I. B. Ivanov, H. Yoshimura, and K. Nagayama, "Mechanism of formation of two-dimensional crystals from latex particles on substrata," *Prog. Colloid Polym. Sci.*, vol. 93, no. 17, pp. 366–367, 1993, doi: 10.1007/bfb0118623.

[34] P. A. Kralchevsky and N. D. Denkov, "Capillary forces and structuring in

layers of colloid particles," *Curr. Opin. Colloid Interface Sci.*, vol. 6, no. 4, pp. 383–401, 2001, doi: 10.1016/S1359-0294(01)00105-4.

[35] S. Gu, J. Onishi, Y. Kobayashi, D. Nagao, and M. Konno, "Preparation and colloidal stability of monodisperse magnetic polymer particles," *J. Colloid Interface Sci.*, vol. 289, no. 2, pp. 419–426, 2005, doi: 10.1016/j.jcis.2005.03.073.

[36] W. Wang and B. Gu, "Self-assembly of two- and three-dimensional particle arrays by manipulating the hydrophobicity of silica nanospheres," *J. Phys. Chem. B*, vol. 109, no. 47, pp. 22175–22180, 2005, doi: 10.1021/jp053692s.

[37] D. Nagao, R. Kameyama, Y. Kobayashi, and M. Konno, "Multiformity of particle arrays assembled with a simple dip-coating," *Colloids Surfaces A Physicochem. Eng. Asp.*, vol. 311, no. 1–3, pp. 26–31, 2007, doi: 10.1016/j.colsurfa.2007.08.031.

[38] R. Micheletto, H. Fukuda, and M. Ohtsu, "A Simple Method for the Production of a Two-Dimensional, Ordered Array of Small Latex Particles," *Langmuir*, vol. 11, no. 9, pp. 3333–3336, 1995, doi: 10.1021/la00009a012.

[39] P. Jiang and M. J. McFarland, "Large-scale fabrication of wafer-size colloidal crystals, macroporous polymers and nanocomposites by spin-coating," *J. Am. Chem. Soc.*, vol. 126, no. 42, pp. 13778–13786, 2004, doi: 10.1021/ja0470923.

[40] Y. B. Zheng, S. J. Chua, C. H. A. Huan, and Z. L. Miao, "Selective growth of GaAs quantum dots on the triangle nanocavities bounded by SiO2 mask on Si substrate by MBE," *J. Cryst. Growth*, vol. 268, no. 3-4 SPEC. ISS., pp. 369–374, 2004, doi: 10.1016/j.jcrysgro.2004.04.056.

[41] C. W. Kuo, J. Y. Shiu, and P. Chen, "Size- and shape-controlled fabrication of large-area periodic nanopillar arrays," *Chem. Mater.*, vol. 15, no. 15, pp. 2917–2920, 2003, doi: 10.1021/cm0343249.

[42] E. C. Brown, S. K. Wilke, D. A. Boyd, D. G. Goodwin, and S. M. Haile, "Polymer sphere lithography for solid oxide fuel cells: A route to functional, well-defined electrode structures," *J. Mater. Chem.*, vol. 20, no. 11, pp. 2190–2196, 2010, doi: 10.1039/b920973e.

[43] M. Trau, D. A. Seville, and I. A. Aksay, "Field-induced layering of colloidal crystals," *Science (80-.).*, vol. 272, no. 5262, pp. 706–709, 1996, doi: 10.1126/science.272.5262.706.

[44] R. C. Hayward, D. A. Saville, and I. A. Aksay, "Electrophoretic assembly of colloidal crystals with optically tunable micropatterns," *Nature*, vol. 404, no. 6773, pp. 56–59, 2000, doi: 10.1038/35003530.

[45] S. O. Lumsdon, E. W. Kaler, and O. D. Velev, "Two-Dimensional Crystallization of Microspheres by a Coplanar AC Electric Field," *Langmuir*,

vol. 20, no. 6, pp. 2108–2116, 2004, doi: 10.1021/la035812y.

[46] J. Rybczynski, U. Ebels, and M. Giersig, "Large-scale, 2D arrays of magnetic nanoparticles," *Colloids Surfaces A Physicochem. Eng. Asp.*, vol. 219, no. 1–3, pp. 1–6, 2003, doi: 10.1016/S0927-7757(03)00011-6.

[47] M. S. L. Technique *et al.*, "ScienceDirect Facile Fabrication of Large Area Polystyrene Colloidal Crystal," *Chem. Res. Chinese*, vol. 6, pp. 712–714, 2007.

[48] L. M. Goldenberg, J. Wagner, J. Stumpe, B. R. Paulke, and E. Görnitz, "Simple method for the preparation of colloidal particle monolayers at the water/alkane interface," *Langmuir*, vol. 18, no. 14, pp. 5627–5629, 2002, doi: 10.1021/la025745s.

[49] K. Seeger and R. E. Palmer, "Fabrication of ordered arrays of silicon nanopillars," *J. Phys. D. Appl. Phys.*, vol. 32, no. 24, pp. 8–12, 1999, doi: 10.1088/0022-3727/32/24/102.

[50] F. Fan and K. J. Stebe, "Assembly of Colloidal Particles by Evaporation on Surfaces with Patterned Hydrophobicity," *Langmuir*, vol. 20, no. 8, pp. 3062–3067, 2004, doi: 10.1021/la030380c.

[51] M. Himmelhaus, M. Himmelhaus, M. Himmelhaus, and H. Takei, "Self-assembly of polystyrene nano particles into patterns of random-close-packed monolayers via chemically induced adsorption," *Phys. Chem. Chem. Phys.*, vol. 4, no. 3, pp. 496–506, 2002, doi: 10.1039/b108631f.

[52] Q. Zhang, S. Ghosh, S. Samitsu, X. Peng, and I. Ichinose, "Ultrathin freestanding nanoporous membranes prepared from polystyrene nanoparticles," *J. Mater. Chem.*, vol. 21, no. 6, pp. 1684–1688, 2011, doi: 10.1039/c0jm03334k.

[53] Y. Wang *et al.*, "Optical properties of the crescent and coherent applications," *Opt. Express*, vol. 19, no. 9, p. 8303, 2011, doi: 10.1364/oe.19.008303.

[54] H. Takei and N. Shimizu, "Gradient sensitive microscopic probes prepared by gold evaporation and chemisorption on latex spheres," *Langmuir*, vol. 13, no. 7, pp. 1995–1998, 1997, doi: 10.1021/la9621067.

[55] E. Hutter and J. H. Fendler, "Exploitation of localized surface plasmon resonance," *Adv. Mater.*, vol. 16, no. 19, pp. 1685–1706, 2004, doi: 10.1002/adma.200400271.

[56] C. L. H. And and R. P. Van Duyne, "Nanosphere Lithography: A Versatile Nanofabrication Tool for Studies of Size-Dependent Nanoparticle Optics," *J. Phys. Chem. B*, vol. 105, no. 24, pp. 5599–5611, 2001, doi: 10.1007/s11468-013-9665-0.

[57] M. B. Nardelli *et al.*, "Corrected 19 december 2008; see last page," *Science*

(80-.)., vol. 321, no. December, pp. 388–393, 2008.

[58] A. J. Haes and R. P. Van Duyne, "A unified view of propagating and localized surface plasmon resonance biosensors," *Anal. Bioanal. Chem.*, vol. 379, no. 7–8, pp. 920–930, 2004, doi: 10.1007/s00216-004-2708-9.

[59] S. M. Weekes, F. Y. Ogrin, and W. A. Murray, "Fabrication of large-area ferromagnetic arrays using etched nanosphere lithography," *Langmuir*, vol. 20, no. 25, pp. 11208–11212, 2004, doi: 10.1021/la048695v.

[60] H. Zhong, G. Tarrach, P. Wu, A. Drechsler, D. Wei, and J. Yuan, "High resolution magnetic force microscopy of patterned L10-FePt dot arrays by nanosphere lithography," *Nanotechnology*, vol. 19, no. 9, 2008, doi: 10.1088/0957-4484/19/9/095703.

[61] J. Rybczynski, M. Hilgendorff, and M. Giersig, "Nanosphere Lithography — Fabrication of Various Periodic Magnetic Particle Arrays Using Versatile Nanosphere Masks," *Low-Dimensional Syst. Theory, Prep. Some Appl.*, pp. 163–172, 2003, doi: 10.1007/978-94-010-0143-4_14.

[62] C. L. Haynes, A. D. McFarland, M. T. Smith, J. C. Hulteen, and R. P. Van Duyne, "Angle-resolved nanosphere lithography: Manipulation of nanoparticle size, shape, and interparticle spacing," *J. Phys. Chem. B*, vol. 106, no. 8, pp. 1898–1902, 2002, doi: 10.1021/jp013570+.

[63] J. Dickmann, A. Geyer, H. Daembkes, H. Nickel, R. Lösch, and W. Schlapp, "Fabrication of Low Resistance Submicron Gates in Pseudomorphic MODFETs Using Optical Contact Lithography," *J. Electrochem. Soc.*, vol. 138, no. 2, pp. 491–493, 1991, doi: 10.1149/1.2085615.

[64] G. Owen, "Methods for proximity effect correction in electron lithography," *J. Vac. Sci. Technol. B Microelectron. Nanom. Struct.*, vol. 8, no. 6, p. 1889, 1990, doi: 10.1116/1.585179.

[65] A. Shirakawa, I. Sakane, M. Takasaka, and T. Kobayashi, "Sub-5-fs visible pulse generation by pulse-front-matched noncollinear optical parametric amplification," *Appl. Phys. Lett.*, vol. 74, no. 16, pp. 2268–2270, 1999, doi: 10.1063/1.123820.

[66] T. Wada, S. Haraichi, K. Ishii, H. Hiroshima, M. Komuro, and M. Hirayama, " SiO 2 /poly-Si electron beam resist process for nanofabrication ," *J. Vac. Sci. Technol. A Vacuum, Surfaces, Film.*, vol. 14, no. 3, pp. 1850–1854, 1996, doi: 10.1116/1.580348.

[67] S. Cataldo *et al.*, "Hole-mask colloidal nanolithography for large-area low-cost metamaterials and antenna-assisted surface-enhanced infrared absorption substrates," *ACS Nano*, vol. 6, no. 1, pp. 979–985, 2012, doi: 10.1021/nn2047982.

[68] V. Peksa *et al.*, "Testing gold nanostructures fabricated by hole-mask

colloidal lithography as potential substrates for SERS sensors: Sensitivity, signal variability, and the aspect of adsorbate deposition," *Phys. Chem. Chem. Phys.*, vol. 18, no. 29, pp. 19613–19620, 2016, doi: 10.1039/c6cp02752k.

[69] J. Zhao, B. Frank, F. Neubrech, C. Zhang, P. V. Braun, and H. Giessen, "Hole-mask colloidal nanolithography combined with tilted-angle-rotation evaporation: A versatile method for fabrication of low-cost and large-area complex plasmonic nanostructures and metamaterials," *Beilstein J. Nanotechnol.*, vol. 5, no. 1, pp. 577–586, 2014, doi: 10.3762/bjnano.5.68.

[70] G. J. Lin *et al.*, "A broadband and omnidirectional light-harvesting scheme employing nanospheres on Si solar cells," *Nano Energy*, vol. 6, pp. 36–43, 2014, doi: 10.1016/j.nanoen.2014.03.004.

[71] P. Matheu, S. H. Lim, D. Derkacs, C. McPheeters, and E. T. Yu, "Metal and dielectric nanoparticle scattering for improved optical absorption in photovoltaic devices," *Appl. Phys. Lett.*, vol. 93, no. 11, pp. 113108-1–3, 2008, doi: 10.1063/1.2957980.

[72] H. R. Stuart and D. G. Hall, "Island size effects in nanoparticle-enhanced photodetectors," *Appl. Phys. Lett.*, vol. 73, no. 26, pp. 3815–3817, 1998, doi: 10.1063/1.122903.

[73] S. Pillai, K. R. Catchpole, T. Trupke, and M. A. Green, "Surface plasmon enhanced silicon solar cells," *J. Appl. Phys.*, vol. 101, no. 9, pp. 093105-1–7, 2007, doi: 10.1063/1.2734885.

[74] D. Derkacs, S. H. Lim, P. Matheu, W. Mar, and E. T. Yu, "Improved performance of amorphous silicon solar cells via scattering from surface plasmon polaritons in nearby metallic nanoparticles," *Appl. Phys. Lett.*, vol. 89, no. 9, pp. 093103-1–4, 2006, doi: 10.1063/1.2336629.

[75] D. M. Schaadt, B. Feng, and E. T. Yu, "Enhanced semiconductor optical absorption via surface plasmon excitation in metal nanoparticles," *Appl. Phys. Lett.*, vol. 86, no. 6, pp. 063106-1–3, 2005, doi: 10.1063/1.1855423.

[76] S. H. Lim, W. Mar, P. Matheu, D. Derkacs, and E. T. Yu, "Photocurrent spectroscopy of optical absorption enhancement in silicon photodiodes via scattering from surface plasmon polaritons in gold nanoparticles," *J. Appl. Phys.*, vol. 101, no. 10, pp. 104309-1–7, 2007, doi: 10.1063/1.2733649.

[77] S. P. Sundararajan, N. K. Grady, N. Mirin, and N. J. Halas, "Nanoparticle-lnduced enhancement and suppression of photocurrent in a silicon photodiode," *Nano Lett.*, vol. 8, no. 2, pp. 624–630, 2008, doi: 10.1021/nl073030+.

[78] Y. C. Chang, M. E. Pollard, D. N. R. Payne, A. Sprafke, S. Pillai, and D. M. Bagnall, "Large-Area Nanosphere Gratings for Light Trapping and Reduced Surface Losses in Thin Solar Cells," *IEEE J. Photovoltaics*, vol. 9, no. 4, pp.

1012–1019, 2019, doi: 10.1109/JPHOTOV.2019.2918183.

[79] B. Wang and P. W. Leu, “High index of refraction nanosphere coatings for light trapping in crystalline silicon thin film solar cells,” *Nano Energy*, vol. 13, pp. 226–232, 2015, doi: 10.1016/j.nanoen.2014.10.040.

[80] V. Sivakov *et al.*, “Silicon nanowire-based solar cells on glass: Synthesis, optical properties, and cell parameters,” *Nano Lett.*, vol. 9, no. 4, pp. 1549–1554, 2009, doi: 10.1021/nl803641f.

[81] L. Tsakalakos, J. Balch, J. Fronheiser, B. A. Korevaar, O. Sulima, and J. Rand, “Silicon nanowire solar cells,” *Appl. Phys. Lett.*, vol. 91, pp. 233117-1–3, 2007, doi: 10.1063/1.2821113.

[82] D. R. Abujetas, R. Paniagua-Domínguez, and J. A. Sánchez-Gil, “Unraveling the Janus Role of Mie Resonances and Leaky/Guided Modes in Semiconductor Nanowire Absorption for Enhanced Light Harvesting,” *ACS Photonics*, vol. 2, no. 7, pp. 921–929, 2015, doi: 10.1021/acsphotonics.5b00112.

[83] S. W. and X. L. Aixue Shang, Xiongfei Zhai, Cheng Zhang, Yaohui Zhan, “Nanowire and nanohole silicon solar cells: a thorough optoelectronic evaluation,” *Prog. Photovolt Res. Appl.*, vol. 23, pp. 1734–1741, 2015, doi: 10.1002/pip.

[84] B. Hua, B. Wang, M. Yu, P. W. Leu, and Z. Fan, “Rational geometrical design of multi-diameter nanopillars for efficient light harvesting,” *Nano Energy*, vol. 2, no. 5, pp. 951–957, 2013, doi: 10.1016/j.nanoen.2013.03.016.

[85] G. Shalev, S. W. Schmitt, G. Brönstrup, and S. Christiansen, “Maximizing the ultimate absorption efficiency of vertically-aligned semiconductor nanowire arrays with wires of a low absorption cross-section,” *Nano Energy*, vol. 12, pp. 801–809, 2015, doi: 10.1016/j.nanoen.2015.01.048.

[86] K. Q. Peng, X. Wang, L. Li, X. L. Wu, and S. T. Lee, “High-performance silicon nanohole solar cells,” *J. Am. Chem. Soc.*, vol. 132, no. 20, pp. 6872–6873, 2010, doi: 10.1021/ja910082y.

[87] D. H. Choi, S. K. Nam, K. Jung, and J. H. Moon, “2D photonic crystal nanodisk array as electron transport layer for highly efficient perovskite solar cells,” *Nano Energy*, vol. 56, pp. 365–372, 2019, doi: 10.1016/j.nanoen.2018.11.050.

[88] Z. Y. Wang *et al.*, “Broadband optical absorption by tunable Mie resonances in silicon nanocone arrays,” *Sci. Rep.*, vol. 5, pp. 7810-1–6, 2015, doi: 10.1038/srep07810.

[89] B. Wang and P. W. Leu, “Enhanced absorption in silicon nanocone arrays for photovoltaics,” *Nanotechnology*, vol. 23, no. 19, pp. 194003-1–7, 2012, doi: 10.1088/0957-4484/23/19/194003.

[90] C. M. Hsu, S. T. Connor, M. X. Tang, and Y. Cui, “Wafer-scale silicon nanopillars and nanocones by Langmuir-Blodgett assembly and etching,” *Appl. Phys. Lett.*, vol. 93, pp. 133109-1–3, 2008, doi: 10.1063/1.2988893.

[91] T. Gao, E. Stevens, J. Lee, and P. W. Leu, “Designing metal hemispheres on silicon ultrathin film solar cells for plasmonic light trapping,” *Opt. Lett.*, vol. 39, no. 16, pp. 4647–4650, 2014, doi: 10.1364/ol.39.004647.

[92] L. B. Luo *et al.*, “Surface plasmon resonance enhanced highly efficient planar silicon solar cell,” *Nano Energy*, vol. 9, pp. 112–120, 2014, doi: 10.1016/j.nanoen.2014.07.003.

[93] G. Liu *et al.*, “Near-unity, full-spectrum, nanoscale solar absorbers and near-perfect blackbody emitters,” *Sol. Energy Mater. Sol. Cells*, vol. 190, pp. 20–29, 2019, doi: 10.1016/j.solmat.2018.10.011.

[94] V. E. Ferry, L. A. Sweatlock, D. Pacifici, and H. A. Atwater, “Plasmonic nanostructure design for efficient light coupling into solar cells,” *Nano Lett.*, vol. 8, no. 12, pp. 4391–4397, 2008, doi: 10.1021/nl8022548.

[95] T. Wang *et al.*, “Enhancing power conversion efficiency of multicrystalline silicon solar cells by plasmonic effect of Ag nanoparticles embedded in SiN x layer,” *AIP Adv.*, vol. 9, no. 2, pp. 025218-1–4, Feb. 2019, doi: 10.1063/1.5087090.

[96] Z. Sun, X. Zuo, and Y. Yang, “Role of surface metal nanoparticles on the absorption in solar cells,” *Opt. Lett.*, vol. 37, no. 4, pp. 641–643, 2012, doi: 10.1364/ol.37.000641.

[97] Y. A. Akimov, W. S. Koh, and K. Ostrikov, “Enhancement of optical absorption in thin-film solar cells through the excitation of higher-order nanoparticle plasmon modes,” *Opt. Express*, vol. 17, no. 12, pp. 10195–10205, 2009, doi: 10.1364/oe.17.010195.

[98] C. L. Lee, W. S. Goh, S. Y. Chee, and L. K. Yik, “Enhancement of light harvesting efficiency of silicon solar cell utilizing arrays of poly(methyl methacrylate-co-acrylic acid) nano-spheres and nano-spheres with embedded silver nano-particles,” *Photonics Nanostructures - Fundam. Appl.*, vol. 23, pp. 36–44, 2017, doi: 10.1016/j.photonics.2016.11.003.

[99] J. Grandidier, D. M. Callahan, J. N. Munday, and H. A. Atwater, “Light absorption enhancement in thin-film solar cells using whispering gallery modes in dielectric nanospheres,” *Adv. Mater.*, vol. 23, no. 10, pp. 1272–1276, 2011, doi: 10.1002/adma.201004393.

[100] M. H. Elshorbagy, E. López-Fraguas, J. M. Sánchez-Pena, B. García-Cámara, and R. Vergaz, “Boosting ultrathin aSi-H solar cells absorption through a nanoparticle cross-packed metasurface,” *Sol. Energy*, vol. 202, no. January, pp. 10–16, 2020, doi: 10.1016/j.solener.2020.03.075.

[101] J. Grandidier *et al.*, “Solar cell efficiency enhancement via light trapping in printable resonant dielectric nanosphere arrays,” *Phys. Status Solidi Appl. Mater. Sci.*, vol. 210, no. 2, pp. 255–260, 2013, doi: 10.1002/pssa.201228690.

[102] J. Grandidier, D. M. Callahan, J. N. Munday, and H. a Atwater, “Gallium Arsenide Solar Cell Absorption Enhancement Using Whispering Gallery Modes of Dielectric Nanospheres,” *IEEE J. Photovoltaics*, vol. 2, no. 2, pp. 123–128, 2012, doi: 10.1109/JPHOTOV.2011.2180512.

[103] Q. Luo *et al.*, “Enhancing photovoltaic performance of perovskite solar cells with silica nanosphere antireflection coatings,” *Sol. Energy*, vol. 169, no. February, pp. 128–135, 2018, doi: 10.1016/j.solener.2018.04.044.

[104] S. Das *et al.*, “A leaf-inspired photon management scheme using optically tuned bilayer nanoparticles for ultra-thin and highly efficient photovoltaic devices,” *Nano Energy*, vol. 58, no. November 2018, pp. 47–56, 2019, doi: 10.1016/j.nanoen.2018.12.072.

[105] Y. R. Lin, K. Y. Lai, H. P. Wang, and J. H. He, “Slope-tunable Si nanorod arrays with enhanced antireflection and self-cleaning properties,” *Nanoscale*, vol. 2, no. 12, pp. 2765–2768, 2010, doi: 10.1039/c0nr00402b.

[106] B. Wang, T. Gao, and P. W. Leu, “Broadband light absorption enhancement in ultrathin film crystalline silicon solar cells with high index of refraction nanosphere arrays,” *Nano Energy*, vol. 19, pp. 471–475, Jan. 2016, doi: 10.1016/j.nanoen.2015.10.039.

[107] Y. Zhang *et al.*, “Coloring solar cells with simultaneously high efficiency by low-index dielectric nanoparticles,” *Nano Energy*, vol. 62, pp. 682–690, 2019, doi: 10.1016/j.nanoen.2019.05.065.

[108] A. M. Al-Amri, P. H. Fu, K. Y. Lai, H. P. Wang, L. J. Li, and J. H. He, “Efficiency Enhancement of InGaN-Based Solar Cells via Stacking Layers of Light-Harvesting Nanospheres,” *Sci. Rep.*, vol. 6, no. March, pp. 28671-1–7, 2016, doi: 10.1038/srep28671.

[109] G. D. Moon *et al.*, “Assembled monolayers of hydrophilic particles on water surfaces,” *ACS Nano*, vol. 5, no. 11, pp. 8600–8612, 2011, doi: 10.1021/nn202733f.

[110] B. Park, S. Y. Na, and I. Bae, “Uniform two-dimensional crystals of polystyrene nanospheres fabricated by a surfactant- assisted spin-coating method with polyoxyethylene tridecyl ether,” *Sci. Rep.*, vol. 9, no. July, pp. 11453-1–9, 2019, doi: 10.1038/s41598-019-47990-z.

[111] X. Ju, C. Xu, Y. Hu, X. Han, G. Wei, and X. Du, “A review on the development of photovoltaic/concentrated solar power (PV-CSP) hybrid systems,” *Sol. Energy Mater. Sol. Cells*, vol. 161, no. November 2016, pp. 305–327, 2017, doi: 10.1016/j.solmat.2016.12.004.

[112] J. Rieger, “The glass transition temperature of polystyrene,” *J. Therm. Anal.*, vol. 46, no. 3–4, pp. 965–972, 1996, doi: 10.1007/bf01983614.

[113] B. G. A. Talat Ozden, Doga Tolgay, M. Samet Yakut, “AN EXTENDED ANALYSIS OF THE MODELS TO ESTIMATE PHOTOVOLTAIC MODULE TEMPERATURE,” *Turkish J. Eng.*, vol. 4, no. 4, pp. 183–196, 2020, doi: 10.31127/tuje.639378.

[114] “Detailed Explanation of the Finite Element Method (FEM).” https://www.comsol.com/multiphysics/finite-element-method (accessed May 04, 2020).

[115] “Nanophotonic FDTD Simulation Software - Lumerical FDTD.” https://www.lumerical.com/products/fdtd/ (accessed Apr. 27, 2020).

[116] X. Ma, J. Q. Lu, R. S. Brock, K. M. Jacobs, P. Yang, and X. H. Hu, “Determination of complex refractive index of polystyrene microspheres from 370 to 1610 nm,” *Phys. Med. Biol.*, vol. 48, no. 24, pp. 4165–4172, 2003, doi: 10.1088/0031-9155/48/24/013.

[117] K. R. Catchpole and A. Polman, “Design principles for particle plasmon enhanced solar cells,” *Appl. Phys. Lett.*, vol. 93, no. 19, pp. 2008–2010, 2008, doi: 10.1063/1.3021072.

[118] K. Shanks, S. Senthilarasu, and T. K. Mallick, “Optics for concentrating photovoltaics: Trends, limits and opportunities for materials and design,” *Renew. Sustain. Energy Rev.*, vol. 60, pp. 394–407, 2016, doi: 10.1016/j.rser.2016.01.089.

[119] P. J. Dobson, “Introduction to Metal-nanoparticle Plasmonics, by Matthew Pelton and Garnett W. Bryant,” *Contemp. Phys.*, vol. 55, no. 4, pp. 352–353, 2014, doi: 10.1080/00107514.2014.948921.

[120] A. Otto, “Surface enhanced Raman scattering A Otto,” *Vaccum*, vol. 33, no. 10–12, pp. 797–802, 1983.

[121] W. C. Lin, S. H. Huang, C. L. Chen, C. C. Chen, D. P. Tsai, and H. P. Chiang, “Controlling SERS intensity by tuning the size and height of a silver nanoparticle array,” *Appl. Phys. A Mater. Sci. Process.*, vol. 101, no. 1, pp. 185–189, 2010, doi: 10.1007/s00339-010-5777-y.

[122] L. Pérez-Mayen, J. Oliva, A. Torres-Castro, and E. De La Rosa, “SERS substrates fabricated with star-like gold nanoparticles for zeptomole detection of analytes,” *Nanoscale*, vol. 7, no. 22, pp. 10249–10258, 2015, doi: 10.1039/c5nr02004b.

[123] J. M. Calleja and M. Cardona, “Resonant Raman scattering in ZnO,” *Phys. Rev. B*, vol. 16, no. 8, pp. 3753–3761, 1977, doi: 10.1103/PhysRevB.16.3753.

[124] J. B. Renucci, R. N. Tyte, and M. Cardona, “Resonant Raman scattering in

silicon," *Phys. Rev. B*, vol. 11, no. 10, pp. 3885–3895, 1975, doi: 10.1103/PhysRevB.11.3885.

[125] E. O. Potma, C. L. Evans, and X. S. Xie, "Heterodyne coherent anti-Stokes Raman scattering (CARS) imaging," vol. 31, no. 2, pp. 241–243, 2006.

[126] J. P. R. Day *et al.*, "Quantitative coherent anti-stokes raman scattering (CARS) microscopy," *J. Phys. Chem. B*, vol. 115, no. 24, pp. 7713–7725, 2011, doi: 10.1021/jp200606e.

[127] N. Valley, N. Greeneltch, R. P. Van Duyne, and G. C. Schatz, "A look at the origin and magnitude of the chemical contribution to the enhancement mechanism of surface-enhanced Raman spectroscopy (SERS): Theory and experiment," *J. Phys. Chem. Lett.*, vol. 4, no. 16, pp. 2599–2604, 2013, doi: 10.1021/jz4012383.

[128] L. Xia *et al.*, "Visualized method of chemical enhancement mechanism on SERS and TERS," *J. Raman Spectrosc.*, vol. 45, no. 7, pp. 533–540, 2014, doi: 10.1002/jrs.4504.

[129] W. Yue, Z. Wang, J. Whittaker, F. Lopez-Royo, Y. Yang, and A. V. Zayats, "Amplification of surface-enhanced Raman scattering due to substrate-mediated localized surface plasmons in gold nanodimers," *J. Mater. Chem. C*, vol. 5, no. 16, pp. 4075–4084, 2017, doi: 10.1039/c7tc00667e.

[130] K. A. Stoerzinger, J. Y. Lin, and T. W. Odom, "Nanoparticle SERS substrates with 3D Raman-active volumes," *Chem. Sci.*, vol. 2, no. 8, pp. 1435–1439, 2011, doi: 10.1039/c1sc00125f.

[131] W. H. Park and Z. H. Kim, "Charge transfer enhancement in the SERS of a single molecule," *Nano Lett.*, vol. 10, no. 10, pp. 4040–4048, 2010, doi: 10.1021/nl102026p.

[132] P. L. Stiles, J. A. Dieringer, N. C. Shah, and R. P. Van Duyne, "Surface-enhanced Raman spectroscopy," *Annu. Rev. Anal. Chem.*, vol. 1, no. 1, pp. 601–626, 2008, doi: 10.1146/annurev.anchem.1.031207.112814.

[133] S. Gwo, H. Y. Chen, M. H. Lin, L. Sun, and X. Li, "Nanomanipulation and controlled self-assembly of metal nanoparticles and nanocrystals for plasmonics," *Chem. Soc. Rev.*, vol. 45, no. 20, pp. 5672–5716, 2016, doi: 10.1039/c6cs00450d.

[134] A. Dhawan, Y. Du, F. Yan, M. D. Gerhold, V. Misra, and T. Vo-Dinh, "Methodologies for developing surface-enhanced raman scattering (SERS) substrates for detection of chemical and biological molecules," *IEEE Sens. J.*, vol. 10, no. 3, pp. 608–616, 2010, doi: 10.1109/JSEN.2009.2038634.

[135] and D.-Y. W. Zhong-Qun Tian, Bin Ren, "Surface-Enhanced Raman Scattering: From Noble to Transition Metals and from Rough Surfaces to Ordered Nanostructures," *Econ. Bot.*, vol. 106, no. 37, pp. 9463–9482, 2002,

doi: 10.1007/bf02871713.

[136] W. Ahmed, Ö. Demirtaş, İ. M. Öztürk, and A. Bek, "Monolayer Assembly of MultiSpiked Gold Nanoparticles for Surface-Enhanced Raman Spectroscopy-Based Trace Detection of Dyes and Explosives," *ACS Appl. Nano Mater.*, vol. 3, no. 7, pp. 6766–6773, 2020, doi: 10.1021/acsanm.0c01177.

[137] H. Staleva *et al.*, "Nanophotonics: Plasmonics and metal nanoparticles," *Phys. Chem. Chem. Phys.*, vol. 11, no. 28, pp. 5866–5866, 2009, doi: 10.1039/b911746f.

[138] M. Kahraman, P. Daggumati, O. Kurtulus, E. Seker, and S. Wachsmann-Hogiu, "Fabrication and characterization of flexible and tunable plasmonic nanostructures," *Sci. Rep.*, vol. 3, pp. 1–9, 2013, doi: 10.1038/srep03396.

[139] G. C. Schatz, R. P. V. Duyne, J. Zhao, J. A. Dieringer, and X. Zhang, "Wavelength-scanned surface-enhanced resonance raman excitation spectroscopy," *J. Phys. Chem. C*, vol. 112, no. 49, pp. 19302–19310, 2008, doi: 10.1021/jp807837t.

[140] S. Schlücker, "Surface-enhanced raman spectroscopy: Concepts and chemical applications," *Angew. Chemie - Int. Ed.*, vol. 53, no. 19, pp. 4756–4795, 2014, doi: 10.1002/anie.201205748.

[141] G. V. P. Kumar, "Plasmonic nano-architectures for surface enhanced Raman scattering: a review," *J. Nanophotonics*, vol. 6, no. 1, pp. 064503-1–20, 2012, doi: 10.1117/1.jnp.6.064503.

[142] M. Fleischmann, P. J. Hendra, and A. J. McQuillan, "Raman spectra of pyridine adsorbed at a silver electrode," *Chem. Phys. Lett.*, vol. 26, no. 2, pp. 163–166, 1974, doi: 10.1016/0009-2614(74)85388-1.

[143] M. G. Albrecht and J. A. Creighton, "Anomalously Intense Raman Spectra of Pyridine at a Silver Electrode," *J. Am. Chem. Soc.*, vol. 99, no. 15, pp. 5215–5217, 1977, doi: 10.1021/ja00457a071.

[144] D. L. Jeanmaire and R. P. VAN Duyne, "Surface Raman Spectroelectrochemistry Part1. Heterocyclic," *J. Electroanal Chem.*, vol. 84, no. 1, pp. 1–20, 1977, doi: https://doi.org/10.1016/S0022-0728(77)80224-6.

[145] M. Moskovits, "Surface roughness and the enhanced intensity of Raman scattering by molecules adsorbed on metals," *J. Chem. Phys.*, vol. 69, no. 9, pp. 4159–4161, 1978, doi: 10.1063/1.437095.

[146] B. Kim, S. L. Tripp, and A. Wei, "Self-organization of large gold nanoparticle arrays," *J. Am. Chem. Soc.*, vol. 123, no. 32, pp. 7955–7956, 2001, doi: 10.1021/ja0160344.

[147] N. A. Abu Hatab, J. M. Oran, and M. J. Sepaniak, "Surface-enhanced Raman spectroscopy substrates created via electron beam lithography and

nanotransfer printing," *ACS Nano*, vol. 2, no. 2, pp. 377–385, 2008, doi: 10.1021/nn7003487.

[148] P. Colson, C. Henrist, and R. Cloots, "Nanosphere lithography: A powerful method for the controlled manufacturing of nanomaterials," *J. Nanomater.*, vol. 2013, pp. 1–19, 2013, doi: 10.1155/2013/948510.

[149] X. Zhang and R. P. Van Duyne, "Optimized silver film over nanosphere surfaces for the biowarfare agent detection based on surface-enhanced Raman spectroscopy," *Mater. Res. Soc. Symp. Proc.*, vol. 876, pp. 207–212, 2005, doi: 10.1557/proc-876-r8.54.

[150] X. Zhang, M. A. Yonzon, D. A. Stuart, and R. P. Van Duyne, "Surface-enhanced Raman spectroscopy biosensors: Excitation spectroscopy for optimisation of substrates fabricated by nanosphere lithography," *IEE Proc. Nanobiotechnology*, vol. 152, no. 6, pp. 195–206, 2005, doi: 10.1049/ip-nbt:20050009.

[151] M. E. Abdelsalam, S. Mahajan, P. N. Bartlett, J. J. Baumberg, and A. E. Rusell, "SERS at structured palladium and platinum surfaces," *J. Am. Chem. Soc.*, vol. 129, no. 23, pp. 7399–7406, 2007, doi: 10.1021/ja071269m.

[152] J. Stropp, G. Trachta, G. Brehm, and S. Schneider, "A new version of AgFON substrates for high-throughput analytical SERS applications," *J. Raman Spectrosc.*, vol. 34, no. 1, pp. 26–32, 2003, doi: 10.1002/jrs.931.

[153] W. C. Lin, L. S. Liao, Y. H. Chen, H. C. Chang, D. P. Tsai, and H. P. Chiang, "Size Dependence of Nanoparticle-SERS Enhancement from Silver Film over Nanosphere (AgFON) Substrate," *Plasmonics*, vol. 6, no. 2, pp. 201–206, 2011, doi: 10.1007/s11468-010-9188-x.

[154] G. N. Xiao, W. Bin Huang, and Z. H. Li, "Rapid and Sensitive Detection of Malachite Green and Melamine with Silver Film over Nanospheres by Surface-Enhanced Raman Scattering," *Plasmonics*, vol. 12, no. 4, pp. 1169–1175, 2017, doi: 10.1007/s11468-016-0372-5.

[155] J. Lee, Q. Zhang, S. Park, A. Choe, Z. Fan, and H. Ko, "Particle-Film Plasmons on Periodic Silver Film over Nanosphere (AgFON): A Hybrid Plasmonic Nanoarchitecture for Surface-Enhanced Raman Spectroscopy," *ACS Appl. Mater. Interfaces*, vol. 8, no. 1, pp. 634–642, 2016, doi: 10.1021/acsami.5b09753.

[156] E. Flores-Romero, E. Rodríguez-Sevilla, and J. C. Cheang-Wong, "Silver films over silica microspheres (AgFOSM) as SERS substrates," *Photonics Nanostructures - Fundam. Appl.*, vol. 28, pp. 81–87, 2018, doi: 10.1016/j.photonics.2017.12.001.

[157] L. Baia, M. Baia, J. Popp, and S. Astilean, "Gold films deposited over regular arrays of polystyrene nanospheres as highly effective SERS substrates from

visible to NIR," *J. Phys. Chem. B*, vol. 110, no. 47, pp. 23982–23986, 2006, doi: 10.1021/jp064458k.

[158] C. Farcau, M. Giloan, E. Vinteler, and S. Astilean, "Understanding plasmon resonances of metal-coated colloidal crystal monolayers," *Appl. Phys. B Lasers Opt.*, vol. 106, no. 4, pp. 849–856, 2012, doi: 10.1007/s00340-011-4849-9.

[159] X. Zhang, M. A. Young, O. Lyandres, and R. P. Van Duyne, "Rapid detection of an anthrax biomarker by surface-enhanced Raman spectroscopy," *J. Am. Chem. Soc.*, vol. 127, no. 12, pp. 4484–4489, 2005, doi: 10.1021/ja043623b.

[160] K. Ma, J. Yuen, and N. Shah, " transcutaneous glucose sensing using surface-enhanced spatially offset Raman spectroscopy: multiple rats, improved hypoglycemic accuracy, low incident power," *Anal. Chem*, pp. 9146–9152, 2011, [Online]. Available: http://pubs.acs.org/doi/abs/10.1021/ac202343e.

[161] O. Lyandres, N. C. Shah, C. R. Yonzon, J. T. Walsh, M. R. Glucksberg, and R. P. Van Duyne, "Real-time glucose sensing by surface-enhanced Raman spectroscopy in bovine plasma facilitated by a mixed decanethiol/mercaptohexanol partition layer," *Anal. Chem.*, vol. 77, no. 19, pp. 6134–6139, 2005, doi: 10.1021/ac051357u.

[162] M. Himmelhaus and H. Takei, "Cap-shaped gold nanoparticles for an optical biosensor," *Sensors Actuators, B Chem.*, vol. 63, no. 1, pp. 24–30, 2000, doi: 10.1016/S0925-4005(99)00393-7.

[163] H. T. Ngo, H. N. Wang, A. M. Fales, and T. Vo-Dinh, "Label-free DNA biosensor based on SERS molecular sentinel on nanowave chip," *Anal. Chem.*, vol. 85, no. 13, pp. 6378–6383, 2013, doi: 10.1021/ac400763c.

[164] X. Zhu, L. Shi, X. Liu, J. Zi, and Z. Wang, "A mechanically tunable plasmonic structure composed of a monolayer array of metal-capped colloidal spheres on an elastomeric substrate," *Nano Res.*, vol. 3, no. 11, pp. 807–812, 2010, doi: 10.1007/s12274-010-0048-y.

[165] J. Wang *et al.*, "A controlled Ag-Au bimetallic nanoshelled microsphere array and its improved surface-enhanced Raman scattering effect," *RSC Adv.*, vol. 4, no. 17, pp. 8758–8763, 2014, doi: 10.1039/c3ra47882c.

[166] N. G. Greeneltch, M. G. Blaber, G. C. Schatz, and R. P. Van Duyne, "Plasmon-sampled surface-enhanced raman excitation spectroscopy on silver immobilized nanorod assemblies and optimization for near infrared (λex = 1064 nm) studies," *J. Phys. Chem. C*, vol. 117, no. 6, pp. 2554–2558, 2013, doi: 10.1021/jp310846j.

[167] W. M. Ingram, C. Han, Q. Zhang, and Y. Zhao, "Optimization of Ag-Coated Polystyrene Nanosphere Substrates for Quantitative Surface-Enhanced Raman Spectroscopy Analysis," *J. Phys. Chem. C*, vol. 119, no. 49, pp.

27639–27648, 2015, doi: 10.1021/acs.jpcc.5b06896.

[168] N. Seyedpour Esmaeilzad *et al.*, “Nanosphere Concentrated Photovoltaics with Shape Control,” *Adv. Opt. Mater.*, vol. 9, no. 3, pp. 1–11, 2021, doi: 10.1002/adom.202000943.

[169] P. B. Johnson and R. W. Christy, “Optical Constant of the Nobel Metals,” *Phys. Rev. B*, vol. 6, no. 12, pp. 4370–4379, 1972.

CURRICULUM VITAE

PERSONAL INFORMATION

Surname, Name: Seyedpour Esmaeilzad, Seyedehnasim
Nationality: Iranian (IR)
Date and Place of Birth: 5 May 1989, Tabriz
Marital Status: Married
Phone: +90 5380120160
email: e189101@metu.edu.tr

EDUCATION

Degree	Institution	Year of Graduation
MS	METU Electrical and Electronics Engineering	2015
BS	University of Tabriz Electrical and Electronics Engineering	2011

WORK EXPERIENCE

Year	Place	Enrollment
2018-Present	TED University, Dept. of Electrical and Electronics Engineering	Teaching Assistant
2012-2018	METU Dept. of Electrical and Electronics Engineering.	Research Assistant

FOREIGN LANGUAGES

Advanced English, Persian, Azeri, Turkish

PUBLICATIONS

1. **Seyedpour Esmaeilzad N**, Demir A K, Hajivandi J, Ciftpinar H, Turan R, Kurt H and Bek A 2021 Nanosphere Concentrated Photovoltaics with Shape Control Adv. Opt. Mater. 9 1–11
2. **Seyedpour Esmaeilzad N**, Demirtas.Ö, Demir A and Bek A Shape and Deposition Angle Control of Silver Film-over-Nanosphere SERS Substrates, submitted to Nanotechnology

3. E. Erdil, K. Topallı, **N. S. Esmaeilzad**, O. Zorlu, H. Külah, and O.A. Civi, "Reconfigurable Nested Ring-Split Ring Transmitarray Unit Cell Employing the Element Rotation Method by Microfluidics," IEEE Transactions on Antennas & Propagation, 2014, DOI:10.1109/TAP.2014.2387424.
4. Özge Demirtas, Ghazanfar Ali Khan, **Nasim Seyedpour Esmaeilzad**, R. M. Faheem Iftikhar, İ. Murat Öztürk, A. Kemal Demir, Waqqar Ahmed, Alpan Bek, "SERS-based trace detection by size and shape controlled noble metal particles with high benefit-cost ratio," Proc. SPIE 11797, Plasmonics: Design, Materials, Fabrication, Characterization, and Applications XIX, 1179713 (1 August 2021); https://doi.org/10.1117/12.2594112
5. **Nasim Seyedpour Esmaeilzad**, Hande Ciftpinar, Rasit Turan, Alpan Bek, "Concentrated Photovoltaics Using Shape-modified Nanospheres, " PVCON 2020.
6. İDİKUT F. , Borra M. Z. , **Seyedpour S. E**. BEK A. "Subsurface Silicon Processing by Microsphere Focusing of Ultrafast Infrared Laser," OPLAL 2019 : 2nd International Conference on Optics, Photonics and Lasers (OPAL' 2019)
7. **Nasim Seyedpour Esmaeilzad,** İbrahim Murat Öztürk, Mona Zolfaghariborra, and Alpan Bek, "Nanosphere Colloidal Coating for Improvement of Solar Cell Efficiency, " EuPVSEC 2018.
8. Navid Hosseini, **N. S. Esmaeilzad**, O.A. Civi, "Tunable Frequency Antenna Integrated With Microfluidic Channel," IEEE AP-S Symposium on Antennas and Propagation 2015.
9. Emre Erdil, Kagan Topalli, **N. S. Esmaeilzad**, Özge Zorlu, Haluk Kulah, Ozlem Aydin Civi "A Reconfigurable Nested Ring-Split Ring Transmit array Unit Cell by Microfluidic Technology," Eucap2014 (8th European Conference on Antennas and Propagation).
10. Emre Erdil, Kagan Topalli, **N. S. Esmaeilzad**, Özge Zorlu, Haluk Kulah, Ozlem Aydin Civi "Microfluidic Reconfigurable Nested Split Ring-Regular Ring Transmitarray Unit Cell," General Assembly and Scientific Symposium (URSI GASS), 2014 XXXIth URSI.